METHOD FOR MEASUREMENT OF RESIDUAL STRESS AND COEFFICIENT OF THERMAL EXPANSION OF LAMINATED COMPOSITES

By

DONALD G. MYERS II

A THESIS PRESENTED TO THE GRADUATE SCHOOL
OF THE UNIVERSITY OF FLORIDA IN PARTIAL FULFILLMENT
OF THE REQUIREMENTS FOR THE DEGREE OF
MASTER OF SCIENCE

UNIVERSITY OF FLORIDA

2004

This thesis is dedicated to my family, loved ones, and in the memory of my father.

ACKNOWLEDGMENTS

I would like to thank my advisor, Dr. Peter Ifju, for all of his support and advice. I would also like to thank my other committee members, Dr. Raphael Haftka and Dr. Bhavani Sankar, for their advice. Thomas Singer, William Schulz, and Lucian Speriatu were fellow assistants in the Experimental Stress Analysis Lab that provided invaluable assistance in my efforts. I would also like to extend a thank you to Dr. Leishan Chen for all of his assistance. Together all of these people along with my various professors have made my time at the University of Florida a wonderful educational experience. Finally I would like to say thank you to my entire family and loved ones for everything they have done for me throughout my life.

TABLE OF CONTENTS

page

APPENDIX

LIST OF TABLES

LIST OF FIGURES

Abstract of Thesis Presented to the Graduate School
of the University of Florida in Partial Fulfillment of the
Requirements for the Degree of Master of Science

METHOD FOR MEASUREMENT OF RESIDUAL STRESS AND COEFFICIENT OF THERMAL EXPANSION OF LAMINATED COMPOSITES

By

Donald G. Myers II

May 2004

Chair: Peter G. Ifju
Major Department: Mechanical and Aerospace Engineering

The development of residual stresses in laminated composites is a very important area of extensive research. Residual stress can dramatically reduce the strength of a component built of a laminated composite. The existence of these residuals stresses and strength degradation can lead to catastrophic material failures as seen in the X-33. A method has been proposed to measure and quantify these stresses as well as determine the thermal expansion coefficient of laminated composites as a function of temperature. This method relies on the combination of existing techniques in a manner that will allow for the acquisition of stress values across a wide range of temperatures. The first technique employed is a novel strain measurement method know as the Cure Referencing Method. This technique is based on transferring a moiré grating onto a specimen during the cure process. The grating becomes a part of the specimen at cure temperature during the polymerization of the resin and therefore carries all strain information from the curing process including temperature dependent strains as well as chemical shrinkage

information. The tool with which the grating was transferred to the specimen is used as a reference from which all relative deformations are calculated. This process is implemented on laminates of three differing stacking sequences, each of which provides its own unique data point. The results from this method provide data points from which the next technique references the strains and stresses as a function of temperature. After strain measurements are taken from the moiré specimen, they are fitted with strain gages in the x and y directions. Strain values are observed as a function of temperature as the specimens are exposed to temperatures between cure and cryogenic conditions. The strain gage readings are compensated for temperature effects and are referenced to the strain values at room temperature given by the cure referencing method. The resulting values of strain represent the total surface strain at any given temperature for the various laminates. The surface strain on the unidirectional laminate represents the free expansion state any lamina would reach if not constrained. This value is used to determine residual strain present in different layers of the multidirectional laminates. The coefficient of thermal expansion is also calculated as a function of temperature from the strain gage readings. Basic material testing is also conducted and the values of longitudinal, transverse, and shear moduli are presented. Variability in these measurements is also reported in conjunction with other work at the University of Florida to perform reliability based optimization. Once the residual strain and material properties are calculated they are transformed into stress by the usual stress-strain relations. The final ply level residual stress is plotted as a function of temperature. The results of surface strain measurements are compared to classical lamination theory analytical predictions.

CHAPTER 1
INTRODUCTION

Throughout history one of the primary goals of engineers has been to develop structures and materials that are lighter, stronger, and tougher than those that already exist. The introduction of advanced structural composites (ASCs) has helped to achieve that goal. Composite materials are those that consist of two or more separate materials that are combined macroscopically into a structural unit [13]. The prevalence of these composite materials has skyrocketed since the 1960s and are now used in structures as advanced as satellites, space structures, and military aircraft and in everyday sporting goods around the house such as skis and golf clubs.

1.1 Historical Background

Despite the boom in significance since the development of ASCs in the 1960s, basic man-made composite materials have been around for thousands of years. Some examples can be seen as early as the times of the great Egyptian kingdoms when brick was made of clay and straw, and in South and Central America where the people used plant fibers in native pottery [13]. Both of these are examples of one of the most predominant composite materials, fiber reinforced composites. Other examples of fiber-reinforced composites include glass/epoxy, steel-reinforced concrete, and graphite/epoxy, the subject of this investigation.

The motivation for the use of fiber-reinforcement in materials comes from research by Griffith published in 1920 that demonstrated that some materials are stronger and

stiffer as fibers than in bulk form [14]. Some reasons for this increase in strength include less material flaws, orientation of molecular chains, and lower dislocation densities.

Along with all the obvious advantages, advanced fiber-reinforced composite materials have their shortcomings as well. A primary performance weakness is that most of the strength exists in the direction of the fiber and the material performs poorly in transverse directions. Transverse reinforcement is necessary to make the material useful and this is done usually by orienting the fibers at various angles.

Using composite materials also poses other problems for designers. These materials are much more difficult to analyze and characterize. Many of the design and analysis techniques that have been used for years on other materials cannot be applied directly to composite materials. Because they consist of more than one material they are often orthotropic in nature. Also, once several layers of lamina are assembled into a laminate, to correct the transverse weakness or tailored to achieve desired directional strengths, a complex interaction between layers develops. This is a macroscopic issue while on the microscopic level there is also a complex interaction that takes place within each lamina between the fiber and matrix material.

Due to these analysis difficulties, the behavior of composite materials is not fully understood and this lack of understanding can lead to devastating mechanical failures. It is the goal of this paper to detail a combination of methods that can be used to characterize a material system and then provide a detailed set of data and information on the IM7/977-2 material system.

1.2 Failure of the X-33 Fuel Tank

For several years, efforts have been underway to develop a reusable launch vehicle (RLV) to replace the aging space shuttle fleet. The goal is to develop a vehicle that is

entirely self-contained without the need of external fuel and propulsion components such as the external fuel tank and solid rocket boosters seen on the current space shuttles. The vehicle is to be able to takeoff, perform its mission in space, and return to earth entirely under its own power. The development of the X-33 was an attempt to achieve these goals.

The design of the X-33 called for an internal liquid hydrogen (LH_2) fuel tank [12]. This tank was to be an integrated part of the structure designed to provide both fuel storage and carry structural loads. One of the most important factors in the design of an RLV is to reduce the takeoff weight as much as possible. Manufacturing a tank consisting of ASCs was seen as the best way to do this.

The X-33's fuel tank and aft fuselage were designed to consist of two LH_2 fuel tanks, with each composed of several "lobes" made of graphite/epoxy and having bonded woven composite joints. Each lobe was a sandwich panel with face sheets consisting of the IM7/977-2 material system and a Korex® core. The tanks were to store the LH_2 fuel as well as be part of the primary aft structure designed to distribute thrust, inertial, landing gear, and aero-control surface loads.

The first of two tanks was designed and delivered by Lockheed Martin to NASA at the Marshall Space Flight Center for preflight testing. The preflight testing was designed to verify that the tank was able to withstand the cryogenic loading conditions of –423º F (20º K) as well as the expected flight loads. The planned testing sequence consisted of:

1. A partial liquid nitrogen (LN_2) fill and proof test to 32 psig, followed by a leak check at 34 psi of gaseous helium
2. A LH_2 fill and structural load application. The test was to consist of six conditions: a proof pressure test at 42 psig and five loading tests at 5 to 42 psig
3. A final 34 psig gaseous helium test

It would be seen soon after testing began that the design was not feasible for its intended purpose.

In early November of 1999 the fuel tank began the first combined mechanical loading and LH_2 storage test. It had been previously been filled and leak tested with LN_2 and LH_2 in the absence of external loads. This time the initial pressure and loading tests were successful and the tank was drained of LH_2. Fifteen minutes after the tank was drained a major mechanical failure took place as the outer facesheet and core material debonded from the inner facesheet. The following lists the observations that were made during the test and time leading up to the failure.

The first observation was that at the time of fueling there was an expected decrease in the pressure of the sandwich core resulting from the temperature change within the tank. The second observation was an unanticipated increase in the core pressures as the tank neared full capacity and pressurization. A third observation was the continued increase in core pressures as the tank was drained. This event was expected, as the temperature increase would reverse the initial trend seen in observation one and pressure should have returned to ambient conditions. Fourth was the incident of the composite sandwich failure. At the time of the failure core pressures were between 50 and 60 psia. These pressures rapidly dropped to atmospheric as the region failed. Finally, the remaining sections of the core that did not experience a failure had internal pressures above the expected ambient a full 13 hours later.

Review and analysis of the data resulted in the following failure sequence. The rise in pressure in the second observation was most likely the result of seepage of H_2 into the core through the inner facesheet. The method of transportation was though mirocracks

that had developed in the inner facesheet due to the stresses and strains cause by the cryogenic environment. As the tank was filled with LH_2, the cooling caused a vacuum in the core, which helped to pull in GH_2 until the area was covered with the liquid. LH_2 was then also able to penetrate the facesheet through the microcracks. As the tank was emptied some of the fluid was able to travel back through the microcracks and be removed from the tank. However, before all of the fluid had passed back into the interior of the tank the pressure and strain decreased closing the microcracks and trapping some of the fluid inside the core. As the temperature continued to climb the pressure of the vaporizing H_2 resulted in a buildup until the outer facesheet and core debonded from the inner facesheet.

The properties of the laminates were estimated from existing databases. Also it was assumed that 5000 microstrain ($\mu\varepsilon$) was an adequate allowable level to limit permeability. The above failure observed in the X-33 project is a perfect example of how the behavior of ASCs are not fully understood and how this lack of information can result in catastrophic failures. The design group failed to adequately cover combined thermal/mechanical effects. It is this thermal effect, or processed induced residual effects, that are not fully understood and result in considerable structural issues.

The failure of the X-33 and what it means to the future of composite implementation is the driving force behind this thesis. This work will propose combined methods that can be used to better evaluate the IM7/977-2 of the X-33 and other composite material properties as they are subjected to extreme thermal conditions. This material characterization can be used to remove the some of the assumptions that are

made in current composite design and replace them with concrete experimentally determined values.

1.3 Residual Strains and Stresses

Root failure of the X-33 was most likely the failure to understand and accurately predict the residual strains and stresses that develop in a composite as a result of curing and the exposure to changing temperatures, especially low temperatures. When a polymeric fiber reinforced composite is manufactured it usually undergoes a process where the resin is heated, the fibers are wetted, and cure takes place at high temperatures [37]. During this process and subsequent conditions residual strains and stresses will develop within the laminate.

The developing stresses arise on two different scales. Stresses will occur that develop between the fiber and matrix in each lamina of a composite. The study of these effects is termed micro-mechanics, where a laminate is examined on the fiber scale. Another area of interest is the examination of what happens to a composite on the macro-mechanical or ply scale. It is on this scale that the following research will focus.

On the ply scale residual strains and stress develop due to the mismatch in the thermal expansion coefficients of the fiber and matrix as well as the development of chemical shrinkage. As a lamina is cured its matrix constituent undergoes polymerization. Epoxy resins undergo condensation polymerization, where two reacting monomers are brought together to form a new molecule of the desired compound [13]. In the case of many ASCs this is a two-step process. The production of prepreg tape consists of wetting the fibers and allowing the matrix to partially cure. The polymerization process concludes when these prepreg materials are arranged into the desired stacking sequences and then are heated to the desired cure temperature. As this

process takes place the matrix undergoes a volumetric change known as chemical shrinkage while the fibers remain volumetrically unchanged. This event adds to the mismatch in expansion of the fibers and matrix, where the matrix is subject to higher expansion and contraction than the fiber.

Residual stresses develop when the desired expansion of the lamina is restricted. As the angles of the lamina are varied from ply to ply, the lower contraction of the fiber will constrain the contraction of the matrix. When temperatures are decreased, as in the case of the X-33, the matrix desires to contract but instead is subjected to tensile stress as this deformation is opposed. If all of the fibers are aligned with each other there is no stress present on the ply scale. A cross-ply [0/90] stacking sequence will result in the highest level of residual stress.

The residual stresses that develop during processing and operating conditions are not negligible. They can consume large amounts of a laminate's strength. If these stresses are not accurately understood they can lead to drastic material failures as in the case of the X-33, where the tensile stresses that developed in the matrix material likely exceeded its critical tensile strength. Once this occurred, micro-cracks were able to develop allowing the seepage the hydrogen into the core. The development of microcracks in other structures will allow the fibers to be exposed to possibly degrading environmental conditions as well as possible chemical attack in storage facilities.

1.4 Structural Reliability

The existence of the overwhelming thermal stresses that resulted in the failure of the X-33 demonstrates the need to better understand the nature of composite materials and appropriately design for their implementation. The examination of structural

reliability of a component during the design process is a step that must be taken to prevent such failures.

Previously, the design process worked to build reliability based on a factor-of-safety approach [48]. This is a deterministic approach to the issue of reliability where worst case scenarios are proposed, investigated, and accounted for by adding a safety margin in the design. This approach has been used for years in metallic structures and can provide adequate reliability for composites but not to the same degree. This is because composite material performance exhibits a larger statistical distribution and variation than metals. Reliability-based design methods are being developed to account for this problem.

Probabilistic design methods are moving to the forefront in composite design. Probabilistic design is an integrated process that works to define and develop functional relationships between various design factors and material properties. A statistical variation in one variable will have consequences to the others and those changes can be designed for. The probabilistic approach uses statistical characterization instead of proposed worst case values to define a variable and determine its magnitude and frequency. The amount of data and how well the variables are defined will influence the extreme values.

A typical probabilistic design approach has the following fundamental elements:

1. Identify all possible uncertain variables on all scales of the structure, including all variables at the constituent scale, all stages of fabrication and assembly, and the possible applied loads.
2. Assign a probabilistic distribution function for each variable.
3. Process all random variables through and analyzer that can handle micro- and macro-mechanics laminate theories, structural mechanics, and probability theories.

4. Extract useful information from the analysis and compare them to probabilistic design parameters.

To be able to carry out the above procedure the following aspects must be characterized as random variables:

- Material mechanical properties
- External loads during operation
- Manufacturing process variability
- Environmental effects
- Environmental history during operation
- Effect of flaws or damage locations
- Predictive Accuracy

The probabilistic approach to analysis and design has become a significant area of academic interest. Qu et al have investigated areas of interest that are particularly of importance to the future of RLV design. They performed reliability-based optimization of composite laminates for cryogenic environments [41]. It was found that under these conditions that the optimized weight was sensitive to transverse lamina strength and thermal stresses as they are related to CTE and lay-up sequence. When the confidence in these values is low the thickness of the laminate is significantly greater leading to a higher vehicle weight.

1.5 Research Objectives

The work of Qu et al has been carried on at the University of Florida and parallels the work in this thesis. The goals of this thesis were to establish a simple testing method to determine residual strains, stresses, and coefficient of thermal expansion as a function of temperature, and to measure these properties on the IM7/977-2 material system that was used in the X-33 fuel tank development. In addition to this, various moduli were to be experimentally determined and statistical data was to be supplied to the optimization group for further probabilistic analysis and design.

CHAPTER 2
RESIDUAL STRESS CHARACTERIZATION TECHNIQUES

2.1 Introduction

Since the introduction of advanced structural composites the need to understand their behavior has lead to extensive research in the area of residual stress determination. Many existing methods have been devised to aid in residual stress characterization. Some of these methods have been derived from existing tests used on other materials while others have been developed from scratch. Each of these methods has it own advantages and disadvantages. As a whole they can be useful in characterizing certain aspects of residual stress and its effects. Most do have the same substantial flaw that will be pointed out in this research. None, with the exception of the Cure Referencing Method (CRM), developed at the University of Florida and used extensively in this work, have the ability to account for the residual stress that results from the chemical shrinkage involved in the curing of an ASC. This chapter will give a brief history of and detail the existing traditional methods that are often used to characterize residual stress in laminated composites.

Existing methods are usually grouped into two broad groups, those that are destructive in nature and those that are non-destructive. Destructive testing usually involves damaging or removing a section of material from a test specimen. The result is a specimen that can no longer be used for most applications. Non-destructive tests are generally preferred over destructive tests for obvious reasons. A specimen exposed to non-destructive means of testing has not lost any usefulness as a structural component.

Tests can also be repeated on the same specimen to ensure accuracy. These methods also often provide a means with which to test the effects of time on a component.

2.2 Destructive Testing Techniques

2.2.1 Hole-Drilling Method

One of the oldest and most accepted methods for the determination of residual stresses is that of the hole-drilling technique. Mathar first proposed this technique as early as the middle 1930s [33]. Since that time it has been employed to characterize residual stresses present in metal structures and other isotropic materials. When a hole is introduced into a stressed body the stresses are relaxed and become zero. This results in a change in the surrounding strain field, which can be measured and correlated to the relaxed stresses. This was the heart of Mathar's work.

The most commonly used application of the hole-drilling techniques involved drilling a small blind hole near the application point of a strain gage rosette [35]. The rosette can then measure the relaxed strain and the data can be used to calculate the residual stress that was present before the creation of the hole. Since the middle to late 1960s efforts have been underway to extend the use of this technique from isotropic to orthotropic materials [1,28,42,43]. The extension of this method into orthotropic materials does not yield results as readily as in isotropic materials. The solution method is numerically intense. Many assumptions must be made in order to simplify the resulting solutions. The highly orthotropic nature of composites also adds further difficulty in the measurements themselves. Obtaining measurement precision around the hole is extremely difficult especially in the fiber direction, even for high precision techniques such as moiré interferometry [36].

2.2.2 Cutting Method

The cutting method is another technique that relies on the same principles as those in the hole drilling method. Again, stress is relaxed by the removal of material. This time a notch is removed from a specimen resulting in the creation of a free edge. Lee devised a method where a moiré interferometry grating was applied to the specimen to record the resulting strain field [30,31]. The resulting strain field was calculated and related to the residual stresses by the used of finite element analysis.

This method is not without its faults and has yet to be fully accepted in the experimental community. Niu poses many questions based on the application of the grating [37]. The grating was applied after an edge of the composite had been trimmed. This resulted in some of the residual stresses being released prior to data recording and the creation of a very complex strain field under the surface. The resulting measurements that were made contained data that was based on a stress field different from the original residual stress.

A second technique derived to employ the cutting method was proposed by Sunderland et al. [46]. The successive grooving technique involved cutting a groove through the thickness at successive depths. Strain gages were placed opposite the groove and recorded the changing strain field. The residual stress was then calculated from the strain by use of a numerical 2-D model for each layer.

2.2.3 Ply Sectioning Method

Yet another destructive technique devised to study residual stresses in laminated composites has been proposed by Joh et al. [24]. This method made use of moiré interferometry. The deformation caused by sectioning and releasing a layer from the constraints imposed by an adjacent layer was measured. The resulting release of stress

could be easily calculated from the deformation strains. The problems resulting from the cutting method are resolved by obtaining a small strip specimen from the edge of the larger specimen resulting in a plane stress state.

Another manner in which to use ply sectioning involves the nature of warping seen in an unbalanced composite laminate. The outside layers of a laminate can be machined away resulting in the unbalanced, warped structure [3,32]. The resulting warpage is measured and can be used as an input in classical lamination theory to calculate the corresponding residual stresses.

2.2.4 First Ply Failure

The first ply failure method makes use of the maximum stress criterion to calculate the existing residual stresses [16,27]. Hahn and Kim recorded strains and loads while loading a cross ply, [0/90], specimen to failure. Elastic assumptions were used to calculate the load at which the first ply failed. This load was compared to the corresponding strength of a unidirectional specimen and the difference was called the residual stress. Kam also attempted to consider the visco-elastic effect on this methodology [25].

2.3 Non-Destructive Techniques

2.3.1 Warpage

Warpage will result in unbalanced, asymmetric multidirectional laminates. The destructive method of Joh et al. made use of this fact in its calculation of stress from deformation strain resulting from sectioning. Asymmetric laminates can also be intentionally manufactured so that the warpage can be measured. This method has been an area of extensive investigation [8,10,17,22,23,26,27,32,51]. CLT provides the usual means by which the stresses are calculated from the observed warpage.

The combination of warpage and CLT has also been used to devise a method to measure and quantify polymer matrix cure shrinkage [8,9]. Daniel manufactured a laminate directly onto an existing and previously cured identical laminate having the same CTE and manufacturing procedure. Any resulting warpage was strictly the result of the chemical shrinkage. The curvature was measured and stresses were again calculated using CLT and the resulting stresses were directly related to chemical shrinkage.

2.3.2 Embedded Strain Gages

Embedded strain gages function by becoming an intimate part of the laminate being measured. Any deformation of the laminate is directly seen and measured by the strain gage. The most common strain gages used for this method are the electrical resistance and fiber optic strain gage.

The first efforts to measure residual stress in this manner were made by Daniel [5,6,7]. High temperature electrical resistance strain gages were cured directly in the laminate by placing them between the lamina plies. The strain gages were then directly exposed to any deformation of the laminate. A compensation method was derived to account for the varying characteristics of the gage as it went through a given temperature range. A similar method of compensation is used and described in this thesis. The main drawback to the method described by Daniel was the introduction of a foreign body to the laminate. This can drastically alter the material properties at the location as well as create a void that will lead to incorrect measurements.

Fiber optics represents the second set of strain gages. This gage seems to be gaining favor in the experimental community. Several recent studies have been conducted with these gages [2,29,47,49]. In this technique a fiber optic is laid or embedded in the composite as if it were one of the fibers. Again there is a concern with

the introduction of a foreign body into the heart of the laminate. If the optical fiber is not on the same size scale as the material fiber then there is potential for significant errors based on the change in the laminate material properties.

2.3.3 X-ray Diffraction

The use of X-ray diffraction in determining stresses was proposed by Predecki and Barrett in 1979 [40]. Their work was extended to measure residual stresses by Fenn, Jones, and Wells [11]. With this technique metal particles become part of the matrix material and experience similar deformations. X-ray measurements are made on the embedded metal particles and the resulting stresses are correlated to the residual stresses in the composite. As with the embedding of strain gages, the introduction of metal particles could result in a change in the laminate properties.

2.3.4 Electrical Resistance

Graphite and Carbon fibers are electrical conductors and therefore a laminate made from them will have a measure of electrical conductivity and resistance. Researchers are looking into a technique where the electrical resistance of a laminate can be used to measure the development of stresses [38,50]. Wang and Chung have observed the change in resistance across the thickness of a laminate and have set out to correlate the measured resistance with stresses present in the composite. Park, Lee, and Lee set out to achieve cure monitoring and strain-stress sensing based on a similar technique.

2.3.5 Cure Referencing Method

The Cure Referencing Method is a technique developed recently by Niu, Ifju, and Kilday to record process induced strains[20,21,37]. CRM uses the full-field laser based optical method of moiré interferometry to document strains on the surface of laminates that initiate during the high temperature curing process. The method involves replicating

a high frequency diffraction grating on the specimen while in the autoclave. This method will be key to the research done in this thesis. A detailed description of the application of CRM will follow.

CHAPTER 3
CURE REFERENCING METHOD

Several distinct experimental techniques were used in conjunction with one another to develop residual strain, stress, and coefficient of thermal expansion values across a wide temperature range. The following chapters will describe in detail the processes and methods used in the research. These processes and experimental techniques include material lay-up procedures, basic material property characterization, the Cure Referencing Method (CRM), and basic strain gage techniques.

3.1 Selected Laminates

The first step in developing a better understanding for the issues at hand was to manufacture a desired test specimen. Three different composite laminates have been chosen for study. A composite laminate consists of two or more layers or plies of lamina arranged in any stacking sequence. Three different stacking sequences of IM7/977-2 were selected for study based on their relative importance. These laminates were:

1. Unidirectional (UNI): $[0_{13}]$
2. Reusable Launch Vehicle (RLV): Quasi-isotropic lay-up $[45/90_3/\text{-}45/\bar{0}_3]_S$
3. Optimized Angle Ply (OAP): $[(\pm 25)]_{3S}$

The unidirectional stacking sequence was selected for its ability to provide insight into some of the material properties of the material system [19]. It will be seen later how the strain values obtained from the unidirectional material are used directly in the analysis to calculate residual strain and stress in the other laminates.

The RLV was, as its name implies, taken directly from the stacking sequence selected by Lockheed Martin for the design of the X-33 LH_2 fuel tanks. It was designed

as a somewhat quasi-isotropic laminate to allow for maximum strength in all directions. Quasi-isotropic lay-ups are very common in structural applications of ASCs. However, it was not designed to account for the loss in strength that is associated with the development of thermal residual stresses.

The lay-up selected as the optimized angle ply was the result of work done in an effort to account for thermal stresses while still maintaining a level of mechanical strength. This effort resulted from a reliability optimization performed by Qu [41], of a LH_2 fuel tank constructed from an IM600/133 graphite/epoxy material system. The stacking sequence for the tank was $[\pm\theta_1/\pm\theta_2]_s$. Optimal designs had ply angles θ_1 and θ_2 near 25^o, and nearly equal; the stacking sequence was thus simplified to $[\pm\theta]_s$. Monte Carlo simulation gave a probability of failure of approximately 1 in 15,000 for the $[\pm 25^o]_s$ design. It should be noted that this optimized ply sequence was for a different, but similar material system.

These laminates were chosen for the study of the residual strain, stress and CTE. Different sequences were used in the basic material property determination and they will be described briefly in a following chapter.

3.2 Cure Referencing Method

The CRM is a technique developed at the University of Florida by Dr. Peter Ifju and Xiaokai Niu. It is a non-destructive novel testing method designed to accurately determine process induced and residual strains that are associated with the manufacturing, cure, and thermal loading of an ASC. This method is based on a full-field measurement technique know as moiré interferometry in which a diffraction grating is placed on a test piece during the cure cycle. The following section aims to describe CRM and the procedures behind its implementation.

3.3 Moiré Interferometry

Moiré Interferometry is a very precise and sensitive laser based optical technique that allows the development of a contour map of the in-plane displacements [39]. This technique provides a displacement sensitivity of 0.417 μm per fringe order. Moiré relies on the interference properties of light that results in the development of dark and light bands known as fringes. For this interference to be observed, two diffraction gratings must be compared to one another. One diffraction grating must be replicated to the desired part or specimen that is to be deformed while another grating is to remain unaltered to serve as a reference. This unaltered grating may be one applied to an un-deformed specimen or the master grating that is used to transfer the pattern to specimens as described in the next section. The moiré interferometer is tuned with the reference grating. "Tuned" refers to aligning the interaction of the laser and reference grating in a manner so that the displacement field is nullified, or no fringes are present. This is necessary so that only the deformation of the specimen is recorded by the presence of fringes. The deformation that develops in a specimen can be observed at anytime under any loading condition as long as the reference grating is still intact. In this study the deformation given by moiré was only observed for a mechanically unloaded specimen at room temperature. A four-beam moiré interferometer, schematically represented in Figure 3-1, was used to record the deformation data.

The interferometer used in this experiment was a 2400 line/mm four-beam system seen in Figure 3-2. The interferometer consisted of a 10 milliwatt Helium Neon laser with a 632 nm wavelength and a 108 mm diameter parabolic mirror. The field of view provided was 38.1mm or 1.5 inches in diameter.

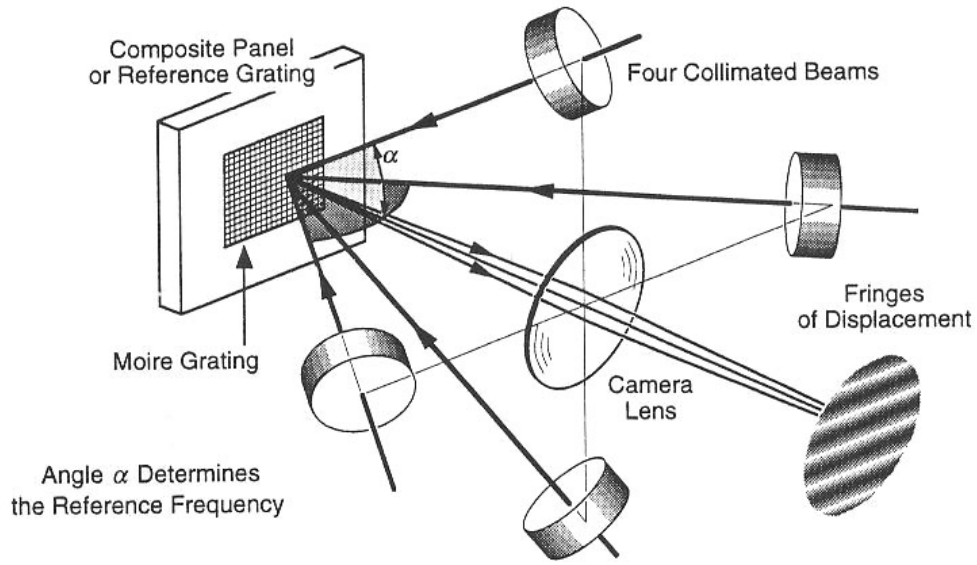

Figure 3-1: Schematic of a four-beam moiré interferometer

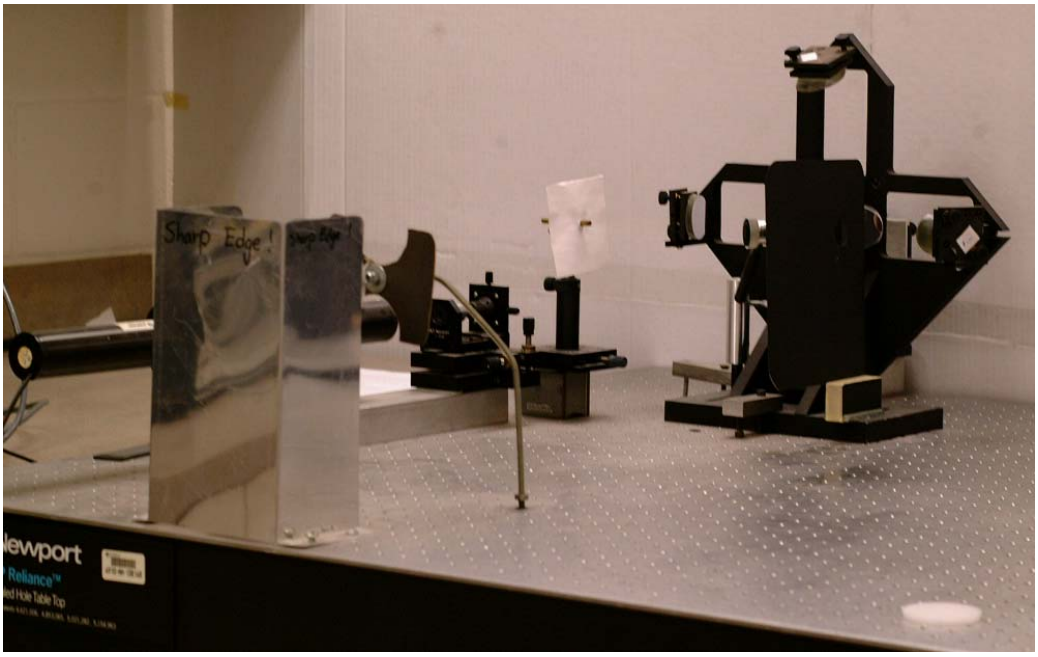

Figure 3-2: Image of moiré interferometer used in testing

3.4 Diffraction Gratings

Application of a diffraction grating to a part during cure is the central idea and procedure behind CRM. Before this grating was applied to a specimen it was carefully

produced in a several step method derived from the process developed by Niu [37] described next.

The development of an appropriate diffraction grating to be attached to a specimen followed these procedures and is seen schematically in Figure 3-3:

5. A grating was replicated at room temperature onto Astrositall glass (ULE) using silicone rubber from an original photoresist master grating. The glass had dimension of 3"x 4.5"x 0.5". The silicone rubber was a two-part mixture (GE RTV 615). The silicone mixture was centrifuged so that all air bubbles could be removed form the mixture.

6. The silicone grating was then placed into a vacuum deposition chamber where a very thin layer of aluminum was deposited onto its surface. This layer was deposited so that another piece of Astrositall could be easily separated from its surface in a later step.

7. The aluminum coated silicone grating was then used to replicate onto the Astrositall autoclave tool. This grating was made of 3501-6 epoxy. Both pieces of Astrositall were placed into a heating/vacuum chamber where they were heated to 177º C and allowed to soak for approximately one hour. A small piece of 3501-6 was pulled from the freezer and placed into a metal tray where it could be heated. A vacuum was applied to the chamber after heating and liquefying the epoxy for 15 minutes so that any trapped gas bubbles were removed from the epoxy. All three components, the two pieces of Astrositall and the heated epoxy, were removed from the oven. Rapidly, the liquid epoxy was poured into a small pool on the clean Astrositall and then the aluminized silicone grating was placed squarely on top. The two pieces of Astrositall were returned to the oven and a small weight was placed on top so that the grating would be very thin. They were cured at 177º C for 10 hours.

8. The autoclave tool was then separated and prepared for use. The autoclave tool was separated from the silicone tool by use of the instrument seen in Figure 3-4. After separating, the autoclave tool was sent into the vacuum deposition chamber, where two layers of aluminum were cast onto the grating. Each layer of aluminum was separated by a thin layer of dilute Kodak Photo Flo solution that was applied between the first and second deposition of aluminum. The orientation of the grating lines on the tool was determined by the use of an alignment device similar to one described by Post et. Al [39]. A straight line was marked on the tool so that the fibers of the composite specimens were easily aligned with the direction of the grating.

9. A thin layer of 3501-6 was then cast onto the autoclave tool directly on top of the grating surface. A Teflon coated tool, seen in 3.5, was then used to apply the thin film of epoxy. As in a previous step some of the components, the autoclave tool

and Teflon coated device, were heated for one hour at 177º C. At several intervals during this hour the Teflon device was removed and the Teflon was tightened to ensure a uniform film of epoxy. After the initial hour, a small piece of 3501-6 was then placed into the metal tray where it was heated for 15 minutes and then vacuumed to remove air bubbles. The components were removed and a thin pool of epoxy was poured onto the grating surface. The Teflon device was lowered into the pool at an angle to push out any possible entrapped air bubbles. The epoxy was cured at 177º C for a period of 10 hours. After cure the autoclave tool was removed from the oven and the Teflon device was disassembled leaving only the sheet of Teflon on the tool. This sheet of Teflon was removed from the surface of the tool by pulling back at a sharp angle.

After completion of the diffraction grating preparation, the grating was transferred to the specimen by the following method.

3.5 Curing Procedure

As with most advanced composite materials, the laminates in this study were cured in an autoclave (Figure 3-6). The autoclave is a pressurized oven that has vacuum line connections inside the pressurized chamber. After selection of an appropriate laminate the following steps were implemented [18]. It should be noted that the following procedure was specific to the implementation of CRM. Other laminates were produced using the same basic procedure and cure cycle with the only difference being that they are cured without the addition of the ultra-low expansion Astrositall glass and grating application.

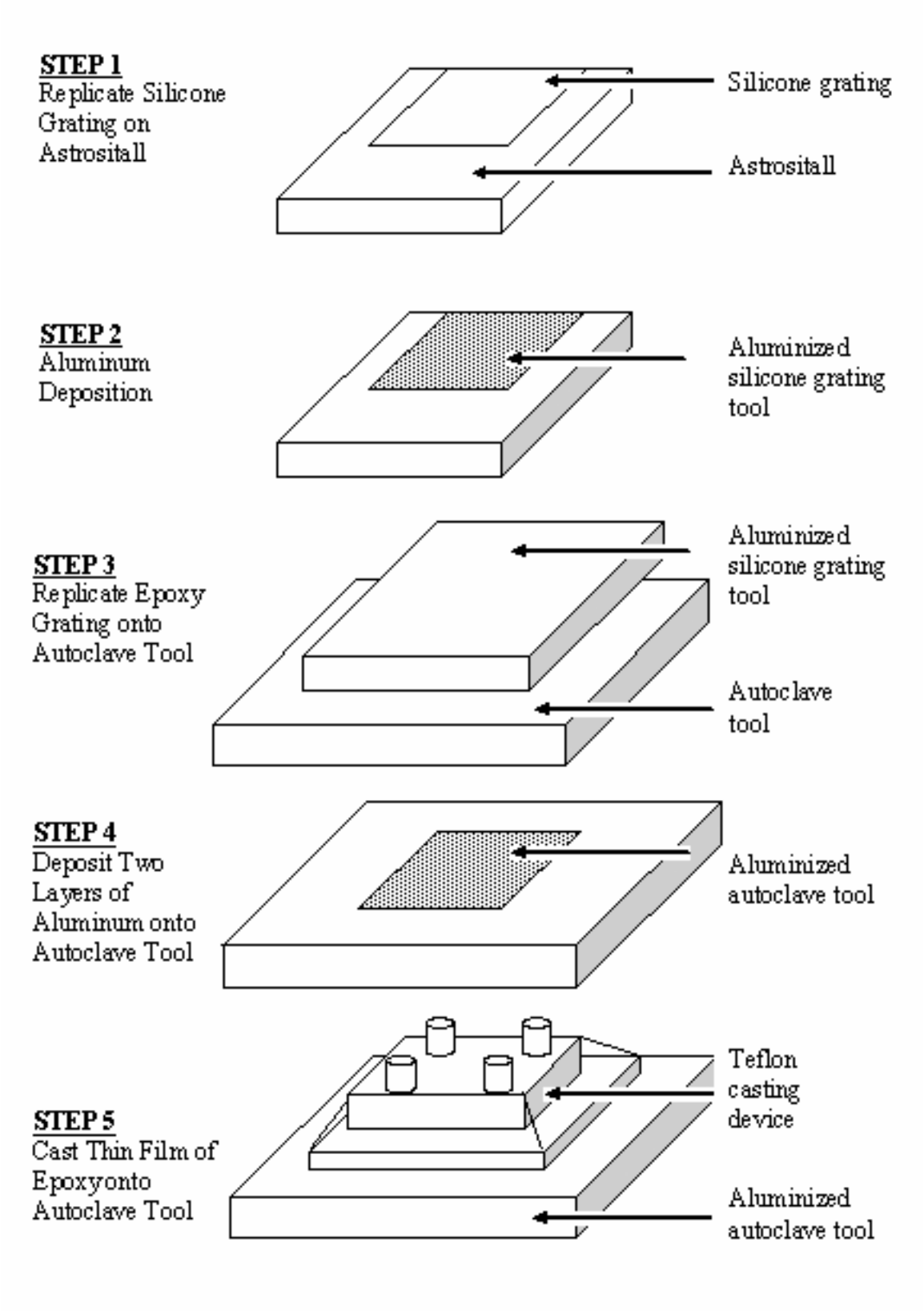

Figure 3-3: Replication schematic

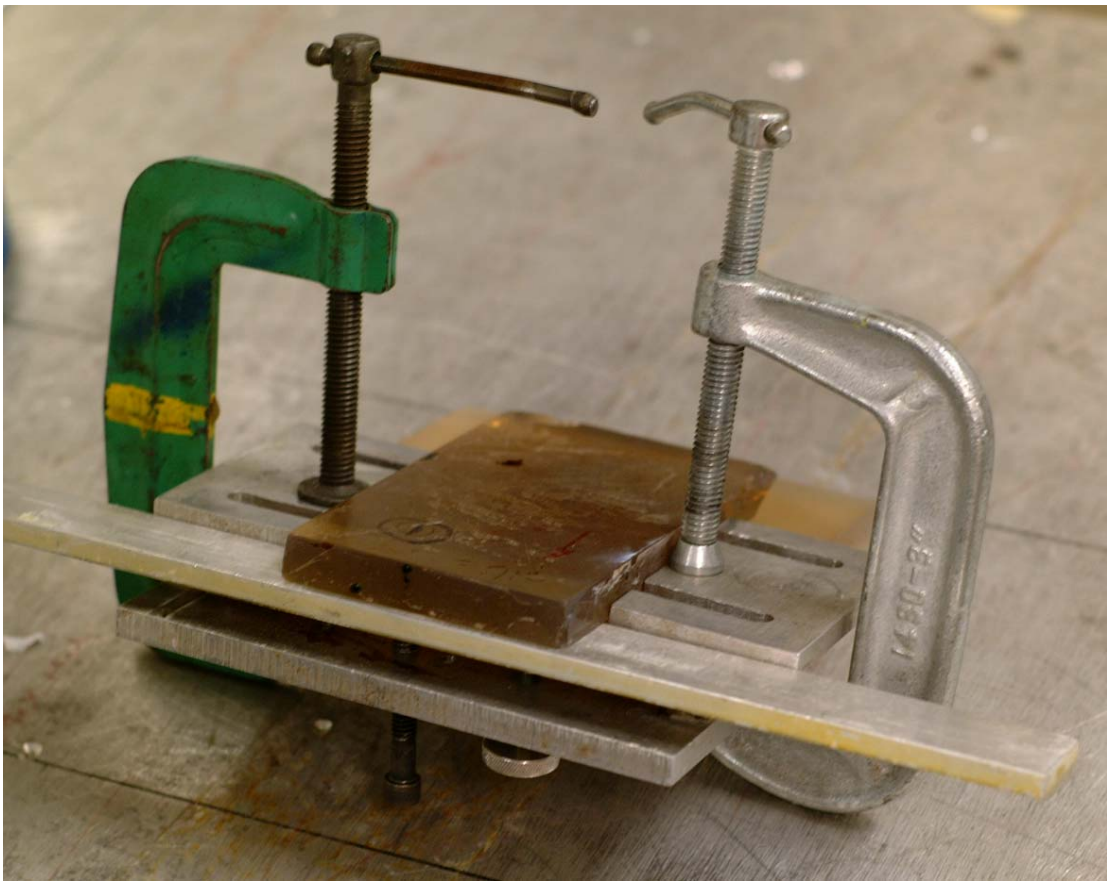

Figure 3-4: Tool separation device

Figure 3-5: Teflon coated epoxy film casting device

10. Lay-up: Individual sheets were cut to size from a roll of prepreg. Those sheets were then arranged and "stacked" in the proper sequence paying heavy attention to maintaining the correct angles.

11. Vacuum bagging: Figure 3-7 shows a schematic of the vacuum bag assembly. The ULE tool with the grating side up was placed at the base of the assembly. The surface was then covered with a non-porous release film. A hole of approximately 1.5" diameter was cut into the release film. The hole allows for the grating to be exposed to the composite surface during the cure cycle. The thickness of the film was important. It was critical that it was as minimal as possible so that it did not indent the surface of the composite during the cure process as the resin began to polymerize. The prepreg laminate was then placed on top of the release film, centered over the ULE tool. The non-porous release film placed between the tool and the laminate prevented the epoxy from curing to the tool. A layer of porous release film was placed on the upper surface of the laminate, which provided two functions. It allowed for excess resin to be drawn off the laminate and into the bleeder cloth, as well as facilitated the separation from the bleeder cloth. The bleeder cloth was a porous material that absorbs excess resin drawn out of the laminate via vacuum. Absorbing this excess resin allowed for an appropriate fiber volume fraction to be achieved. The breather cloth, which was the same material as the bleeder cloth, was used to distribute the vacuum throughout the entire bag. Another layer of non-porous release film was placed between the bleeder and the breather cloths so that excess resin was not transferred into the breather material. This could have resulted in resin being drawn into the vacuum line or clogging the breather cloth which then would have prevented an even vacuum distribution on the laminate during cure. Finally the ULE and laminate assembly were placed into a vacuum bag. The bag was sealed with a sealant tape and placed in the autoclave for curing.

12. Cure preparation: The vacuum bag was placed inside the oven and connected to the vacuum line. Vacuum was applied and a leak check was performed. It was imperative that the vacuum integrity was maintained throughout the necessary portions of the curing process.

13. Cure: Execute the cure cycle appropriate for the given material. The cure cycle for the IM7/977-2 can be seen in 3-8.

Figure 3-6: Autoclave oven

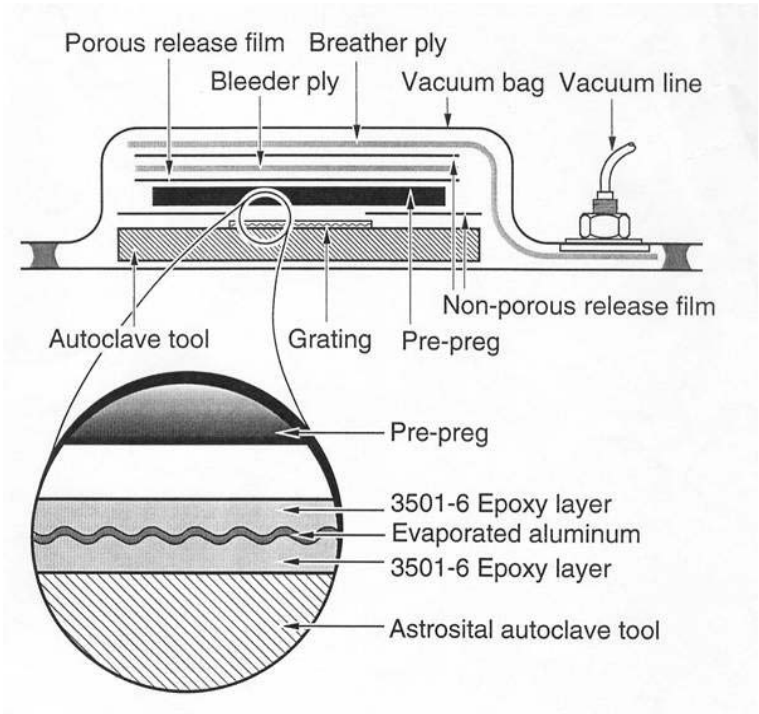

Figure 3-7: Vacuum bag assembly schematic

3.6 Moiré Measurement Technique

After the specimens have gone through the cure cycle the reflective grating was present on the surface (Figure 3-9). The specimens were then returned to the moiré interferometer where the deformation measurements were taken. There are many sources of potential error in this technique if the proper steps were not taken to insure accurate measurements.

The first step that must be taken was to properly tune the moiré interferometer. The virtual grating must be tuned accurately to 2400 lines/mm in both the horizontal and vertical field, U and V respectively. This was done by directing the second order diffraction of the reference grating back to the fiber optic tip for all adjustable mirrors. Then fine-tuning was done for each field by adjusting the U and V field mirrors until both displayed null fields. The exact position of the master grating was noted so that the specimen was also placed at the exact same position. Failing to do so would have introduced errors due to the imperfection in the collimated laser beam.

On each specimen a circle of know radius was scribed into the reflective grating. This established the gage length over which the fringe numbers would be counted. Each specimen was then placed into the tuned interferometer with a rotation at 90° from the reference grating. This rotation was needed because the grating surfaces of the specimens were the mirror image of the reference grating. The resulting fringes were photographed using Polaroid ISO 400/27° black and white instant sheet film. Images were taken and recorded from all of the different laminate specimens at room temperature.

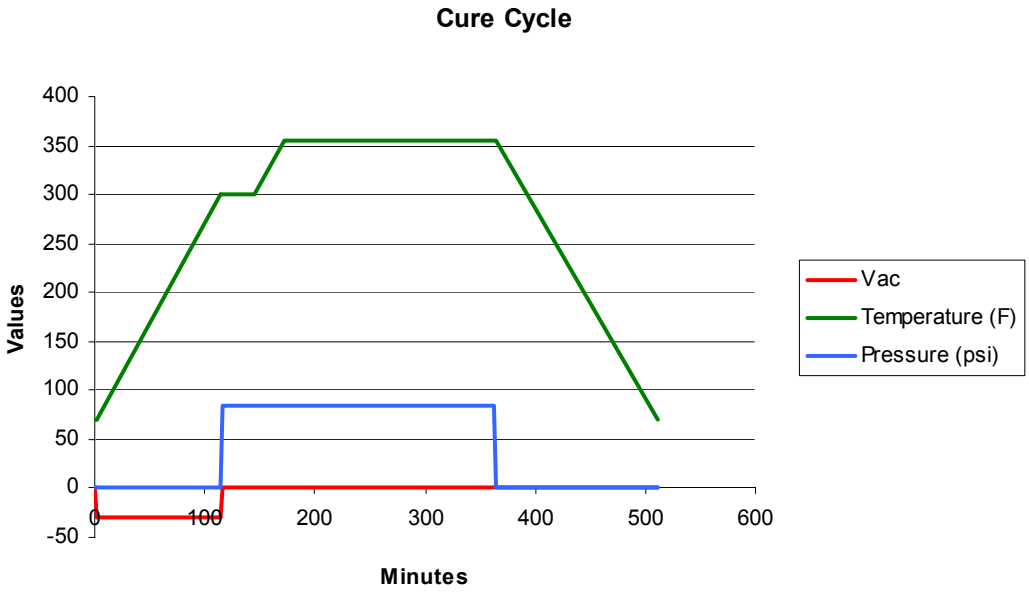

Figure 3-8: IM7/977-2 cure cycle

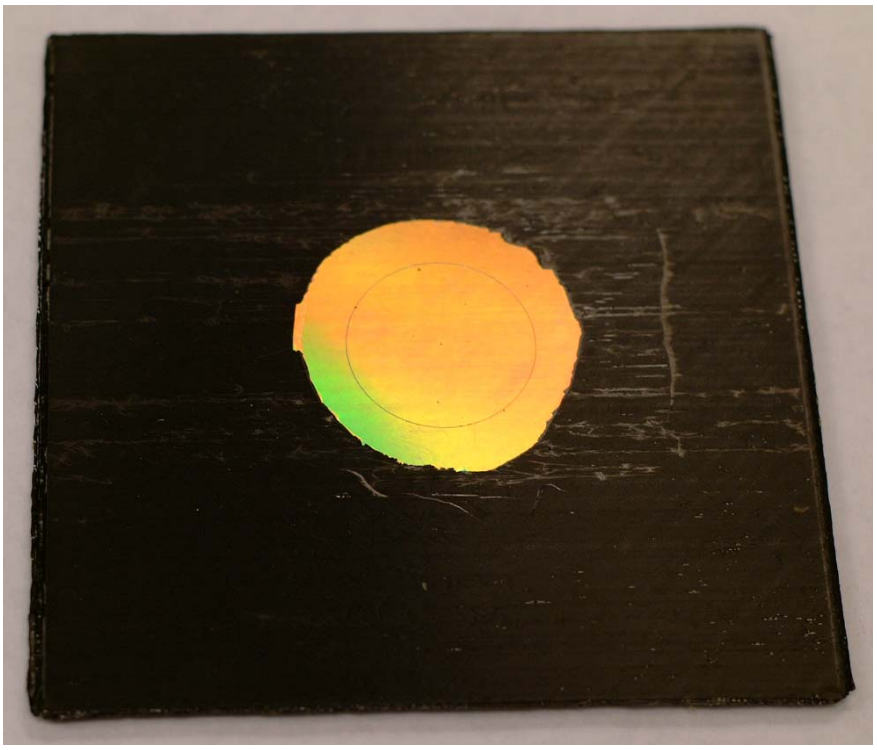

Figure 3-9: Moiré grating on specimen

3.7 Data Analysis

The experimental technique and methods described previously resulted in the acquisition of the very characteristic pattern of light and dark fringes of moiré interferometry. These fringe patterns were used to directly determine the in-plane displacements and strains. The relationship between fringe order N and displacement was as follows:

$$U = \frac{N_x}{f} \tag{3.1}$$

$$V = \frac{N_y}{f} \tag{3.2}$$

where f was the frequency of the virtual grating; f=2400 lines/mm.

The absolute surface strain was also determined from the fringe pattern analysis by the following relations:

$$\varepsilon_x = \frac{\partial U}{\partial x} = \frac{1}{f}\left[\frac{\partial N_x}{\partial x}\right] = \frac{1}{f}\left[\frac{\Delta N_x}{\Delta x}\right] \tag{3.3}$$

$$\varepsilon_y = \frac{\partial V}{\partial x} = \frac{1}{f}\left[\frac{\partial N_y}{\partial y}\right] = \frac{1}{f}\left[\frac{\Delta N_y}{\Delta y}\right]. \tag{3.4}$$

These equations were used to determine the strain on the surface of both the unidirectional and multidirectional laminates. These strains were a result of the thermal contraction, which was a function of the temperature difference between the cure temperature and operating temperature; chemical shrinkage of the matrix, which was not temperature dependent, occurring only during cure; and the thermal expansion of the autoclave tool, which was neglected in the analysis [19].

The resulting characteristic images of each laminate stacking sequence are displayed in Appendix A and the corresponding values of the surface strain given by

CRM can be seen in Tables 3-1 through 3-3. The values seen in the table represent the values of surface strain that were present at room temperature. These measurements were extended throughout the range from cure to LN_2 temperatures by a method to be discussed next.

3.8 Error Sources

Several sources of error were potentially present during the implementation of CRM. These sources included the improper implementation of moiré interferometry, manufacturing defects in the laminate specimens, and misalignment of CRM grating surface. Without taking precautions to avoid possible error sources, the indicated strains of the CRM method could be significantly misleading.

Table 3-1: Total surface strain on unidirectional laminates at 24°C

Specimen	x-direction	y-direction
UNI-13-06-04	0	-6890
UNI-13-02-03	0	-6500
UNI-13-03-02	0	-7220
UNI-13-B2-02	0	-6955
UNI-13-02-05	0	-6824
Average	0	-6877.8
COV	----	3.77%

Table 3-2: Total surface strain on optimized angle ply at 24°C

Specimen	x-direction	y-direction
OAP-12-B3-01	787	-4920
OAP-12-03-02	820	-5250
OAP-16-04-01	919	-4950
OAP-16-02-02	1030	-5510
OAP-20-07-05	1033	-5250
Average	917.8	-5176
COV	12.5%	4.72%

Table 3-3: Total surface strain on RLV laminate at 24°C

Specimen	x-direction	y-direction
RLV-A1-01	-610	-190
RLV-02-02	-525	-197
RLV-03-03	-525	-220
RLV-05-04	-590	-230
Average	-562.5	-209.25
COV	6.78%	7.80%

The implementation of moiré interferometry has many possible sources of error itself. Improper tuning of the interferometer, misalignment of specimens, improper specimen orientation and placement, and vibration can all lead to potential problems. Fortunately, these issues are somewhat easily accounted for and all the proper steps were taken to avoid improper strain reading as a result of these problems.

Other sources of errors were not as easy to account for. Manufacturing defects are a common event in laminate production. Inclusions of foreign matter can often lead to incorrect results. The existence of these inclusions on a large scale is easy to detect while testing due to the large deviations they can cause from expected or previous results. Manufacturing the laminates in a clean working area and examining each layer prior to joining eliminated this problem. One source of error that was not ruled out was misalignment of the layers themselves during manufacturing. All laminates were cut and aligned as carefully as possible by hand but the element of human error still existed. It was possible that misalignments of $\pm 2.5°$ through the thickness developed. This misalignment can result in a change in the characteristics of the laminate.

Similar to the alignment of the fibers during manufacturing, the autoclave tool and the grating on its surface was aligned by hand onto the specimen. The greatest care was taken to apply the grating as accurately as possible, but a possible slight offset from the desired axis of measurement may have resulted. This offset would have lead to the

measurement of strain in a direction different than what was desired. For example, if the strain in the fiber direction after cure is desired and the grating was not aligned perfectly in the x, or fiber direction, as in the case of the unidirectional laminate, the measured displacement would be higher than the true displacement.

A very important aspect of accuracy was the ability to read the fringe order information. From equations (3.3) and (3.4) it is seen that any inaccuracy in the reading of the correct fringe order would have lead directly to measurement errors. Different fringe pattern densities often required adjustments on gage factor as the images must be magnified to see the fringes. Different magnifications assured that all patterns could be read to less than one fringe order. In the case where the gage length was 0.5", a misread of one fringe would have resulted in an error of approximately 33 με. In the case of a 0.25" gage length a misread of one fringe would have led to double the previous, up to 66 με.

3.9 Conclusions

The Cure Referencing Method has been applied to find the total surface displacement on various laminate stacking sequences. The calculated surface strains represent the sum of the contraction from thermal effects as well as chemical shrinkage that resulted from polymerization. The strains have been averaged and the coefficient of variation has been calculated for each stacking sequences. Any COV measurements will be provided to the optimization group for future reliability analysis.

The experimental results were relatively repeatable. All of the COVs were quite low with the exception of the x-direction OAP values. This indicated quite consistent and reliable results.

The unidirectional laminates showed the highest value of surface strain, followed by the OAP, and finally the RLV laminates. The high strain level indicated that the unidirectional and OAP laminates were relatively free to contract. Conversely, the RLV laminate showed a very low strain value which indicated a high level of constraint. The data from these tests are revisited in the combination of CRM and strain gage results in Chapter 4.

CHAPTER 4
STRAIN GAGE METHODS

The second technique of experimentation that was used in this study was that of basic thermal expansion testing methods conducted with modern strain gage technology. This method was used to gather real time surface strain data as the temperature was varied over the test range. Later it will be shown how information gathered with this testing procedure was used in conjunction with CRM and material property testing to develop residual strains, stresses, and CTE as a function of temperature.

4.1 Acquisition Theory

When strain gages are used to acquire strain as a result of temperature change the output cannot be treated as the true strain on the surface. The output of the gage is actually termed the thermal output. It is caused by two factors, the change in the resistivity of the grid alloy with change in temperature and the difference in thermal expansion coefficients between the gage and the test material [34]. The resulting resistance change is the sum of resistivity and differential expansion effects are

$$\frac{\Delta R}{R} = \left[\beta_G + (\alpha_S - \alpha_G)F_G\right]\Delta T \tag{4.1}$$

where $\Delta R/R$ is unit resistance change, β_G is the thermal coefficient of resistance of the grid material, $\alpha_S - \alpha_G$ is the difference in specimen and grid thermal expansions, F_G is the gage factor of the strain gage, and ΔT is an arbitrary temperature change from a reference temperature. The strain that is indicated from the change in gage resistance was then

$$\varepsilon_i = \frac{\Delta R / R}{F_I} \tag{4.2}$$

where F_I is the gage factor setting of the instrument. The gage factor of the instrument was set to that of the gage so that the resulting thermal output, or strain, output by a gage on a specimen was

$$\varepsilon_{T(G/S)} = \frac{\beta_G}{F_G}\Delta T + \left(\varepsilon_S - \varepsilon_G\right) \tag{4.3}$$

From this output it was necessary to remove the gage contribution so that only the surface expansion of the specimen was recorded. This was accomplished by placing the same gage type from the same lot number onto a reference material of a known expansion coefficient and expansion curve as a function of temperature. When the reference material was exposed to identical conditions as the specimen the reference material gives a thermal output of

$$\varepsilon_{T(G/R)} = \frac{\beta_G}{F_G}\Delta T + \left(\varepsilon_R - \varepsilon_G\right) \tag{4.4}$$

The gage output was measured on the reference material then the theoretical strain at a given temperature was removed from the total output yielding the gage contribution to the thermal output [18]. This output was then subtracted from the thermal output of the specimen and gage reading, yielding only the thermal induced strain on the surface as

$$\varepsilon_S = \varepsilon_{T(G/S)} - \varepsilon_{T(G/R)} \tag{4.5}$$

The acquired strain readings were later combined with CRM data.

4.2 Specimen Preparation

To ensure the continuity of the measurements, the same specimens used for the CRM procedure were used for the strain gage experiments. The CRM specimens were

sectioned so that the gratings were not damaged, yet a large enough area for strain gage application was obtained. This yielded specimens of approximately 1" x 4".

The specimens were conditioned and sanded as recommended by Vishay Measurements Group for strain gage application. The test covered a wide range of temperatures that demanded special attention to gage and application techniques. For this reason M-Bond 610 was selected as the adhesive system and two WK-13-250BG-350 gages were applied to each side, one directed in the x-direction and the other in the y-direction. These gages were selected for their performance characteristics over the proposed test temperature range. Each gage was aligned in the proper orientation by use of mylar tape across the terminals. The gage backing and specimen surface were coated with M-Bond 610 and were exposed to the air for approximately 15 minutes. After drying, the gages were pressed down onto the specimen and covered with a thin Teflon film. Pressure pads were placed over the gages and then they were clamped at 40 psi with 2" spring clamps. The assembly was then placed in a cool oven and the temperature was increased to 121º C at a rate of 5º C/min. and then was allowed to cure for 3 ½ hours. The tape was peeled off of the specimens and they were returned to the oven to be post cured for two hours at 135º C. A schematic and example of the resulting specimens are seen in Figures 4-1 and 4-2.

Decoupling the strain gage expansion effects accurately was crucial to maintain the validity of testing results. The reference materials were prepared following the exact same procedures, making use of the same gages and bonding techniques, as those used for the preparation of the composite specimens (Figure 4-3).

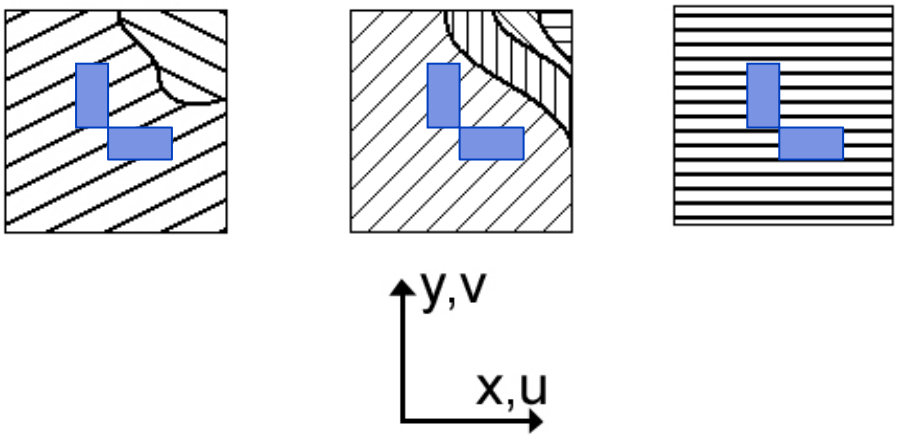

Figure 4-1: Schematic of strain gage alignment

Figure 4-2: Gauging of sectioned specimen

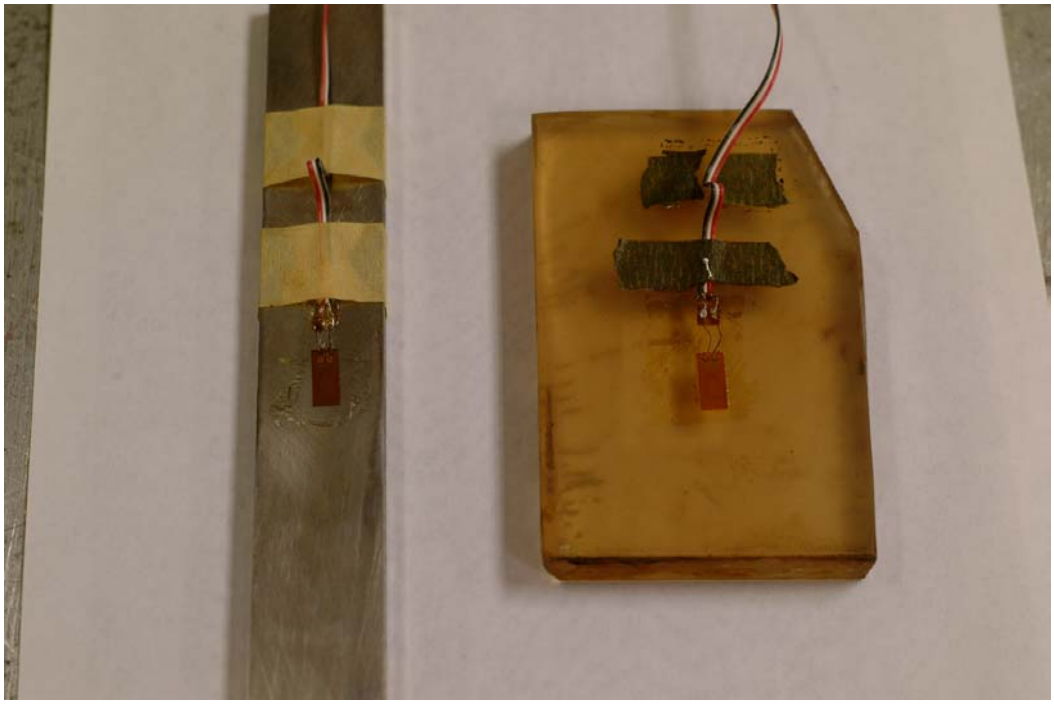

Figure 4-3: Gauging of reference materials

4.3 Testing Procedure

The failure of the X-33 provided motivation for this work as well as the environmental conditions under which the residual strains, stresses, and CTE were studied. The composite specimens were observed and investigated over a wide range of temperatures, from the harsh conditions of the cryogenic realm up to the temperatures at which they were cured. The following section describes the methods that were used to test and acquire data in these conditions.

After all preparations were made to the specimens and reference material they were placed in a Sun Systems Model EC1x environmental chamber. Each test consisted of three specimens and the reference material being exposed to the desired conditions as controlled by the environmental chamber. Due to the extensive amount of time that was necessary to run and collect data, each test was divided into separate cryogenic and elevated temperature runs.

4.3.1 Cryogenic Tests

A LN_2 tank was attached to the environmental chamber as seen in Figure 4-4. The chamber was then able to regulate the temperature by controlling the release of LN_2. The specimens and reference material were then supported on a rack covered with Teflon (Figure 4-5). The Teflon ensured that the specimens were free to expand and contract without being exposed to friction that might inhibit this deformation. Lead wires were passed through a port in the chamber to the data acquisition set up. The chamber door was returned and sealed while the proper connections were made to the acquisition hardware.

Each gage was read in a quarter-bridge configuration (Figure 4-6). The lead wires were passed directly to a STB AD808FB Optim Electronics quarter-bridge completion module. The completed bridges were directed into a National Instruments SCXI-1322 breakout board attached to a NI SCXI-1122 sixteen-channel Isolated Transducer Multiplexer Module for Signal Conditioning. The signal conditioning board was part of a SCXI-1000 four slot chassis that directed the data into a Dell Dimension 8100 through a NI PCI 6035E data acquisition card. The data and hardware was manipulated by a NI LabVIEW program.

The chamber temperature was set for 20º C and the specimens were allowed to soak there for 15 minutes. This temperature was selected as the starting point due to the material property values of the reference material. The National Institute for Standards

Figure 4-4: Environmental chamber and LN_2

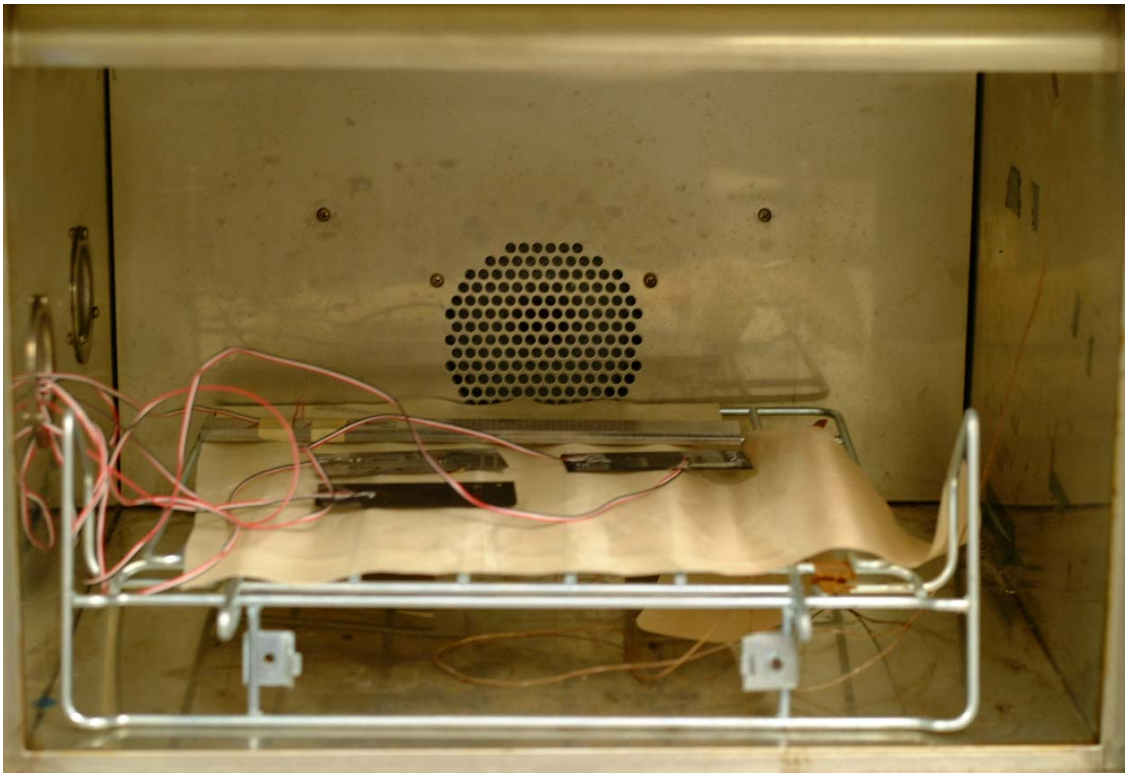

Figure 4-5: Laminate coupons wired and placed inside environmental chamber

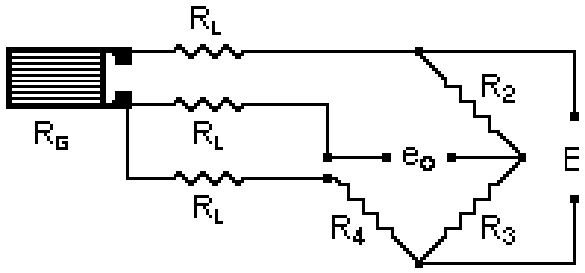

Figure 4-6: Quarter-bridge schematic

and Testing has established the thermal expansion data for the reference material, Ti6-4Al-4V, as a deviation from this temperature. The titanium reference expands as:

$$\left(-1.711E^{2}+-2.140E^{-1}\times T_{k}+4.807E^{-3}\times T_{k}^{2}+-7.111E^{-6}\times T_{k}^{3}\right)\times 10 \qquad (4.6)$$

This equation is accurate to within 1.5% from temperatures of 24°K to 300°K. A reading was taken at this point and the corresponding voltages were stored and used as tare voltages that were removed from all subsequent measurements.

After acquiring the tare voltages at 20º C the temperature in the environmental chamber was reduced to 5º C. The specimens were again allowed to remain at that temperature for 15 minutes so that temperature was constant through the thickness. Another set of readings was taken at this temperature. The LabVIEW program that was written to manipulate the incoming data took the raw voltages and proceeded to compensate for several factors. The initial voltages read in the tare measurement were removed from the new voltage readings. The new gage factor for the corresponding temperature was calculated and then the raw voltage was converted into strain and adjusted for transverse sensitivity errors. This was done for all gages inside the chamber. The converted strain readings represented the total thermal output of the gages and the gage contribution was decoupled as follows. LabVIEW calculated the actual strain experienced by the reference material according to equation 4.6 and compared it to what

was read. The difference in the readings corresponded to the gage contribution to the thermal output. This difference was calculated then subtracted from all other strain readings resulting in the true surface strain on the specimens. This was recorded and saved versus the temperature.

The same procedure was followed throughout the experiment. Dwell times were increased as the temperature was lowered since it took more time for the specimens and reference material to reach thermal equilibrium. Thermal equilibrium was verified by taking several strain readings within a few minutes of each other. If the drift in the calculated strain was observed to be very small, on the order of 2 to 5 microstrain per 3 minutes then the final reading was recorded and the experiment proceeded to the next temperature.

The experiment terminated with the final reading at -190º C. This was the lowest temperature that was obtainable using this environmental chamber and LN_2. The chamber temperature was returned to room temperature in several steps so as not to thermally shock the specimens. The specimens and reference material were removed from the chamber and it was heated to remove all moisture. This procedure was followed for all specimens.

4.3.2 Elevated Temperature

Following the cryogenic testing the specimens were exposed to elevated temperatures from room temperature to the upper limit of the composite cure temperature. The same specimens were used for the elevated temperature tests so that a curve across the entire test range could be created for each individual specimen. The only difference was in the solder that was used to connect the lead wires, as the solder appropriate for exposure to cryogenic temperature is not applicable at elevated

temperatures. The conductivity of both solders was very similar, thus the effect of this change was negligible. The same hardware and software programs were used to collect the data from elevated testing.

The chamber with specimens and reference material inside was again set at 20º C where after a dwell time tare readings were taken. This initial point was selected in order to obtain a continuous graph of the surface strains. It was not set at 20º C to account for the reference material, as a small piece of Astrositall was gauged and used as a reference instead of the titanium. The data available for the titanium reference was not valid into the upper limits of the high temperature test. The Astrositall has an extremely low expansion coefficient so that in the test range its actual surface strain was treated as zero.

The chamber was heated to 24º C and allowed to dwell there. This temperature location was necessary since it corresponds to the room temperature at which the CRM measurements were made. The need for the correspondence in temperature locations will be discussed later. The dwell time needed for the elevated temperature test was much longer than that of the cryogenic test due to the slower heat absorption of the Astrositall reference material.

The LabVIEW program followed the same methodology for the calculation of the true surface stain. The only difference being that the reference material was different and had a different expansion curve. The Astrositall was treated as non-expanding throughout the entire test. Therefore, any indicated strain on the reference material was immediately subtracted from the specimen readings as the gage thermal contribution.

The temperature intervals began as 15º C increments. After the temperature reached 90º C the increments were increased to 20º C. The test concluded when the

chamber was raised to 182º C, which corresponds to the composite cure temperature. As before, when conditions began to deviate much from room temperature the dwell times were increased. Thermal equilibrium was verified with the same technique as previously discussed.

4.4 Data Analysis and Results

The data obtained directly from the above methods did not directly provide the total surface strain present the laminate as a function of temperature. What was observed through the strain gage testing was the relative change in surface strain as the temperature was varied from 20º C. The strain data has to be coupled with the CRM data in order to encompass all surface strains.

CRM was able to capture the entire strain induced on the surface of the laminate as it went through cure and was brought down to room temperature, which was 24º C. These strain values for the various laminates were highlighted previously (Tables 3-1 through 3-3). The data acquired through the use of strain gages must be referenced to those values. This was the reason for the strain measurement taken at 24º C by the strain gages.

The total surface strain as a function of temperature was calculated and plotted in Microsoft Excel. The total surface strain present at any given temperature was:

$$\varepsilon_{lam} = \varepsilon_T + \varepsilon_{CRM} - \varepsilon_{24} \tag{4.7}$$

where ϵ_T is the strain calculated by the strain gages at any temperature, ϵ_{CRM} is the strain recorded by CRM at 24º C for a particular specimen, and ϵ_{24} is the strain recorded by the strain gages at 24º C. Figures 4-4 through 4-6 show the resulting total surface strains as a function of temperature on the various specimens of each laminate sequence.

All of the curves demonstrate fairly smooth behavior. The total surface strain results for different specimens of each stacking sequence are in good agreement with each other and no large deviations are observed among different specimens of the same laminate and the average COV across the entire temperature range is acceptable for each (Table 4-1). The surface strains have been averaged for each laminate (Figure 4-7).

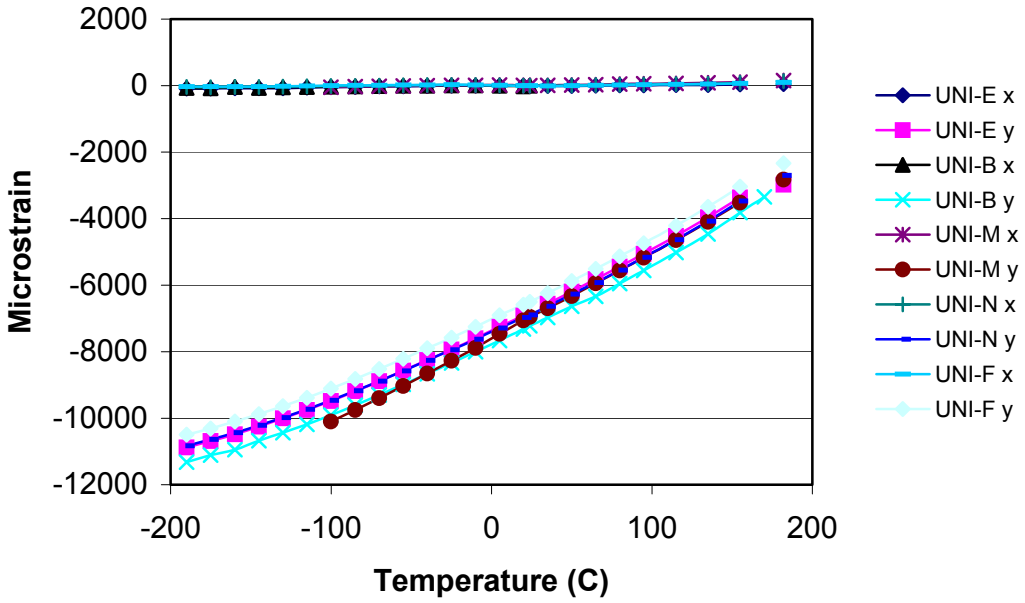

Figure 4-7: Unidirectional laminate surface strain

A crucial observation to be made is that the strains do not return to zero as the temperature is returned to cure. The cure temperature is often referred to as a stress free state, hence strain is also expected to be zero at this point. This is only true during the curing of the laminate because during cure the epoxy undergoes polymerization, which is a one-time event. The resulting strain from this event, referred to as chemical shrinkage is always present, is often overlooked, and can contribute a large amount of strain to a given laminate (Tables 4-2 through 4-4). The stress measurement techniques described previously, and an analytical prediction tool discussed later, known as Classical

Lamination Theory (CLT), do not have the ability to account for this phenomenon. CRM provides a tool that can accurately predict and calculate this effect.

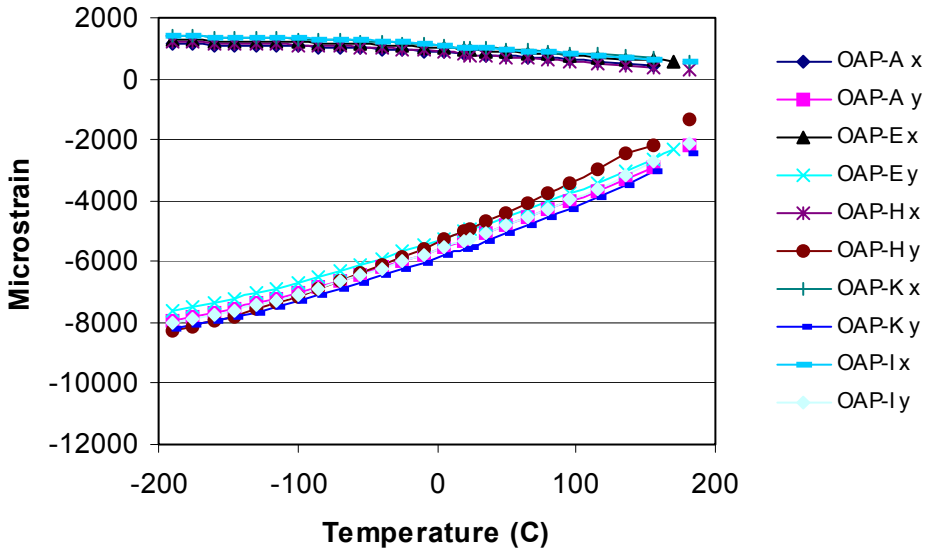

Figure 4-8: OAP laminate surface strain

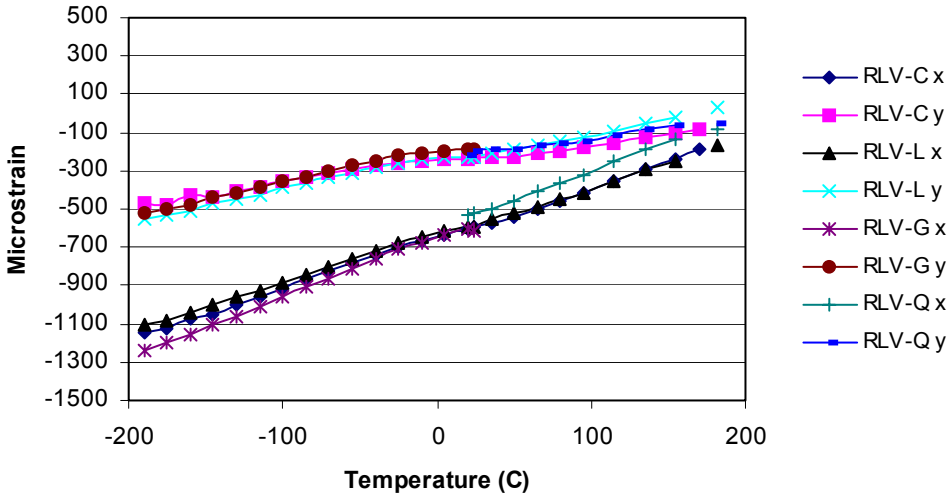

Figure 4-9: RLV laminate surface strain

The strain data was also transformed into a linear coefficient of thermal expansion from cure to the testing temperature. The data was taken in 15°C and 20°C intervals allowing the CTE of the laminates to be calculated as a function of temperature. The

change in strain over the temperature interval was divided by that interval from cure to cryogenic. CTE was calculated for each direction in the various specimens as:

$$CTE_x = \frac{\left(\varepsilon_{T2x} - \varepsilon_{T1x}\right)}{(T_2 - T_1)} \tag{4.8}$$

$$CTE_y = \frac{\left(\varepsilon_{T2y} - \varepsilon_{T1y}\right)}{(T_2 - T_1)} \tag{4.9}$$

The CTE values as a function of temperature are displayed in Figure 4.11. Over the test range the change in CTE appears to be quite linear and trend lines were created as such. The linear fit of the CTE of the unidirectional laminate will later be used to refine Classical Lamination Theory predictions.

4.5 Error Sources

Just as in the case of CRM any misalignment in the orientations during manufacturing would have led to incorrect measured values. Also, since the strain gage readings were combined with those of CRM, any problems that may have been encountered during the alignment of the displacement gratings would have propagated into the combined measurements. The most likely source for a large error would have resulted from the misalignment of a strain gage on the specimen.

Strain gages are extremely sensitive to misalignment when placed on composite specimens. In some cases a $\pm 4°$ misalignment of a strain gage would have led to errors as large as $\pm 17\%$ in an axial gage measurement, while a $\pm 65\%$ error could exist in a similar transverse measurement. However, in this case the sensitivity to misalignment was not as dramatic. On the unidirectional laminates the gages were aligned along the 0º and 90º directions. It was assumed that enough effort was centered on strain gage alignment that less than $\pm 2°$ offset was induced. This desired alignment dropped

possible misalignment errors approximately to less than 5% in the case of gages off axis by $\pm 2°$. In the case of the OAP laminate a $\pm 2°$ offset leads to an error of about 3%. The somewhat quasi-isotropic nature of the RLV laminate again helped to minimize the effects of gage misalignment keeping errors on the order of 5%.

4.6 Conclusions

A method of measuring relative surface strains as they develop as a function of temperature has been outlined. Proper compensation methods to account for temperature effects on measurement techniques have been discussed and automated in a LabVIEW data acquisition program. Measurements of surface strain have been made across a large temperature range and the CRM and gage values have been combined in a manner to account for the total surface strain at any given temperature. The surface strains for all specimens have been plotted as a function of temperature and the averages of the different laminates have been compared to each other. The chemical shrinkage component of the total surface strain has been decoupled. Finally, the average CTE of the different laminates has been computed as a function of temperature.

The different runs of the various specimens were quite consistent. The surface strain values were reproducible as a function of temperature from run to run. As in the results from CRM in chapter 3, the unidirectional and OAP laminates continued to display a higher strain level than the RLV laminate. The same conclusion is reached, that the increasing offset of ply angles has lead to a lower strain which resulted from high constraint imposed in the RLV laminate.

The decoupled chemical shrinkage terms were quite large for the transverse direction of the unidirectional and OAP laminates. These large values indicate that any

work that neglects the chemical shrinkage components will neglect a significant strain event. These values were not seen in the RLV due to the usual constraint mechanisms.

The CTE was seen to tend toward zero as the temperature was decreased. This event was observed less in the RLV laminate since the CTE was already quite low, again due to high constraint. The trend toward zero was expected as molecules will tend to slow in all motion as the temperature is reduced. The CTE observed in the unidirectional laminates was taken to be the CTE of the material system and is used in CLT calculations in Chapter 7 as α_1 and α_2.

Table 4-1: Average COV of surface strains across temperature range

Laminate	COV x-direction	COV y-direction
UNI	-----	4.26%
OAP	13.55%	6.10%
RLV	9.59%	10.10%

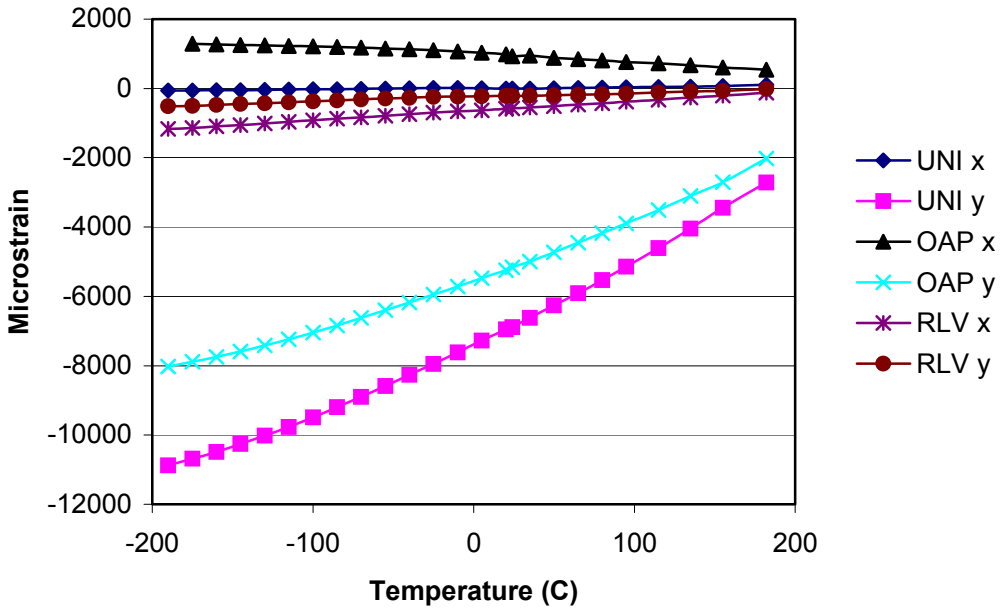

Figure 4-10: Average of laminate surface strains

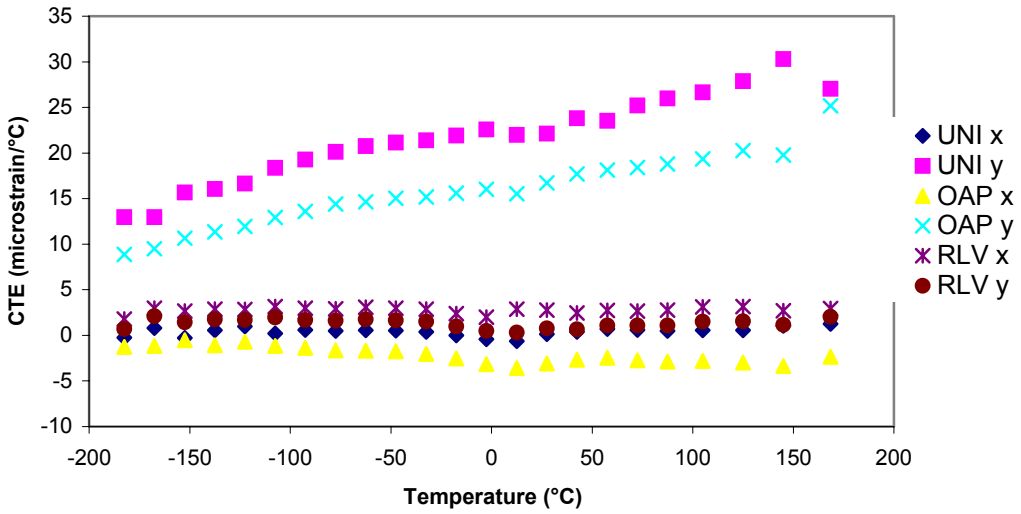

Figure 4-11: Coefficient of thermal expansion

Table 4-2: Unidirectional chemical shrinkage induced strain

Laminate	x-direction	y-direction
UNI B	-----	-----
UNI E	48.5	-2978.5
UNI F	99.3	-2338.5
UNI M	155.9	-2831.1
UNI N	131.1	-2702.0
Average	108.6	-2712.5

Table 4-3: OAP chemical shrinkage induced strain

Laminate	x-direction	y-direction
OAP A	-----	-2164.4
OAP E	-----	-----
OAP H	298.5	-1359.5
OAP I	550.2	-2153.1
OAP K	582.1	-2430.7
Average	476.9	2026.9

Table 4-4: RLV chemical shrinkage induced strain

Laminate	x-direction	y-direction
RLV C	-----	-----
RLV G	-----	-----
RLV L	-169.3	29.3
RLV Q	-83.8	-47.8
Average	-126.55	-9.25

CHAPTER 5
MATERIAL PROPERTY TESTING

Basic material tests include those that provide some of the most elementary yet critical values that can be assigned to a material. The following experiments were performed to obtain the Young's Moduli, E_1 and E_2, Poisson's ratio, ν_{12}, and the shear modulus, G_{12}. These properties are necessary for the prediction of the strains and stresses provided by Classical Lamination Theory (CLT). They must also be used to transform the experimentally measured strains into stresses.

The American Society for Testing and Materials (ASTM) book of standards was used as a guideline for the testing procedures implemented. Standard D 3039 was used as the model for the E_1 and E_2 tests, while standard D 5379 was used to determine the shear modulus.

5.1 E_1 Testing

ASTM standard D3039 is a test method designed to determine the in-plane tensile properties of a polymer matrix composite with high modulus fiber reinforcement [44]. A panel of unidirectional IM7/977-2 was manufactured as discussed in previous sections without the previsions made for the implementation of CRM. The panel had dimensions of 10" in the fiber direction by 6" transversely. The panel was seven layers thick to approach the ASTM recommended thickness of 0.040".

After the panel was cured, test coupons were cut from it having nominal dimensions of 10" x 1". Each coupon was then sanded and conditioned at its midpoint in accordance with Vishay Measurements Group techniques for strain gage application.

One CEA-13-125UT-350 tee gage from Vishay was placed on each side of the coupon with the standard M-bond 200 cyanoacrylate glue. One gage located on each side allows for cancellation of bending effects. The branches of the tee were placed precisely in the fiber and transverse directions allowing for the acquisition of information needed to calculate both the E_1 and ν_{12} properties.

After the coupons were gauged they were then placed in a MTI Phoenix machine where they could be loaded (Figure 5-1). Each specimen was loaded axially in the fiber direction with a crosshead displacement rate of 0.01" per minute. Load versus strain data was acquired nominally at 200-pound intervals with National Instruments data acquisition hardware. The hardware consisted of an SCXI-1000 four slot chassis, SCXI-1322 breakout board, and a SCXI-1122 sixteen-channel Isolated Transducer Multiplexer Module for Signal Conditioning all read into a Dell Dimension 8100 through a NI PCI 6035E data acquisition card. NI LabVIEW software was used to operate and read the acquisition hardware.

5.2 E_2 Testing

ASTM standard 3039 was also used to establish the E_2 testing procedures [44]. In this case a panel of IM7/977-2 was manufactured with dimensions of 6" in the fiber direction by 7" in the transverse direction. The panel was 14 layers thick to bring the thickness nominally to 0.080".

Again the panel was cut into test coupons after the curing process with the test coupons nominally of dimensions 7" x 1". Each specimen was sanded and conditioned as before at its midpoint. One CEA-06-250UN-350 unidirectional gage was applied to

each side of the specimen. The gage was placed on the coupon precisely in the matrix direction, transverse to the fibers.

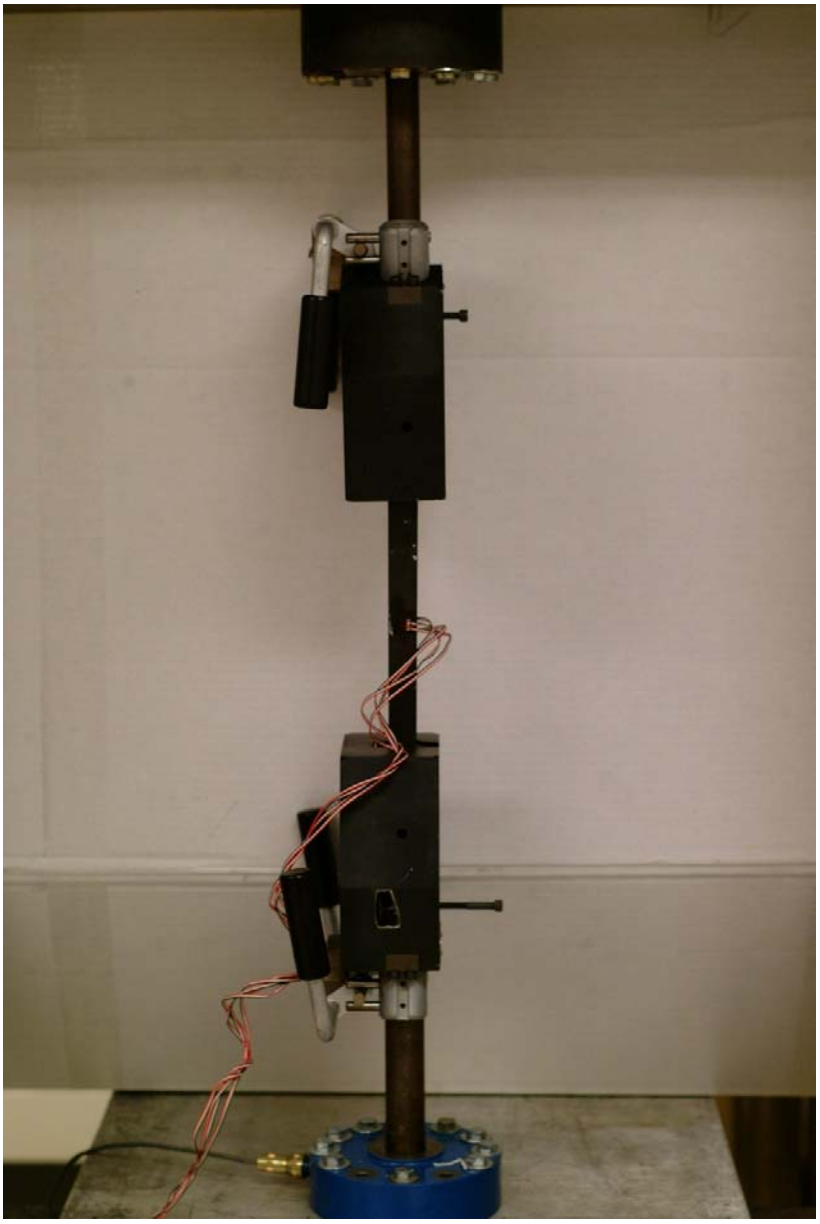

Figure 5-1: E_1 and E_2 testing fixture

As before, after the specimens were prepared they were subjected to load in the MTI Phoenix displacement controlled testing machine. The displacement rate was again 0.01" per minute with load versus strain data acquired at approximately 200-pound intervals. The same NI data acquisition hardware was used for this procedure as in the E_1 testing.

5.3 G_{12} Testing

As with the previous material property tests, the ASTM book of standards was used as the guideline for establishing test setup and procedures. ASTM D 5379 is designed to determine the shear properties of high-modulus fiber reinforced composite materials [45]. A 6" x 6" 13 layer panel of unidirectional IM7/977-2 was manufactured and then cured in the autoclave with the appropriate cure cycle.

After the panel is cured it was sectioned and machined into the proper shape. The testing coupons were machined into the form of a rectangular flat strips with two v-shaped notches centered along the length. A diagram of the appropriate geometry is seen in Figure 5-2. The panel was sent to TMR Engineering for machining of the correct geometry.

The v-notched specimens were then prepared for testing through the application of Vishay micro-measurements N2A-06-C032A-500 shear gages. The specimens were conditioned appropriately and then one gage was applied to each side precisely in the area spanning the concentric notches.

The gauged coupons were then placed in the MTI machine with a special testing fixture seen in Figure 5-3. The specimens were inserted in the fixture and then placed onto the machine in a manner where the notches were along the line-of-action of the

testing machine. The two halves were then tensioned at a rate of 0.01" per minute while the load-shear strain data was collected using the NI hardware.

5.4 Data Analysis and Results

Before each E_1, E_2, and G_{12} test was run the dimensions of the all test coupons were measured. The stress, σ, in each coupon was calculated as a function of cross sectional area, A, and the load applied by the MTI machine, P:

$$\sigma = \frac{P}{A}. \tag{5.1}$$

The stress was then plotted versus the strain in each coupon. The slopes of the resulting graphs (Figures 5-4 and 5-5) were the Young's moduli of each coupon. The various moduli were very similar in value and were averaged. The results of each test are seen in Table 5.1. The E_1 testing yielded an average value of 150.2 GPa for the modulus of elasticity in the fiber direction, while the E_2 testing yielded an average of 8.04 GPa for the transverse or matrix modulus.

The shear specimen results are plotted in Figure 5.6. The shear modulus was calculated in accordance with ASTM Standard D 5379 where a "shear chord" between the values of 1000 and 3000 με was calculated as

$$G^{chord} = \frac{\Delta\tau}{\Delta\gamma} \tag{5.2}$$

The resulting average value for the shear modulus was 4.77 GPa.

The Poisson's ratio was also calculated from the E_1 test by use of the strain readings from the transverse gages. The strains displayed by the longitudinal and transverse gages were compared and Poisson's ratio was calculated as

$$\nu_{12} = \frac{\varepsilon_2}{\varepsilon_1}. \tag{5.3}$$

All calculated Poisson's ratios were very similar and average to 0.342.

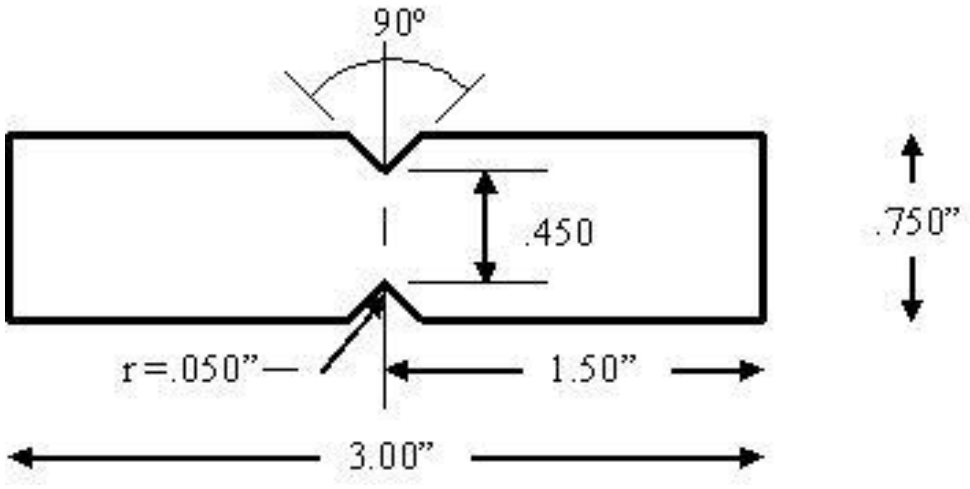

Figure 5-2: Shear test specimen schematic

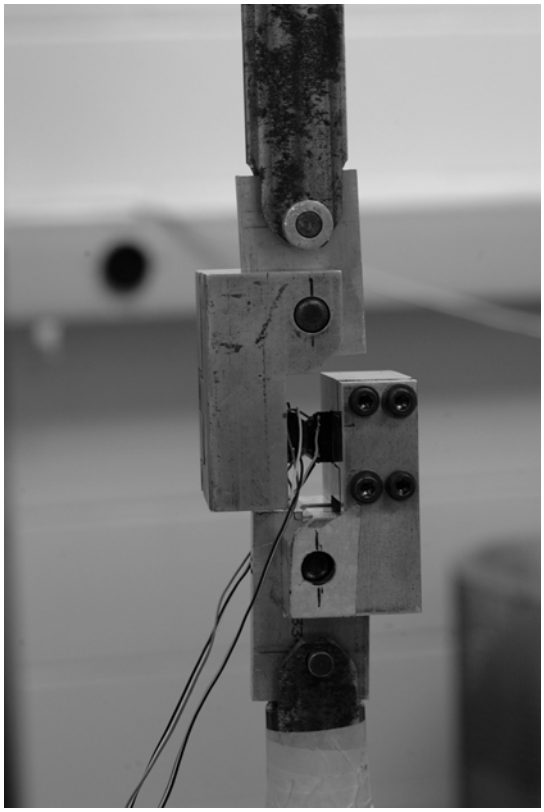

Figure 5-3: Shear Testing Fixture

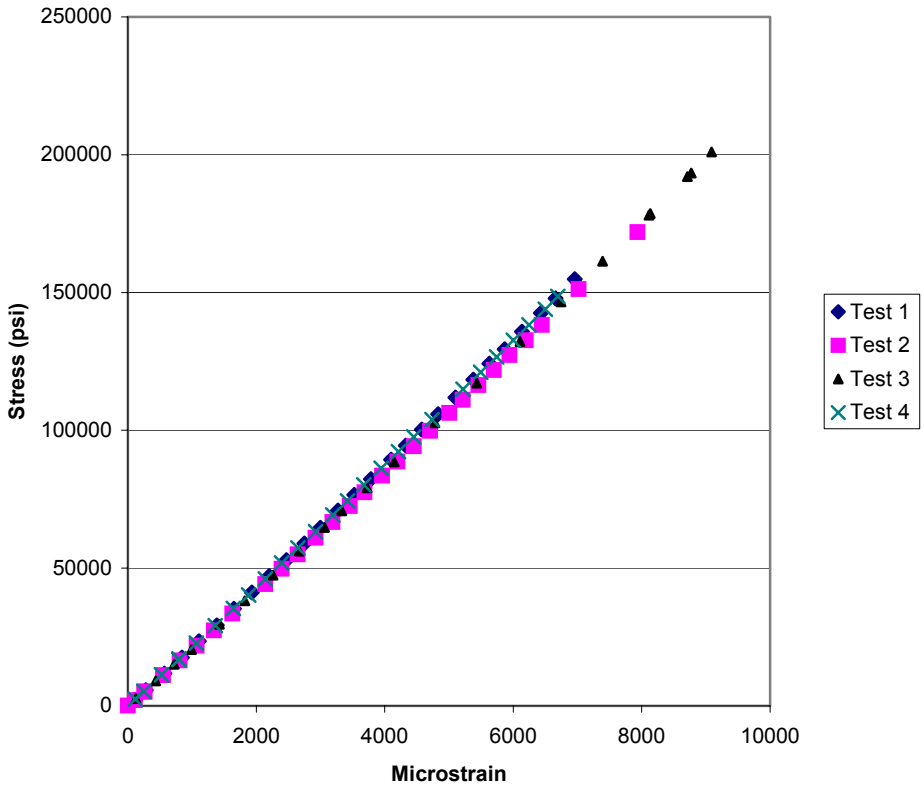

Figure 5-4: E_1 stress/strain curves

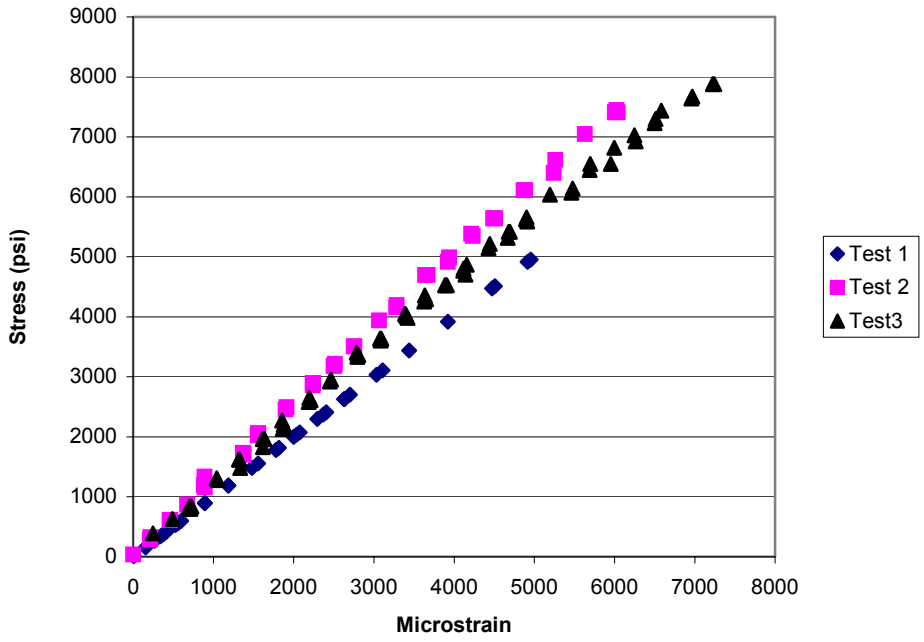

Figure 5-5: E_2 stress/strain curves

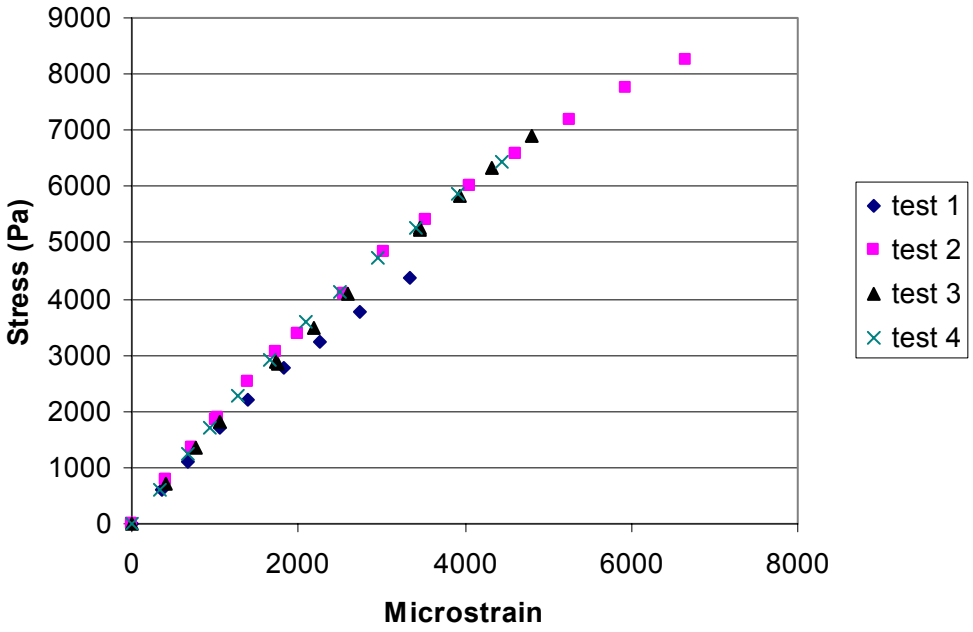

Figure 5-6: G_{12} stress/strain curves

Table 5-1: Results of each tension test

Run	E_1 (GPa)	E_2 (GPa)	υ_{12}	G_{12} (GPa)
1	151.5	7.67	0.345	4.05
2	151.6	8.40	0.343	5.10
3	147.1	8.05	0.343	4.93
4	150.5	-----	0.338	5.00
Ave	150.2	8.04	0.342	4.77
COV	1.40%	4.54%	0.87%	10.16%

5.5 Micro-mechanical Methods

A detailed micro-mechanical approach is also being used by others to develop characteristics of the IM7/977-2 material system [4]. The micro-mechanics approach uses a unit-cell model of the material system. The unit-cell is modeled and analyzed using finite element analysis of solid elements. Periodic boundary conditions are applied to the surface of each cell. This micro-mechanical approach has yielded the E_1, E_2, ν_{12}, and G_{12} properties as well. Table 5-2 compares the results of the micromechanical approach with experimentally determined values.

Table 5-2: Comparison of experimental measurements and micro-mechanics values

Material Property	Experimental Average	General Dynamics	Rockwell	Micro-mechanics	Max Percent Difference	Min Percent Difference
E_1 (GPa)	150.2	169.6	148.2	159	12.1	1.34
E_2 (GPa)	8.04	-----	9.31	9.43	15.9	14.6
ν_{12}	.342	-----	-----	.253	29.9	29.9
G_{12} (GPa)	4.77	4.80	5.17	4.34	9.45	0.63

5.6 Error Sources

Potential sources for error in the determination of material properties included many of those listed in pervious chapters. These potential sources were manufacturing defects, especially layer orientation mistakes, and gage misalignment. Again, misalignment of the strain gages is the most likely to result in the development of significant errors.

For the most part the potential errors were reduced to below 5% due to the orientation of the gage with the fibers in the specific tests. The only case of potential significant error was in the ν_{12} measurement made by measuring the transverse strain on the E_1 specimen. Any transverse measurement was much more sensitive to misalignment, however, again the desired angle helped to alleviate possible error. Transverse measurements were expected to have less than 10% potential error.

5.7 Conclusions

Various material tests have been conducted using ASTM testing standards. The material properties of Young' Modulus in both the fiber and transverse direction have been calculated as well as the resulting Poison's ratio. Further testing was conducted to evaluate the shear modulus of the material system.

The data was very consistent and possessed little scatter in most of the measurements. The COV of the various material properties were very low with the exception of the shear modulus at 10.16%.

Comparisons were made between the experimentally determined material properties and those calculated using a micro-mechanics based simulation. This comparison of material properties yielded widely varying results. The E_1 results agreed quite well and the E_2 results were not extremely different. However, the results for ν_{12} did not yield good agreement. There were several potential sources for the dramatic differences. One significant source of difference could have been the assumptions made in the micro-mechanic model. This is a FE based model that is very depended on boundary conditions. Also this model was applied on a single unit cell assuming a square packing arrangement. These may have been poor assumptions. Just as likely to yield differing results were the potential error sources listed previously. All of the samples for each test were sectioned from one plate specific to that test. If any errors had been made in the lay-up of the plate then those would have been seen in all tested specimens yielding a precise but not accurate result. More material testing should be conducted on specimens from more plates to investigate these differences.

CHAPTER 6
PLY LEVEL RESIDUAL STRAINS AND STRESSES

The residual strains and stresses in a composite result from the mismatch in contraction of the matrix and fibers. This mismatch in contraction is from the combination of drastically different CTEs and the chemical shrinkage event that is limited to the polymer matrix. The follow section will analyze the data acquired from the previous experimental techniques and present the resulting macro-mechanical residual strains and stresses.

6.1 Residual Strain Calculation

By determining the state that each ply would reach if the bonds between them were liberated the stresses that held them together can be defined [18]. This liberated strain will be referred to as the residual strain. Using the assumptions of laminate theory, where plane sections remain plane, for symmetric lay-ups, the strain on the surface matches that at any point in the interior, as long as the location is a few ply thicknesses away from the free edge.

The surface strain in each laminate is first transformed into its fiber and matrix components of each ply:

$$\begin{Bmatrix} \varepsilon_{ply\_1} \\ \varepsilon_{ply\_2} \\ \gamma_{ply\_12} \end{Bmatrix} = [T]_k \cdot \begin{Bmatrix} \varepsilon_{lam\_1} & \varepsilon_{lam\_2} & \gamma_{lam\_12} \end{Bmatrix} \tag{6.1}$$

where ε_{lam} is the total surface strain and $[T]_k$ is the transformation matrix of each ply:

$$[T]=\begin{bmatrix} \cos^2\theta & \sin^2\theta & 2\cos\theta\sin\theta \\ \sin^2\theta & \cos^2\theta & -2\cos\theta\sin\theta \\ -\cos\theta\sin\theta & \cos\theta\sin\theta & \cos^2\theta-\sin^2\theta \end{bmatrix}. \tag{6.2}$$

The residual strain in each ply then becomes:

$$\begin{Bmatrix} \varepsilon_{res\_1} \\ \varepsilon_{res\_2} \\ \gamma_{res\_12} \end{Bmatrix}_k = \begin{Bmatrix} \varepsilon_{uni\_1} \\ \varepsilon_{uni\_2} \\ \gamma_{uni\_12} \end{Bmatrix} - \begin{Bmatrix} \varepsilon_{lply\_1} \\ \varepsilon_{ply\_2} \\ \gamma_{ply\_12} \end{Bmatrix}, \tag{6.3}$$

where $\{\varepsilon_{uni}\}$ is the free expansion surface strain measured from the unidirectional specimens. This surface strain represents the strain that a ply would reach if not constrained by adjacent layers. These calculations are made for each temperature in the experimental test range. Matrix properties are significantly weaker than those of the fiber and the first sign of damage is typically mirocracks in the matrix. For this reason, the residual strains reported will be those in the transverse direction. The residual strains are plotted as a function of temperature for each layer in the OAP and RLV laminates (Figure. 6-1).

6.2 Residual Stress

After residual strain was calculated the stress-strain relations were used to define the corresponding residual stresses:

$$\begin{Bmatrix} \sigma_{res\_1} \\ \sigma_{res\_2} \\ \tau_{res\_12} \end{Bmatrix}_k = \begin{bmatrix} Q_{11} & Q_{12} & 0 \\ Q_{21} & Q_{22} & 0 \\ 0 & 0 & Q_{66} \end{bmatrix}_k \begin{Bmatrix} \varepsilon_{res\_1} \\ \varepsilon_{res\_2} \\ \gamma_{res\_12} \end{Bmatrix}_k. \tag{6.4}$$

The resulting residual stresses in the ply of the OAP and RLV laminates are plotted versus temperature (Figure 6.2).

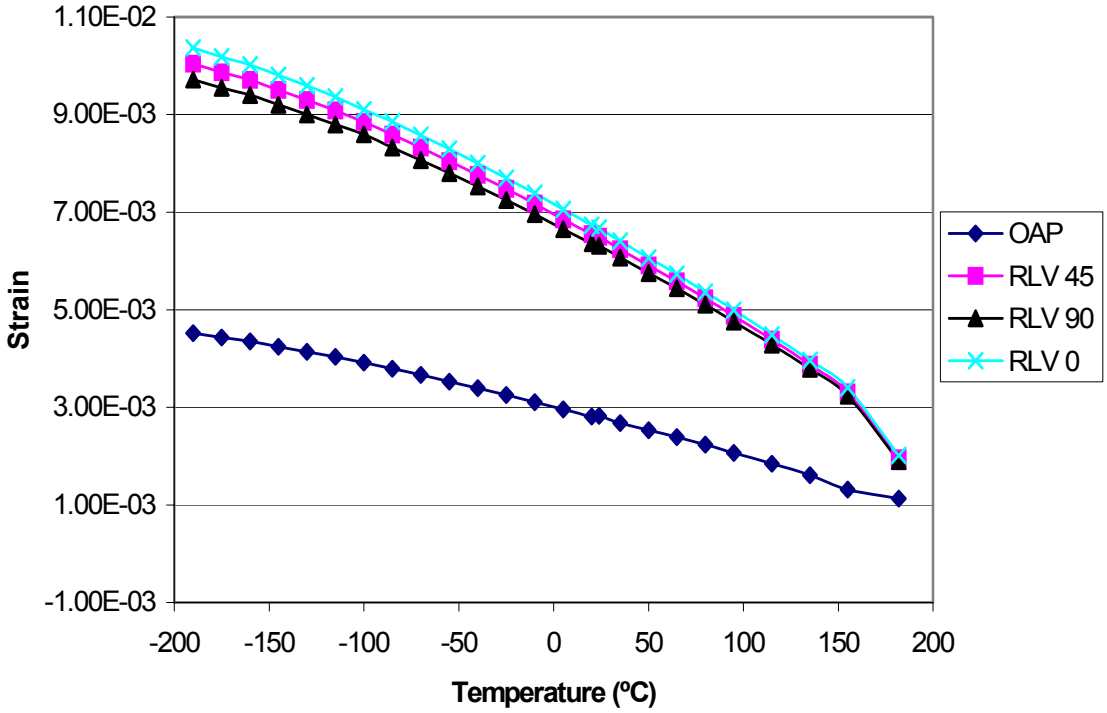

Figure 6-1: Residual strain on selected plies

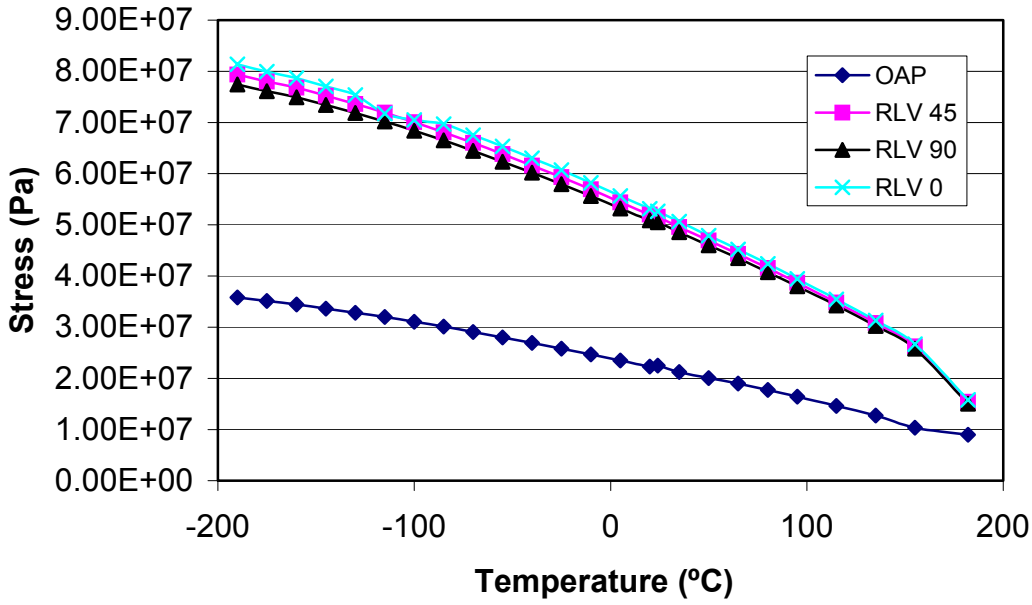

Figure 6-2: Residual stress level on selected plies

6.3 Conclusions

A method to quantify residual strains and stresses based on surface strains has been discussed. This method has been used to display the resulting residual stresses that were present in the different laminates. As expected, the high level of constraint that has been discussed throughout this thesis has lead to high level of residual stress. The OAP has performed much better than the RLV lay-up in reference to the development of thermally induced stresses. The often neglected chemical shrinkage has induced as much as 15.4 MPa of residual stress in the RLV laminate.

From these results it has been made apparent that the chemical shrinkage is not a negligible term and must be determined to fully quantify the extent of residual stress development. It has also been made quite apparent that there is a great need for the development of optimization techniques to account for the interaction of both mechanically and thermally induced stresses.

CHAPTER 7
CLASSICAL LAMINATION THEORY

Classical Lamination Theory (CLT) is a predictive tool that makes it possible to analyze complex coupling effects that may occur in composites. CLT is able to predict strains, displacements, and curvatures that develop in a laminate as it is mechanically loaded as well as those resulting from hygrothermal stresses. It is the thermal contribution to strain that will be investigated in the following section.

CLT is derived from many assumptions, the most basic of which are that individual lamina are perfectly bonded together so that they behave as a "unitary, nonhomogeneous, anisotropic plate" [13]. The most important assumption in CLT is that each ply is assumed to be in a state of plane stress and that interlaminar stresses are neglected.

7.1 Theory Development

Using the coordinate system in Figure 7-1, the laminated plate geometry and ply numbering scheme defined in Figure 7-2, along with several basic assumptions, a set of equations are derived to predict deformations and stresses. The basic assumptions needed in the derivation are:

14. The plate consists of orthotropic lamina bonded together, with principal material axis directed in arbitrary directions with respect to the x and y axes.
15. Edge lengths of the plate must be much greater than the individual ply thicknesses.
16. The u,v,w displacements are small in comparison to the total plate thickness.
17. The in-plane strains ε_x, ε_y, and γ_{xy} are much smaller than one.
18. Transverse shear strains γ_{xz} and γ_{yz} are neglected.
19. The u and v displacements are linear functions of the z coordinate.

20. The transverse normal strain ε_z is neglected.

21. Hooke's Law applies to each ply.

22. Total plate thickness is constant.

23. At the plate surface the transverse shear stresses τ_{xz} and τ_{yz} are zero.

Assumptions 6 and 7 define the displacements as

$$\begin{aligned} u &= u^0(x,y) + zF_1(x,y) \\ v &= v^0(x,y) + zF_2(x,y) \\ w &= w^0(x,y) = w(x,y) \end{aligned} \tag{7.1}$$

where u^0 and v^0 are the displacements in the x and y directions at the middle of the plate. The displacement w is the same at any thickness in the plate with the same x and y coordinates due to assumption 7. Substituting equations 7.1 into the strain-displacement equations for the transverse shear strains and imposing assumption 5 yields

$$\begin{aligned} \gamma_{xy} &= \frac{\partial u}{\partial z} + \frac{\partial w}{\partial x} = F_1(x,y) + \frac{\partial w}{\partial x} = 0 \\ \gamma_{yz} &= \frac{\partial v}{\partial z} + \frac{\partial w}{\partial y} = F_2(x,y) + \frac{\partial w}{\partial y} = 0 \end{aligned} \tag{7.2}$$

and

$$\begin{aligned} F_1(x,y) &= -\frac{\partial w}{\partial x} \\ F_2(x,y) &= -\frac{\partial w}{\partial y} \end{aligned} \tag{7.3}$$

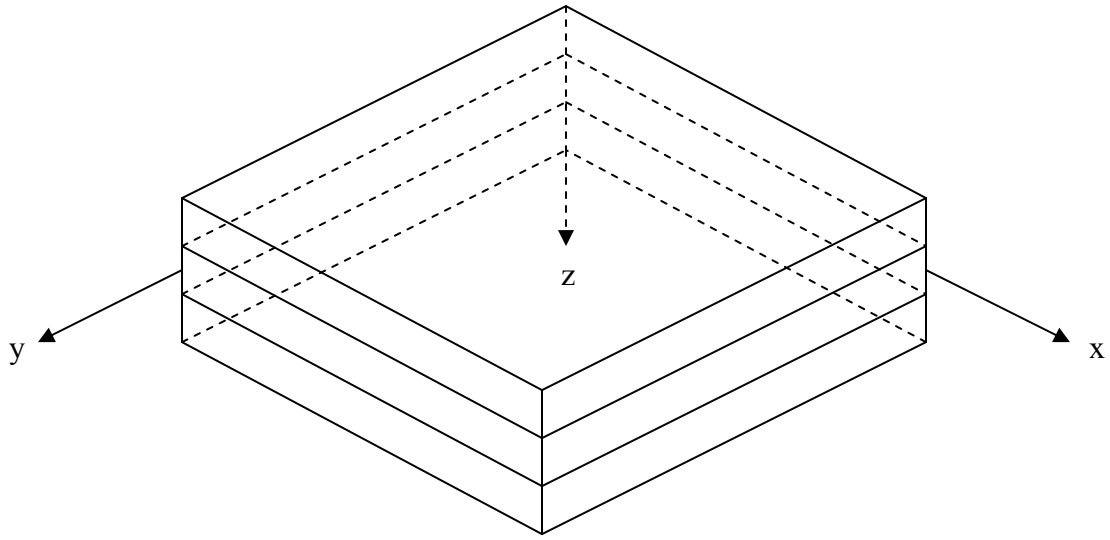

Figure 7-1: Laminate coordinate system

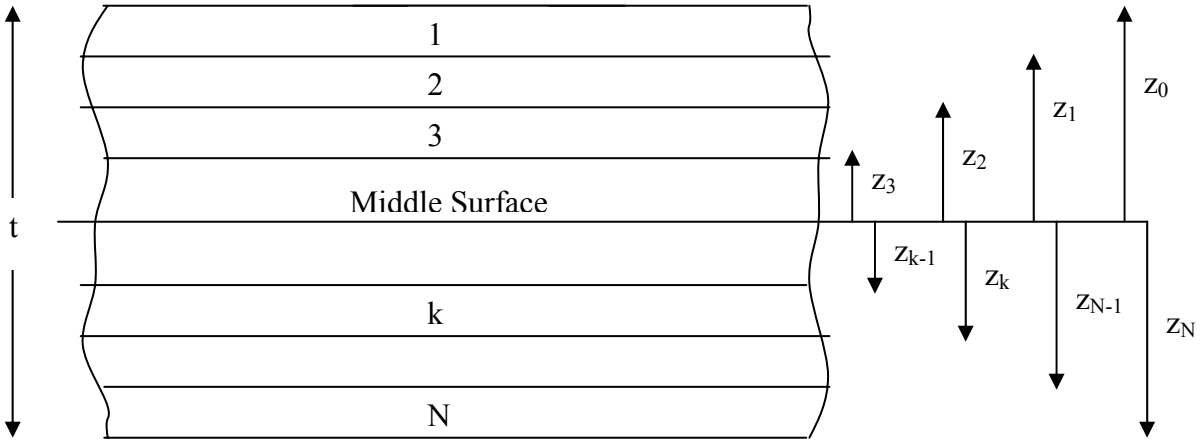

Figure 7-2: Layer schematic and nomenclature

Combining the strain-displacement relations for in-plane strains with Eqs. (7.1) and (7.3) results in

$$\begin{aligned} \varepsilon_x &= \frac{\partial u}{\partial x} = \varepsilon_x^0 + z\kappa_x \\ \varepsilon_y &= \frac{\partial v}{\partial y} = \varepsilon_y^0 + z\kappa_y \\ \gamma_{xy} &= \frac{\partial u}{\partial y} + \frac{\partial v}{\partial x} = \gamma_{xy}^0 + z\kappa_{xy} \end{aligned} \tag{7.4}$$

where mid-laminate strains are

$$\begin{aligned} \varepsilon_x^0 &= \frac{\partial u^0}{\partial x} \\ \varepsilon_y^0 &= \frac{\partial v^0}{\partial y} \\ \gamma_{xy}^0 &= \frac{\partial u^0}{\partial y} + \frac{\partial v^0}{\partial x} \end{aligned} \tag{7.5}$$

and mid-laminate curvatures are given by

$$\begin{aligned} \kappa_x &= -\frac{\partial^2 w}{\partial x^2} \\ \kappa_y &= -\frac{\partial^2 w}{\partial y^2} \\ \kappa_{xy} &= -2\frac{\partial^2 w}{\partial x \partial y} \end{aligned} \tag{7.6}$$

These represent the curvatures associated with the bending at the middle of the laminate in the xz and yz planes as well as the out of plane twisting of the middle surface of the laminate. In our case, as with any symmetric laminate, these curvatures will be zero. They are left in the derivation to give the solution for any arbitrary stacking sequence where curvature may be present.

Equation (7.4) provides a solution for the strain at any given distance from mid-laminate. If the various lamina are of known thickness then the distance of each from mid-laminate is known and the stress-strain relations for the k^{th} lamina can be expressed as

$$\begin{Bmatrix} \sigma_x \\ \sigma_y \\ \tau_{xy} \end{Bmatrix}_k = \begin{bmatrix} \overline{Q}_{11} & \overline{Q}_{12} & \overline{Q}_{16} \\ \overline{Q}_{12} & \overline{Q}_{22} & \overline{Q}_{26} \\ \overline{Q}_{16} & \overline{Q}_{26} & \overline{Q}_{66} \end{bmatrix} = \begin{Bmatrix} \varepsilon_x^0 + z\kappa_x \\ \varepsilon_y^0 + z\kappa_y \\ \gamma_{xy}^0 + z\kappa_{xy} \end{Bmatrix} \tag{7.7}$$

where

$$\left[\overline{Q}\right] = [T]^{-1}[Q][T] \tag{7.8}$$

and

$$\begin{aligned} Q_{11} &= \frac{E_1}{1-\nu_{12}\nu_{21}} \\ Q_{12} &= \frac{\nu_{12}E_2}{1-\nu_{12}\nu_{21}} = Q_{21} \\ Q_{22} &= \frac{E_2}{1-\nu_{12}\nu_{21}} \\ Q_{66} &= G_{12} \end{aligned} \tag{7.9}$$

When determining strains and stresses in a laminated plate it is convenient to look at the forces and moments per unit length as they act on a plate. The force per unit length, N_x, is given by

$$N_x = \int_{-t/2}^{t/2} \sigma_x dz = \sum_{k=1}^{N} \left\{ \int_{z_{k-1}}^{z_k} \left(\sigma_x\right)_k dz \right\} \tag{7.10}$$

and the moment per unit length, M_x, is given by

$$M_x = \int_{-t/2}^{t/2} \sigma_x z dz = \sum_{k=1}^{N} \left\{ \int_{z_{k-1}}^{z_k} \left(\sigma_x\right)_k z dz \right\} \tag{7.11}$$

where t is the laminate thickness, $\left(\sigma_x\right)_k$ is the stress in the kth lamina, z_{k-1} is the distance from mid-laminate to inner surface of the kth lamina, and z_k is the distance to the outer surface of the same lamina. Combining (7.7) with both (7.10) and (7.11) yields the following equations for the force and moment per unit length.

$$\begin{aligned} N_x &= \sum_{k=1}^{N} \int_{z_{k-1}}^{z_k} \left\{ \left(\overline{Q}_{11}\right)_k \left(\varepsilon_x^0 + z\kappa_x\right) + \left(\overline{Q}_{12}\right)_k \left(\varepsilon_y^0 + z\kappa_y\right) + \left(\overline{Q}_{16}\right)_k \left(\gamma_{xy}^0 + z\kappa_{xy}\right) \right\} dz \\ M_x &= \sum_{k=1}^{N} \int_{z_{k-1}}^{z_k} \left\{ \left(\overline{Q}_{11}\right)_k \left(\varepsilon_x^0 + z\kappa_x\right) + \left(\overline{Q}_{12}\right)_k \left(\varepsilon_y^0 + z\kappa_y\right) + \left(\overline{Q}_{16}\right)_k \left(\gamma_{xy}^0 + z\kappa_{xy}\right) \right\} z dz \end{aligned} \tag{7.12}$$

after rearranging (7.12) the force and moment equations can be written as

$$\begin{aligned} N_x &= A_{11}\varepsilon_x^0 + A_{12}\varepsilon_y^0 + A_{16}\gamma_{xy}^0 + B_{11}\kappa_x + B_{12}\kappa_y + B_{16}\kappa_{xy} \\ M_x &= B_{11}\varepsilon_x^0 + B_{12}\varepsilon_y^0 + B_{16}\gamma_{xy}^0 + D_{11}\kappa_x + D_{12}\kappa_y + D_{16}\kappa_{xy} \end{aligned} \tag{7.13}$$

where the laminate extensional stiffness is given by

$$A_{ij} = \int_{-\frac{t}{2}}^{\frac{t}{2}} \left(\overline{Q}_{ij}\right)_k dz = \sum_{k=1}^{N} \left(\overline{Q}_{ij}\right)_k \left(z_k - z_{k-1}\right) \tag{7.14}$$

the laminate coupling stiffness is given by

$$B_{ij} = \int_{-\frac{t}{2}}^{\frac{t}{2}} \left(\overline{Q}_{ij}\right)_k z dz = \frac{1}{2}\sum_{k=1}^{N} \left(\overline{Q}_{ij}\right)_k \left(z_k^2 - z_{k-1}^2\right) \tag{7.15}$$

and the laminate bending stiffness is

$$D_{ij} = \int_{-\frac{t}{2}}^{\frac{t}{2}} \left(\overline{Q}_{ij}\right)_k z^2 dz = \frac{1}{3}\sum_{k=1}^{N} \left(\overline{Q}_{ij}\right)_k \left(z_k^3 - z_{k-1}^3\right) \tag{7.16}$$

Finally the entire set of equations can be expressed as

$$\begin{Bmatrix} N_x \\ N_y \\ N_{xy} \\ M_x \\ M_y \\ M_{xy} \end{Bmatrix} = \begin{bmatrix} A_{11} & A_{12} & A_{16} & B_{11} & B_{12} & B_{16} \\ A_{11} & A_{22} & A_{26} & B_{12} & B_{22} & B_{26} \\ A_{16} & A_{26} & A_{66} & B_{16} & B_{26} & B_{66} \\ B_{11} & B_{12} & B_{16} & D_{11} & D_{12} & D_{16} \\ B_{11} & B_{22} & B_{26} & D_{11} & D_{22} & D_{26} \\ B_{16} & B_{26} & B_{66} & D_{16} & D_{26} & D_{66} \end{bmatrix} \begin{Bmatrix} \varepsilon_x^0 \\ \varepsilon_y^0 \\ \gamma_{xy}^0 \\ \kappa_x \\ \kappa_y \\ \kappa_{xy} \end{Bmatrix} \tag{7.17}$$

The above solution exists for the state in which laminates are not subjected to any thermal or moisture effects. Together these effects are known as hygrothermal effects. It is the thermal component of this stress that is of the greatest concern in this case and therefore the stresses and strains in the laminate must be solved for this hygrothermal effect.

When the moisture and thermal effects are incorporated the resulting stresses on each lamina are

$$\{\sigma\}_k = \left[\overline{Q}\right]_k \left(\{\varepsilon\}_k - \{\alpha\}_k \Delta T - \{\beta\}_k c\right) \tag{7.18}$$

and the total lamina strains equal

$$\{\varepsilon\}_k = \left\{\varepsilon^0\right\} + z\{\kappa\} \tag{7.19}$$

Equation (7.19) is substituted into Eqn. (7.18) giving

$$\{\sigma\}_k = \left[\overline{Q}\right]_k \left(\left\{\varepsilon^0\right\} + z\{\kappa\} - \{\alpha\}_k \Delta T - \{\beta\}_k c\right) \tag{7.20}$$

The force and moment per unit length are then solved in the same manner but this time by integrating (7.20).

$$\begin{aligned}
\{N\} &= \int \{\sigma\}_k dz = \int \left[\overline{Q}\right]_k \left(\left\{\varepsilon^0\right\} + z\{\kappa\} - \{\alpha\}_k \Delta T - \{\beta\}_k c\right) dz \\
\{N\} &= [A]\left\{\varepsilon^0\right\} + [B]\{\kappa\} - \left\{N^T\right\} - \left\{N^M\right\} \\
\{M\} &= \int \{\sigma\}_k z dz = \int \left[\overline{Q}\right]_k \left(\left\{\varepsilon^0\right\} + z\{\kappa\} - \{\alpha\}_k \Delta T - \{\beta\}_k c\right) z dz \\
\{M\} &= [B]\left\{\varepsilon^0\right\} + [D]\{\kappa\} - \left\{M^T\right\} - \left\{M^M\right\}
\end{aligned} \tag{7.21}$$

The contributions of the thermal and moisture components are

$$\begin{aligned}
\left\{N^T\right\} &= \int \left[\overline{Q}\right]_k \{\alpha\}_k \Delta T dz = (\Delta T) \sum_{k=1}^{N} \left[\overline{Q}\right]_k \{\alpha\}_k \left(z_k - z_{k-1}\right) \\
\left\{N^M\right\} &= \int \left[\overline{Q}\right]_k \{\beta\}_k c dz = c \sum_{k=1}^{N} \left[\overline{Q}\right]_k \{\beta\}_k \left(z_k - z_{k-1}\right)
\end{aligned} \tag{7.22}$$

and

$$\begin{aligned}
\left\{M^T\right\} &= \int \left[\overline{Q}\right]_k \{\alpha\}_k \Delta T z dz = \frac{(\Delta T)}{2} \sum_{k=1}^{N} \left[\overline{Q}\right]_k \{\alpha\}_k \left(z_k^2 - z_{k-1}^2\right) \\
\left\{M^M\right\} &= \int \left[\overline{Q}\right]_k \{\beta\}_k c z dz = \frac{c}{2} \sum_{k=1}^{N} \left[\overline{Q}\right]_k \{\beta\}_k \left(z_k^2 - z_{k-1}^2\right)
\end{aligned} \tag{7.23}$$

Finally, the entire solution can be written in matrix form as

$$\begin{Bmatrix} N_x + N_x^T + N_x^M \\ N_y + N_y^T + N_y^M \\ N_{xy} + N_{xy}^T + N_{xy}^M \\ M_x + M_x^T + M_x^M \\ M_y + M_y^T + M_y^M \\ M_{xy} + M_{xy}^T + M_{xy}^M \end{Bmatrix} = \begin{bmatrix} A_{11} & A_{12} & A_{16} & B_{11} & B_{12} & B_{16} \\ A_{11} & A_{22} & A_{26} & B_{12} & B_{22} & B_{26} \\ A_{16} & A_{26} & A_{66} & B_{16} & B_{26} & B_{66} \\ B_{11} & B_{12} & B_{16} & D_{11} & D_{12} & D_{16} \\ B_{11} & B_{22} & B_{26} & D_{11} & D_{22} & D_{26} \\ B_{16} & B_{26} & B_{66} & D_{16} & D_{26} & D_{66} \end{bmatrix} \begin{Bmatrix} \varepsilon_x^0 \\ \varepsilon_y^0 \\ \gamma_{xy}^0 \\ \kappa_x \\ \kappa_y \\ \kappa_{xy} \end{Bmatrix} \tag{7.24}$$

This approach was used to predict the strains on the surface of the laminates and compare them to those measured via experiment. A MatLAB code was authored, primarily by Thomas Singer and William Schulz, to encompass all of the assumptions and calculations involved in CLT (Appendix B). The code was executed at each temperature in which experimental data was collected. CLT makes its predictions based on the material properties of individual lamina. The material properties of E_1, E_2, ν_{12}, G_{12}, and α_1 and α_2 were obtained from previous experiments. The CTE values of α_1 and α_2 have been calculated as functions of temperature from previous analysis. The apparent change in CTE is linear and therefore an average CTE across the test range was used as the input for the CLT program.

7.2 Experimental vs. Analytical Results

CLT results were plotted as a function of temperature and compared to the experimental results (Figures 7-3through 7-5). It can be seen in all cases that there is substantial difference between the results of CLT and experimental data.

Several factors could lead to potential differences in the measured and predicted values. The first potential source is in the assumptions that are made in CLT formulation. The second and most crucial difference is that CLT lacks the ability to interpret the event of chemical shrinkage and the effect it has on laminate strain. If the values at the cure temperature are compared it is seen that CLT predicts no strain at this point, while the

combined experimental techniques show strains that are the result of the chemical shrinkage. Since chemical shrinkage is a one-time event and the resulting strains are an invariant part of the laminate strain they can be added to the results of CLT. Upon the introduction of the chemical shrinkage term into the CLT results it was seen that the graphs collapsed onto each other (Figures 7-6 through 7-8).

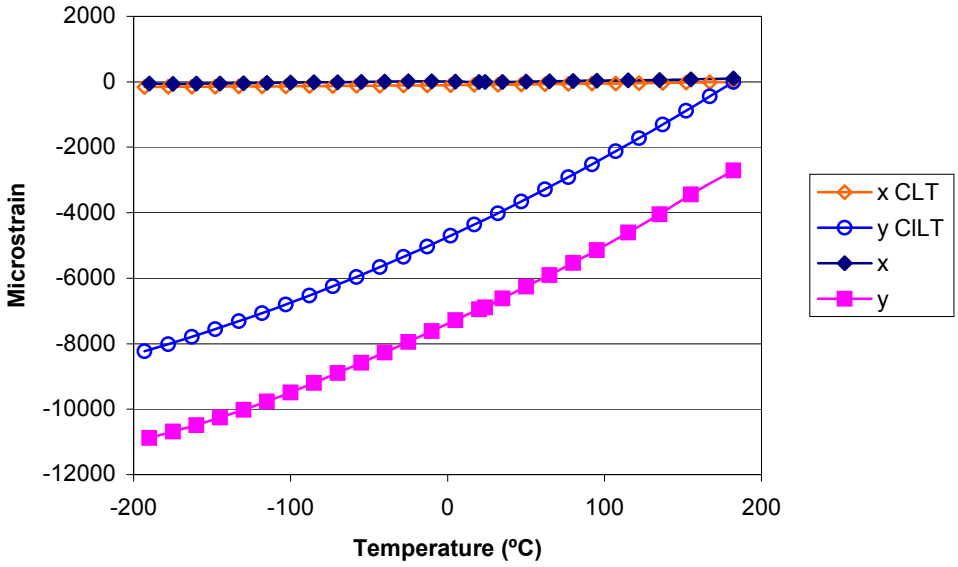

Figure 7-3: Unidirectional CLT and experimental results

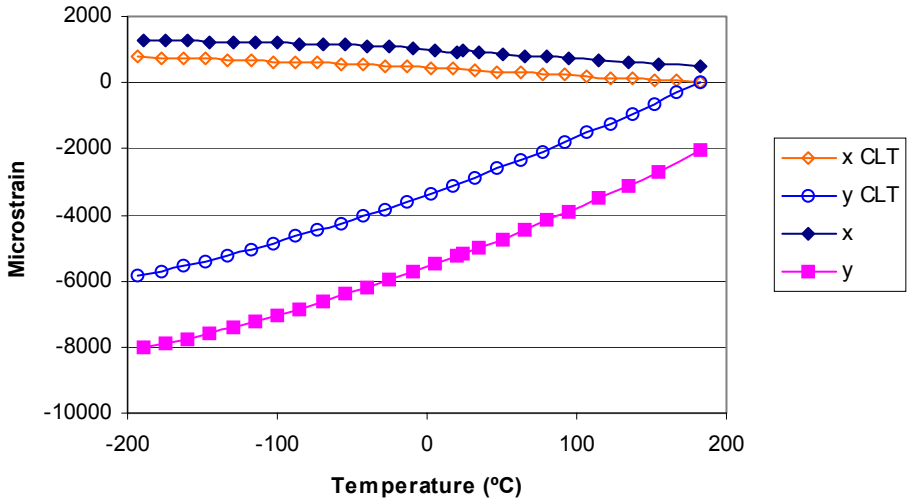

Figure 7-4: OAP CLT and experimental results

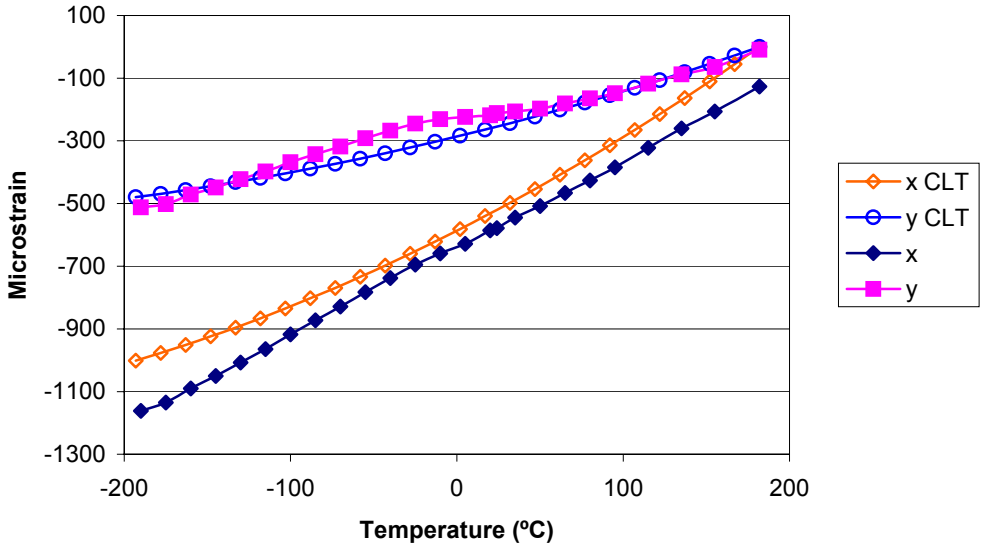

Figure 7-5: RLV CLT and experimental results

The resulting agreement between the CLT and experimental values provides proof of testing concept and a high degree of measurement accuracy.

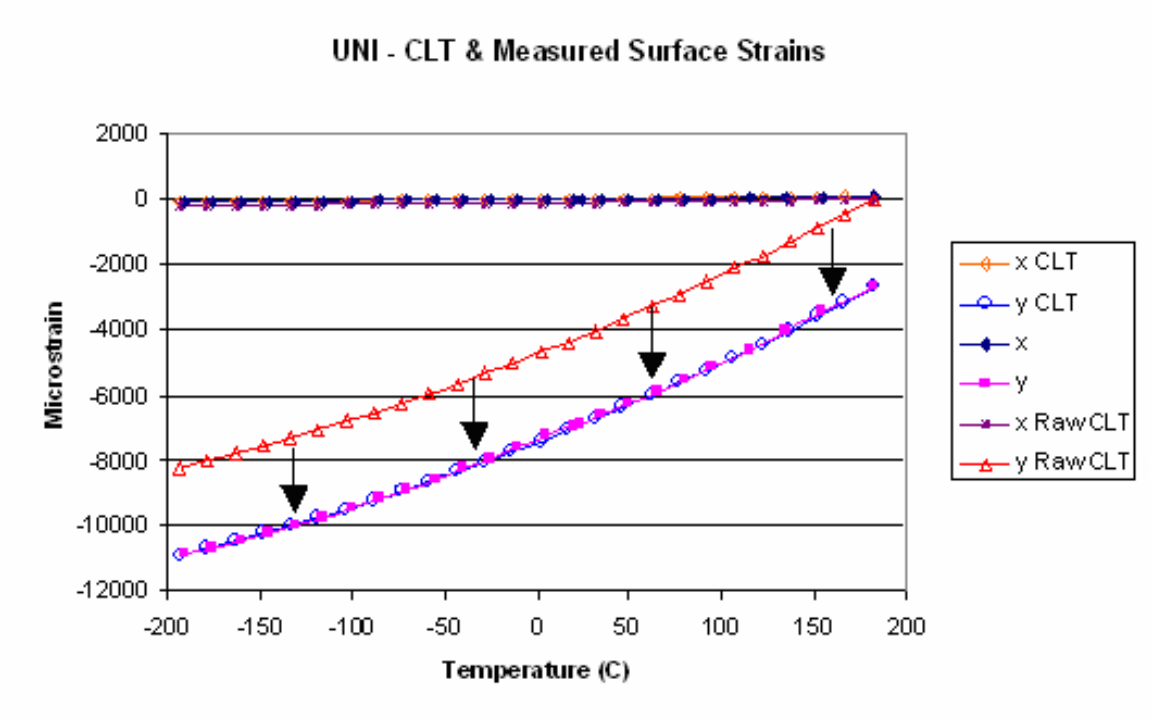

Figure 7-6: Unidirectional CLT shifted for chemical shrinkage

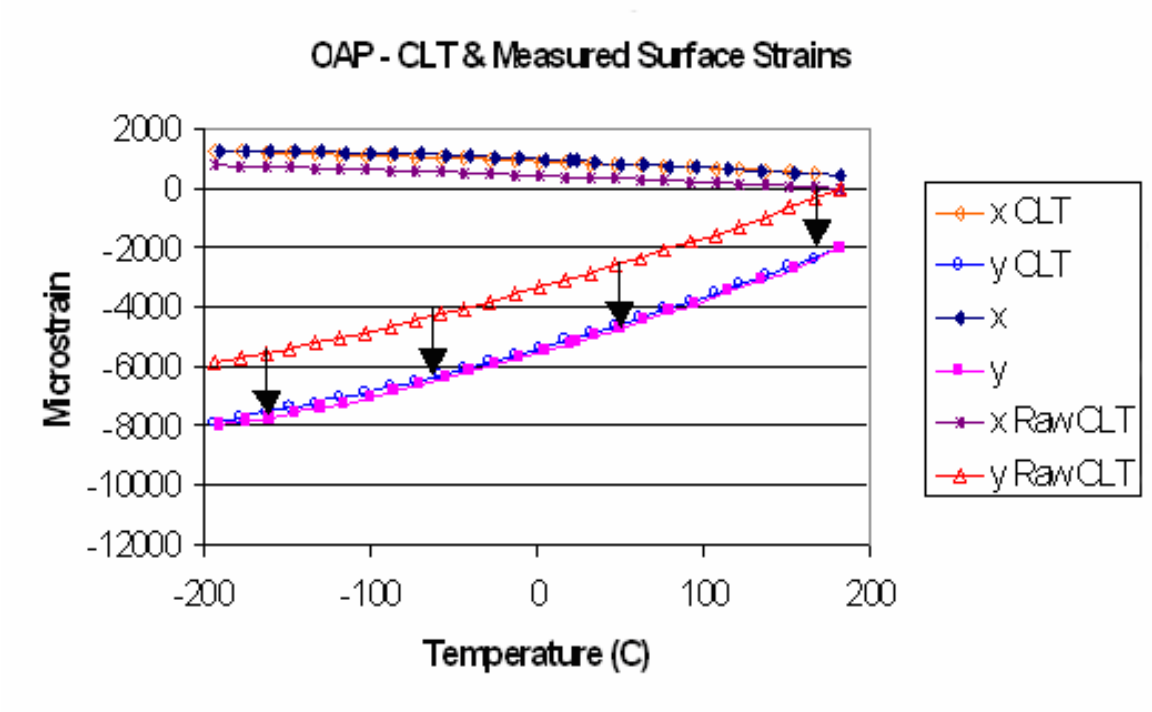

Figure 7-7: OAP CLT shifted for chemical shrinkage

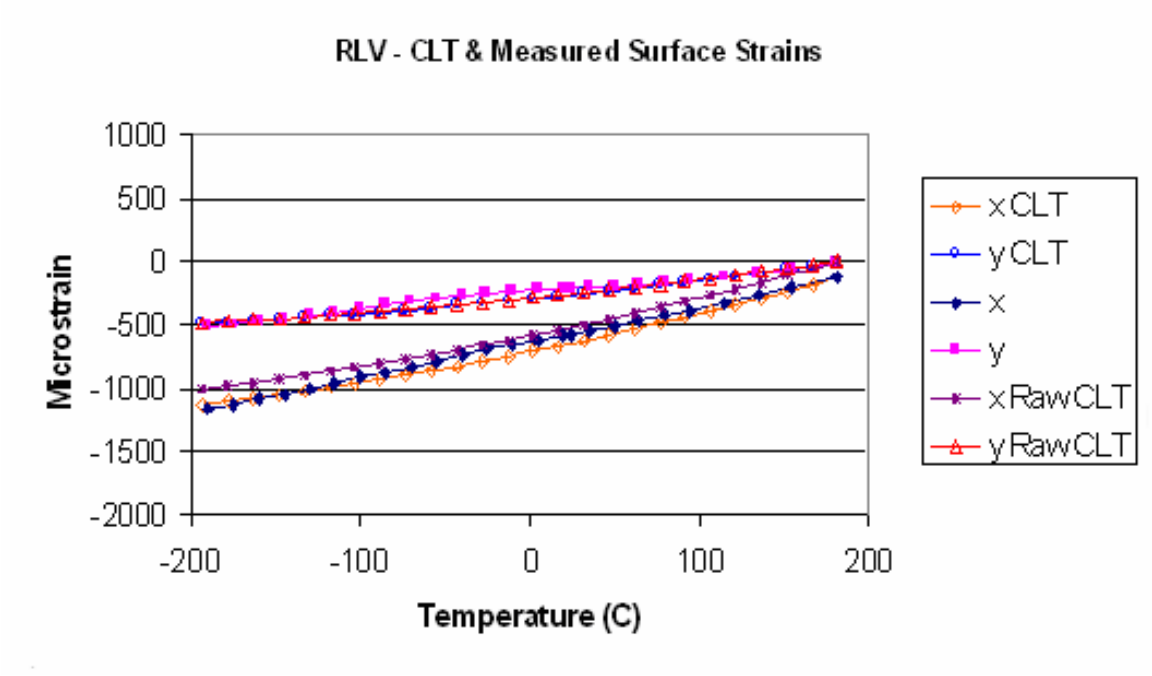

Figure 7-8: RLV CLT shifted for chemical shrinkage

7.3 Conclusions

Classical Laminate theory has been examined and used to predict the surface strains on the different laminates. This examination has taken place as an attempt to verify the experimentally determined results. It is a well known fact that the traditional approach to lamination theory does not have the means to account for chemical shrinkage.

When the two results were compared an interesting phenomenon was observed. The measured and predicted curves appeared to follow nearly the same trends, separated by an offset. When the curves were examined it was seen that this offset was almost exactly equal to that of the chemical shrinkage. When the previously decoupled chemical shrinkage term was added to the analytical results form CLT the offset in the curves vanished and the two results were nearly identically. Several substantial conclusions have been drawn from these results.

First, the fact that the resulting curves coincided with each other throughout the testing range confirmed that the chemical shrinkage can be treated as a one time event, completely independent of temperature effects. Secondly, the fact that the two curves coincided very well provided proof of concept in the strain gage measurements and temperature compensation technique. Last, and perhaps the most important conclusion was that the CRM method did indeed provide a means by which the true total strain present in a laminated composite could be measured. From this result, it is seen that once the chemical shrinkage term is decoupled and defined, the computer based analytical tool of CLT can be used to predict the development of strains anywhere in a given temperature range.

APPENDIX A
CRM IMAGES OF SPECIMENS

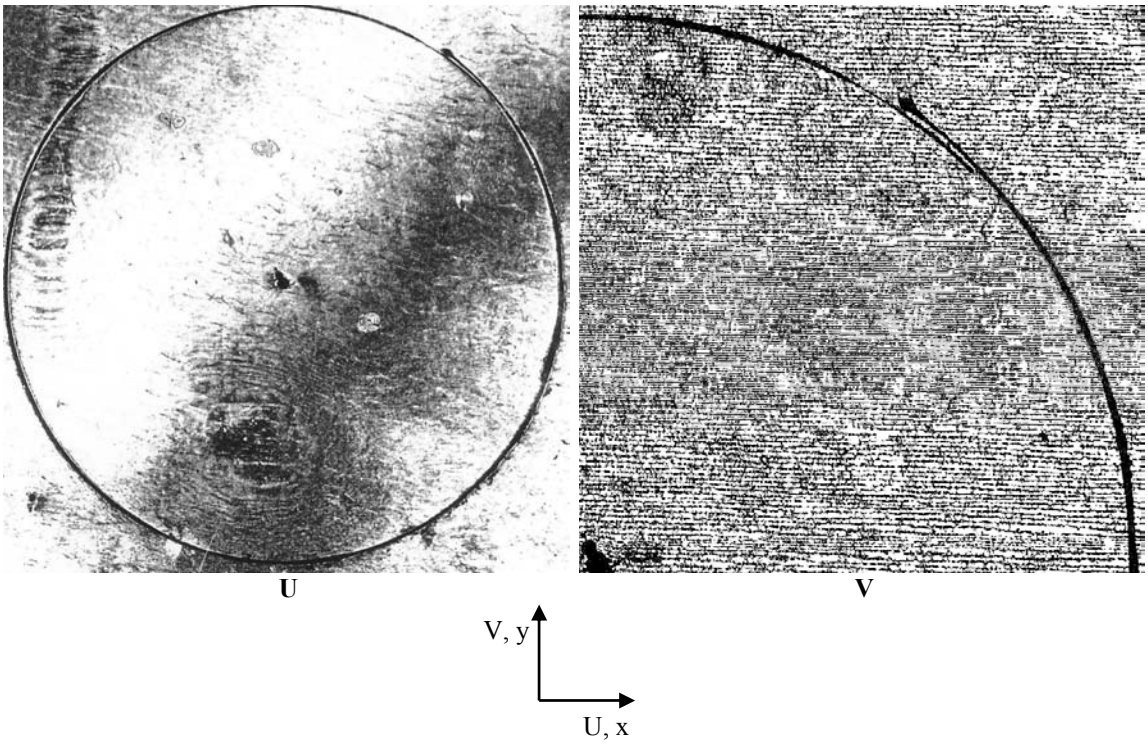

Figure A-1: Unidirectional Laminate Run 1

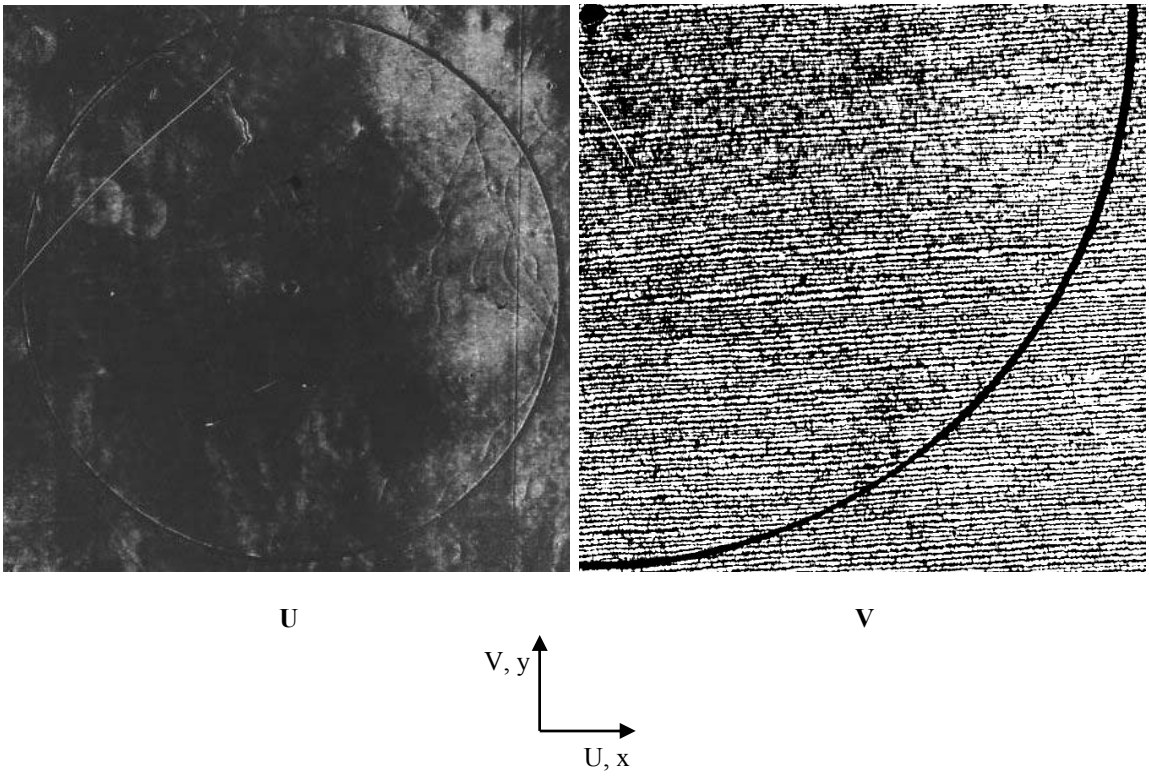

Figure A-2: Unidirectional Laminate Run 2

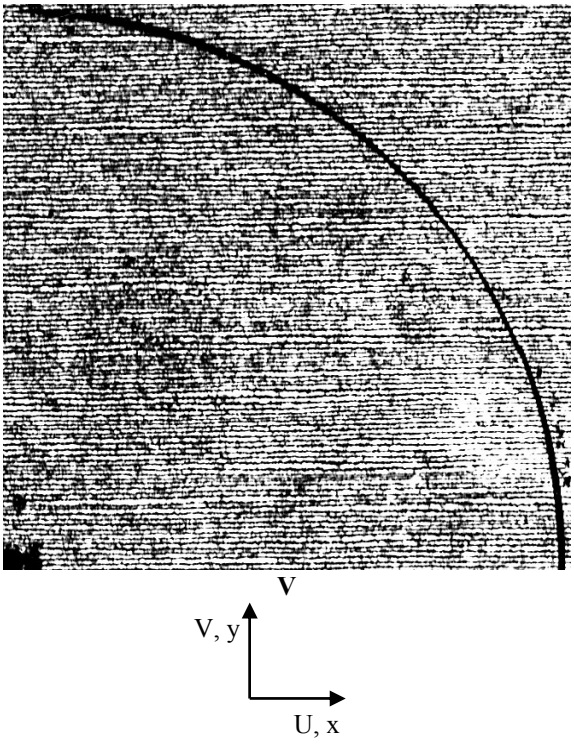

Figure A-3: Unidirectional Laminate Run 3

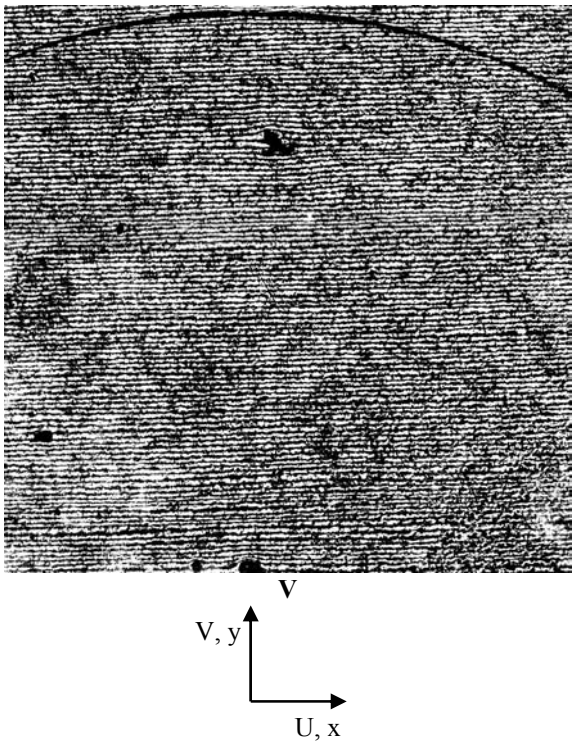

Figure A-4: Unidirectional Laminate Run 4

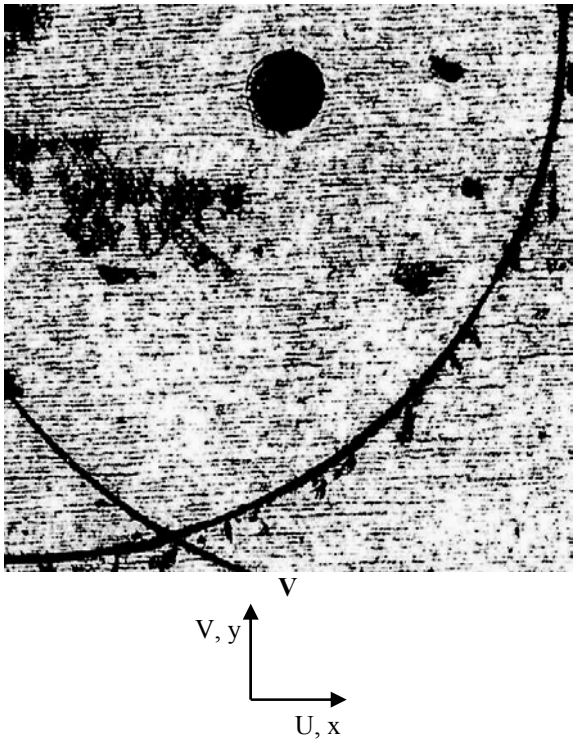

Figure A-5: Unidirectional Laminate Run 5

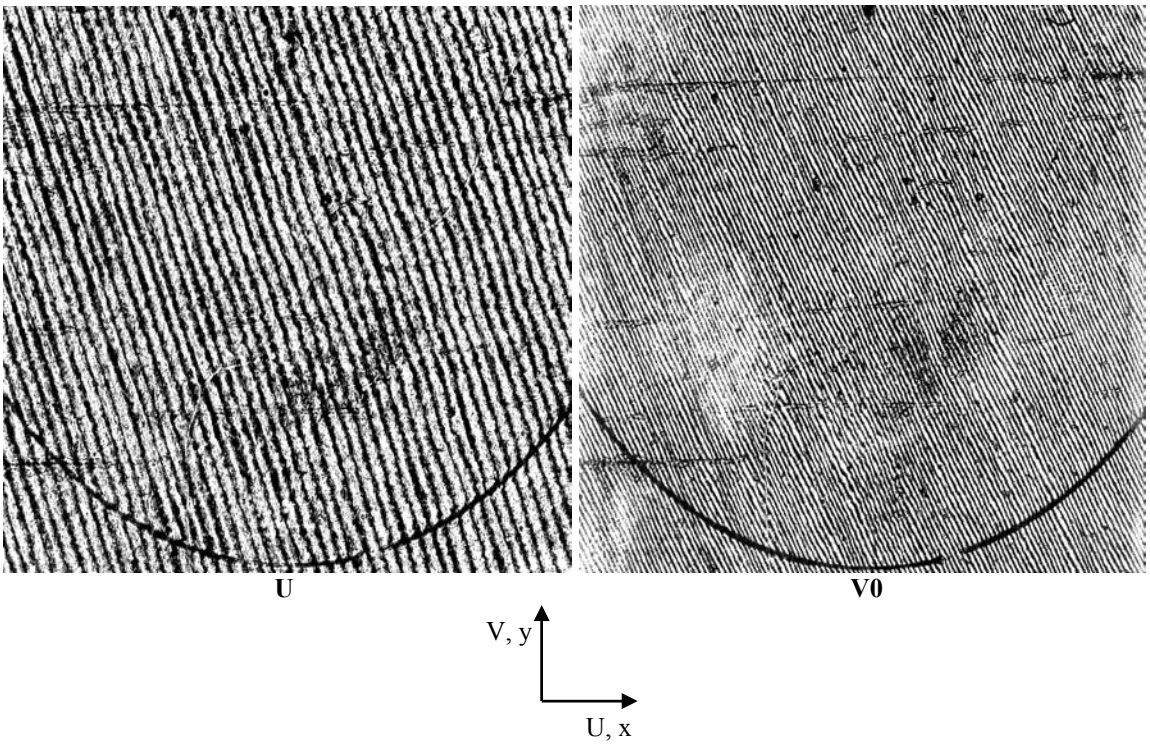

Figure A-6: OAP Laminate Run 1

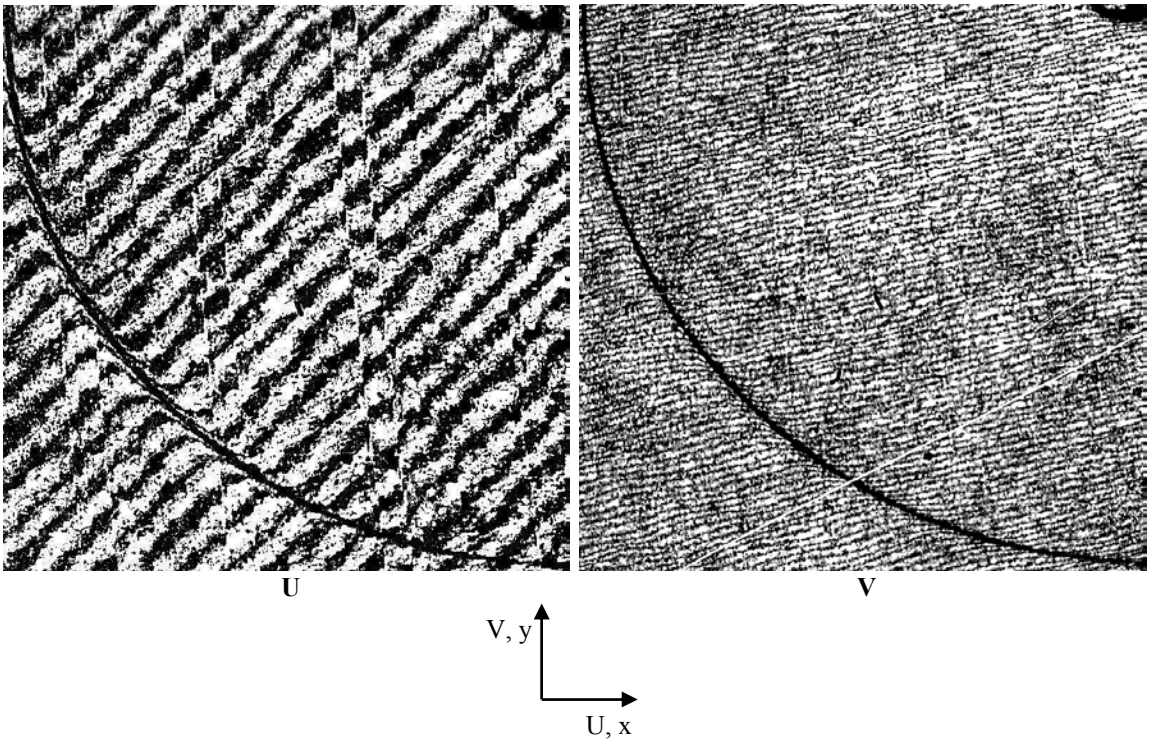

Figure A-7: OAP Laminate Run 2

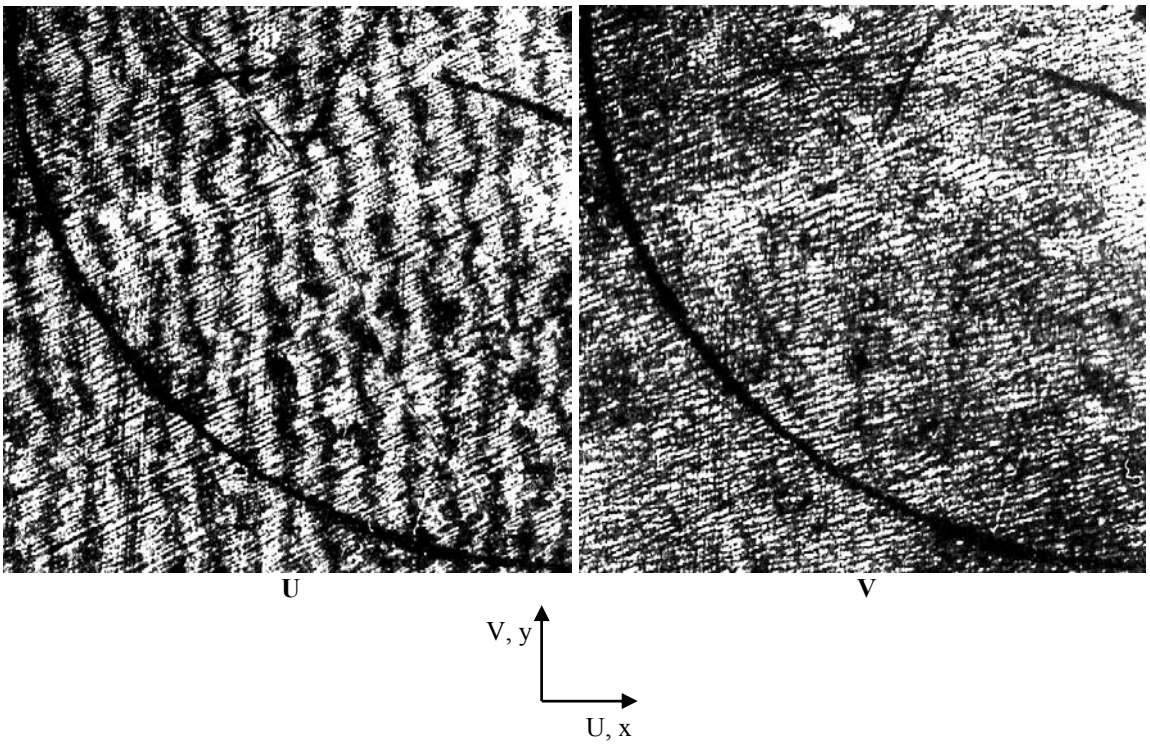

Figure A-8: OAP Laminate Run 3

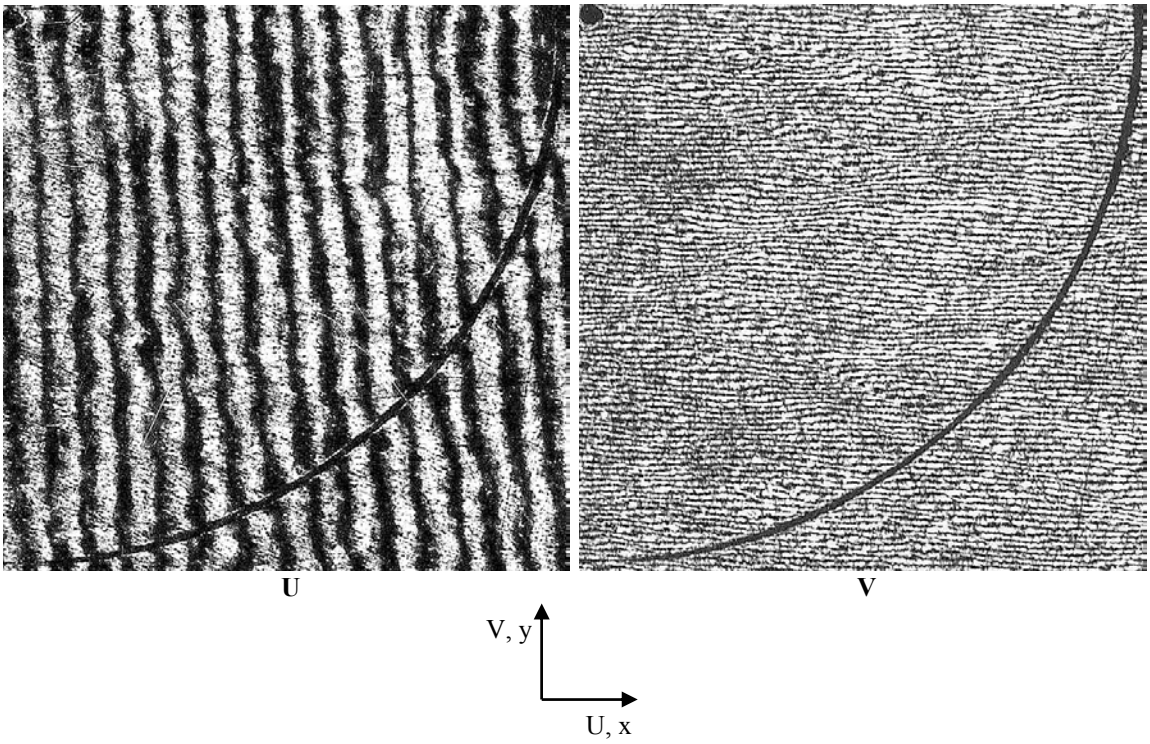

Figure A-9: OAP Laminate Run 4

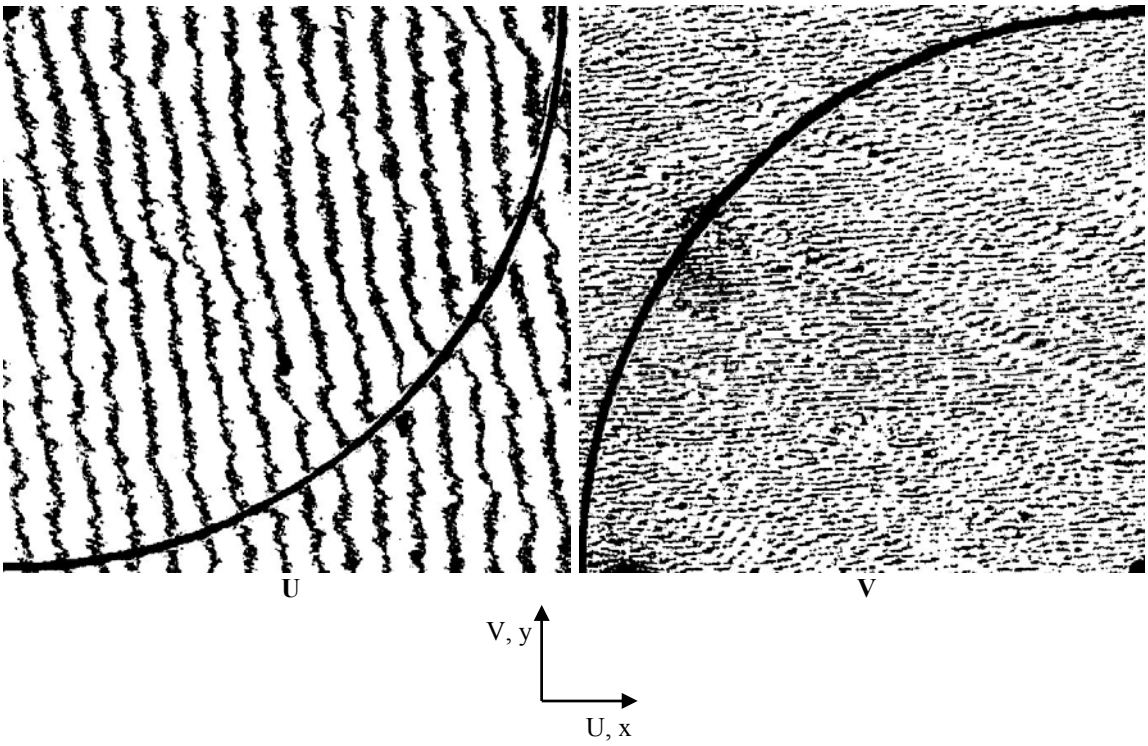

Figure A-10: OAP Laminate Run 5

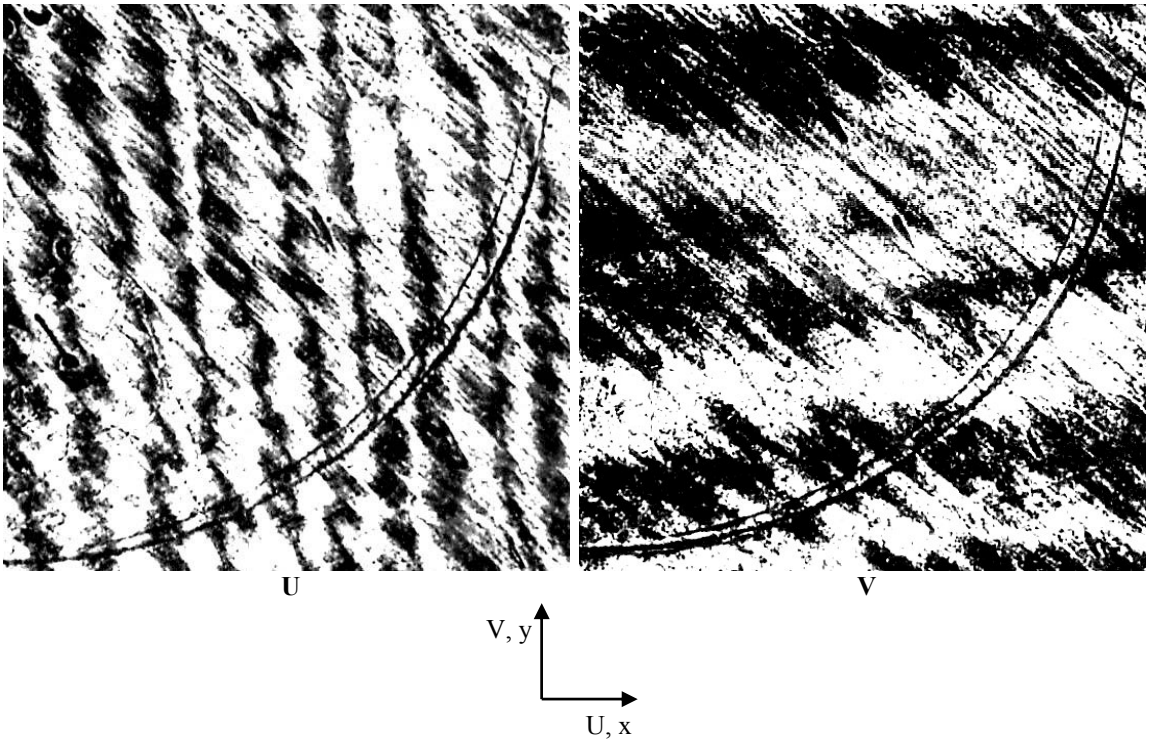

Figure A-11: RLV laminate Run 1

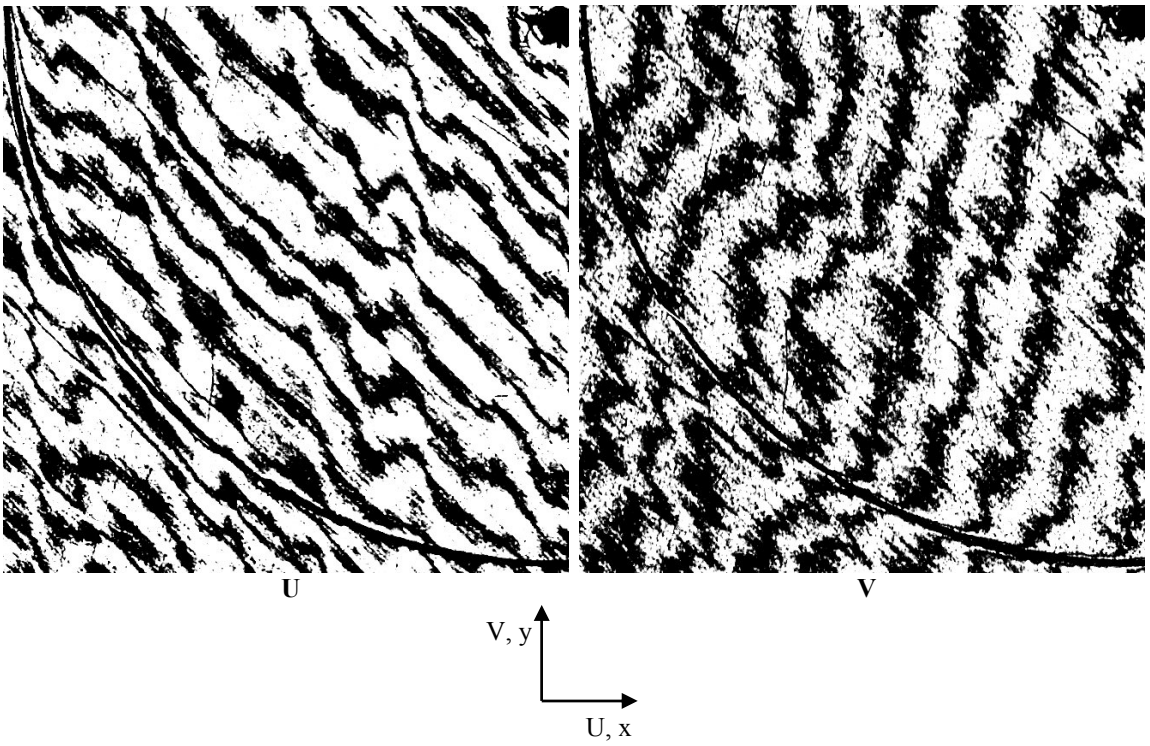

Figure A-12: RLV Laminate Run 2

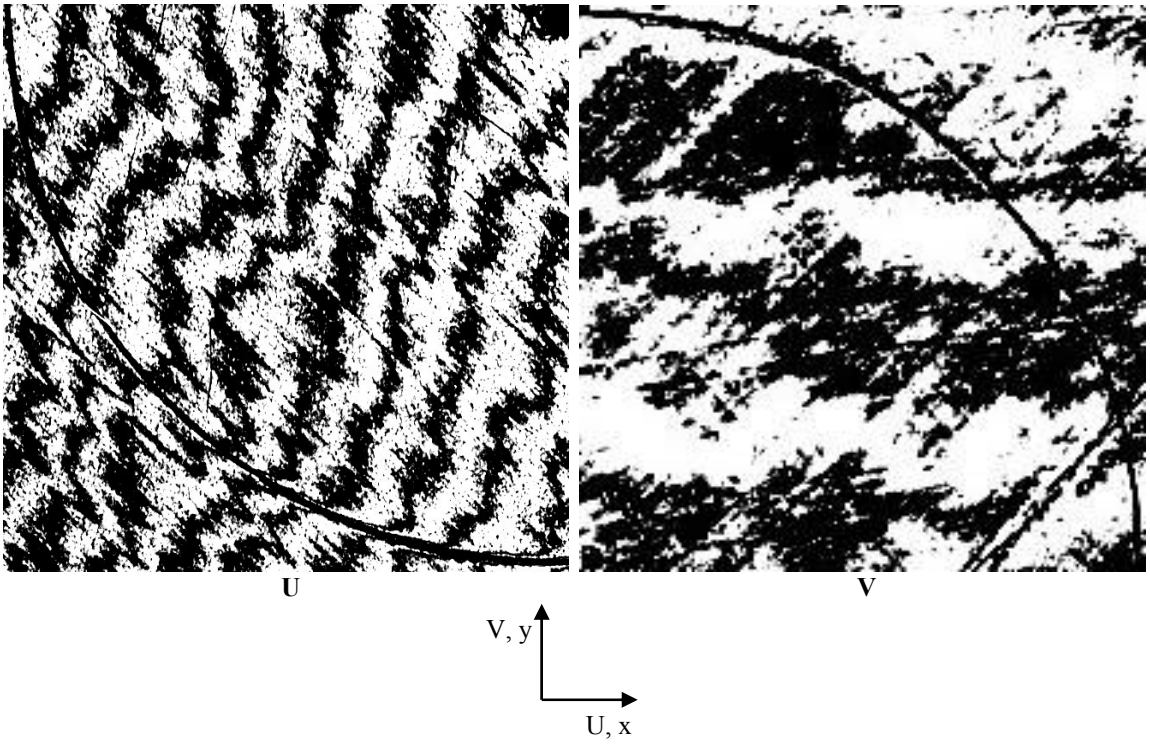

Figure A-13: RLV Laminate Run 3

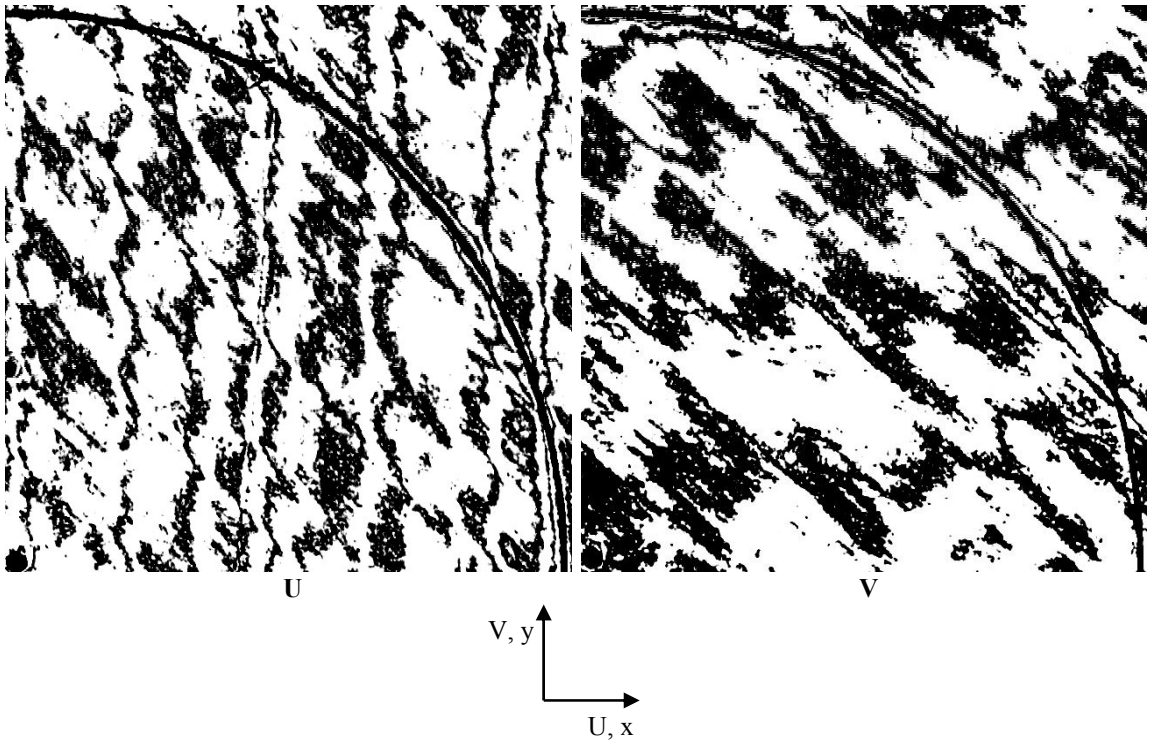

Figure A-14: RLV Laminate Run 4

APPENDIX B
MATLAB CLT CODE

Main Routine: laminatestress

```
function
[strain0,curve,stressx,stress1]=laminatestress(plydir,thick,E1,E2,G12,n
u12,NM,deltaT,c,alpha12,beta12,plots)
% laminatestress uses classical laminate theory to give midplane strain
and curvature, and
% stress (in both the coordinates of the laminate and of the ply) at
the top and bottom of each ply.
% All referenced equations are from Gibson, Principles of Composite
Material Mechanics, 1994
%    strain0: midplane strain, in laminate coords. [e_x;e_y;g_xy].
%    curve: curvature. [K_x;K_y;K_xy].
%    stressx: stress in laminate coords.  stressx is 6 x k, where k is
the number of plys.
%       The kth column gives stress in the x and y directions and shear
in the xy plane at
%       the top and bottom of the kth ply;
[s_x_top;s_y_top;s_xy_top;s_x_bot;s_y_bot;s_xy_bot].
%   stress1: stress in ply coords.  Same as stressx, but the kth column
is in the kth ply
%       coords, with the 1-direction longitudinal, and 2-direction
transverse.
%   plydir: string of the form '[90/+-45/(-+30)3/90bar]s' or column
matrix of ply directions.  Note
%       that the variables make more sense with the z-axis down;
following this convention, the
%       first ply is the most negative.
%   plythick: column vector of ply thicknesses.  If thick is a scalar,
the thickness is applied to
%       all plys.
%   E1: column vector of Young's modulii in the fiber direction of each
ply.  If E1 is a scalar,
%       the modulus is applied to all plys.
%   E2: same as E1, in transverse directions.
%   G12: same as E1, but shear modulii.
%   nu12: same as E1, but Poisson's ratios.
%   NM: column vector of mechanical loading conditions
[N_x;N_y,N_xy;M_x;M_y;M_xy] per unit
%       length.
%   deltaT: change in temperature from cure temp.
%   c: moisture concentration.
%   alpha12: matrix of coeffs of thermal expansion, in material coords.
alpha12
%       is 2xn or 3xn,  where n is the number of plies.  If alpha12 is
2x1 or
```

```
%       3x1, the CTEs are assumed to apply to all plies.  Row 1 is CTE
in the
%       fiber direction, row 2 is CTE in the transverse direction, and
row 3
%       is 0.
%   beta12: matrix of coeffs of hygroscopic expansion.  Same format as
alpha12.
%   plots: 1 plots stressx and stress1 through thickness; 0 or blank
doesn't plot.
% Note: the last 5 inputs are optional.  If only one is entered, it is
taken to be plots.
% If 2 are entered, they are taken as deltaT and alpha.  If 3 are
entered, they are taken
% as deltaT, alpha12, and plots.  If 4 are entered, they are taken as
deltaT, c, alpha12,
% and beta12.


%----------Housekeeping----------
if exist('deltaT')==0
    deltaT=0;
    c=0;
    alpha12=[0;0;0];
    beta12=[0;0;0];
    plots=0;
elseif exist('c')==0
    plots=deltaT;
    deltaT=0;
    c=0;
    alpha12=[0;0;0];
    beta12=[0;0;0];
elseif exist('alpha12')==0
    alpha12=c;
    c=0;
    beta12=[0;0;0];
    plots=0;
elseif exist('beta12')==0
    plots=alpha12;
    alpha12=c;
    c=0;
    beta12=[0;0;0];
elseif exist('plots')==0
    plots=0;
end
%Sets variables not assigned in input

[a,b]=size(NM);
for i=a:5
    NM(i+1,1)=0;
end
%Fills in missing force and moment terms

if ischar(plydir)
    plydir=directions(plydir);
end
%Converts shorthand ply orientation to matrix
```

```
%----------Computation-------------
[m,n]=size(plydir);

[stiff,Q,S,Qbar,Sbar,T,z,z0]=ABD(plydir,thick,E1,E2,G12,nu12);
%Calculates ABD matrix

[Nh,Mh,alpha,beta]=hygrothermal(deltaT,c,alpha12,beta12,Qbar,T,z0,z);
NM=NM+[Nh;Mh];
%Adds hygrothermal forces and moments.  Eqs 7.95, 7.96

invstiff=inv(stiff);
ek=invstiff*NM;
%Solves for midplane strain and curvature.  Eq 7.46

strain0=ek(1:3);
curve=ek(4:6);
%Extracting midplane strain and curvature

strainxtop=strain0+z0*curve;
%Pesky 0-index problem...see below

for k=1:m
    strainx(:,k)=strain0+z(k)*curve;
    botstressx(:,k)=Qbar(:,:,k)*(strainx(:,k)-alpha(:,k)*deltaT-
beta(:,k)*c);
    if k==1
        topstressx(:,k)=Qbar(:,:,k)*(strainxtop-alpha(:,k)*deltaT-
beta(:,k)*c);
    else
        topstressx(:,k)=Qbar(:,:,k)*(strainx(:,k-1)-alpha(:,k)*deltaT-
beta(:,k)*c);
    end
    %Stress in general (x-y) coords.  Eq 7.85
    botstress1(:,k)=T(:,:,k)*botstressx(:,k);
    topstress1(:,k)=T(:,:,k)*topstressx(:,k);
    %Stress in ply (1-2) coords.  Eq 2.31
end

stressx=[topstressx;botstressx];
stress1=[topstress1;botstress1];


%---------Plotting---------
if plots==1
    for k=1:m
        stressxx(2*k-1,1)=stressx(1,k);
        stressxx(2*k,1)=stressx(4,k);
        stressxy(2*k-1,1)=stressx(2,k);
        stressxy(2*k,1)=stressx(5,k);
        stressxxy(2*k-1,1)=stressx(3,k);
        stressxxy(2*k,1)=stressx(6,k);
        stress11(2*k-1,1)=stress1(1,k);
        stress11(2*k,1)=stress1(4,k);
        stress12(2*k-1,1)=stress1(2,k);
        stress12(2*k,1)=stress1(5,k);
```

```
        stress112(2*k-1,1)=stress1(3,k);
        stress112(2*k,1)=stress1(6,k);
    end

    zplot=z0;

    for k=1:m
        zplot(2*k,1)=z(k);
        if k~=m
            zplot(2*k+1,1)=z(k);
        end
    end

    scalex=max(stressxx);
    scaley=max(stressxy);
    scalexy=max(stressxxy);
    scale1=max(stress11);
    scale2=max(stress12);
    scale12=max(stress112);

scalex=max([scalex,scaley,scalexy])+.1*abs(max([scalex,scaley,scalexy])
);

scale1=max([scale1,scale2,scale12])+.1*abs(max([scale1,scale2,scale12])
);

    scalelox=min(stressxx);
    scaleloy=min(stressxy);
    scaleloxy=min(stressxxy);
    scalelo1=min(stress11);
    scalelo2=min(stress12);
    scalelo12=min(stress112);
    scalelox=min(0,min([scalelox,scaleloy,scaleloxy])-
.1*abs(min([scalelox,scaleloy,scaleloxy])));
    scalelo1=min(0,min([scalelo1,scalelo2,scalelo12])-
.1*abs(min([scalelo1,scalelo2,scalelo12])));

        strainxplot=[strain0(1)+curve(1)*z0;strain0(1)+curve(1)*z(m)];
        strainyplot=[strain0(2)+curve(2)*z0;strain0(2)+curve(2)*z(m)];
        strainxyplot=[strain0(3)+curve(3)*z0;strain0(3)+curve(3)*z(m)];
        strainzplot=[z0;z(m)];
        figure;
        plot(strainxplot,strainzplot)
        title('x-strains throughout the thickness, (x,y) coords')
        xlabel('Strain')
        ylabel('Postion')
        axis([-10e-3,20e-3,z0,z(m)])
        figure;
        plot(strainyplot,strainzplot)
        title('y-strains throughout the thickness, (x,y) coords')
        xlabel('Strain')
        ylabel('Postion')
        axis([-10e-3,20e-3,z0,z(m)])
        figure;
        plot(strainxyplot,strainzplot)
        title('Shear strains throughout the thickness, (x,y) coords')
        xlabel('Strain')
```

```
        ylabel('Postion')
        axis([-10e-3,20e-3,z0,z(m)])

    figure;
    plot(stressxx,zplot)
    title('x-stresses throughout the thickness, (x,y) coords')
    xlabel('Stress')
    ylabel('Position')
    axis([scalelox,scalex,z0,z(m)])
    figure;
    plot(stressxy,zplot)
    title('y-stresses throughout the thickness, (x,y) coords')
    xlabel('Stress')
    ylabel('Position')
    axis([scalelox,scalex,z0,z(m)])
    figure;
    plot(stressxxy,zplot)
    title('Shear stresses throughout the thickness, (x,y) coords')
    xlabel('Stress')
    ylabel('Position')
    axis([scalelox,scalex,z0,z(m)])
    figure;
    plot(stress11,zplot)
    title('1-stresses throughout the thickness, ply (1,2) coords')
    xlabel('Stress')
    ylabel('Position')
    axis([scalelo1,scale1,z0,z(m)])
    figure;
    plot(stress12,zplot)
    title('2-stresses throughout the thickness, ply (1,2) coords')
    xlabel('Stress')
    ylabel('Position')
    axis([scalelo1,scale1,z0,z(m)])
    figure;
    plot(stress112,zplot)
    title('Shear stresses throughout the thickness, ply (1,2) coords')
    xlabel('Stress')
    ylabel('Position')
    axis([scalelo1,scale1,z0,z(m)])
end
```

Subroutine: directions

```
function dir=directions(str)
% DIRECTIONS  Converts from shorthand ply angle notation
%   DIRECTIONS(str) outputs a column vector of ply angles as given by
str.
%   str should be a string of the form '[(25)2/+-45/(-+60/0)3/90bar]s'
%   In extended notation, this is
%   [25/25/+45/-45/-60/+60/0/-60/+60/0/-60/+60/0/90/0/+60/-60/0/+60/-
60/0/+60/-60/-45/+45/25/25]
%   Always start with [.  Use / to seperate ply angles.  Use (plys)n to
%   indicate a set of plys repeated n times.  Use +-theta to indicate
%   +theta/-theta, and -+theta to indicate -theta/+theta.  Use bar
after
%   the last ply to indicate a symmetric laminate in which the midplane
```

```
%   passes through the middle of the ply.  End the ply sequence with ].
%   Use s at the end to indicate symmetry (must be used with bar); t or
%   nothing denotes that the full ply sequence has been given.
%
%   It may sound confusing, but it should actually be quite natural if
%   you are familiar with the shorthand notation.
%
%   See also PARENTHESES

str=lower(str);
len=length(str);

if str(len)=='t' & str(len-4:len-2)=='bar'
    error('Hey, dummy, is it symmetric or not?')
end

sym=0;
oddsym=0;

if str(len)=='s'
    sym=1;
    str=str(1:len-2);
elseif str(len)=='t'
    str=str(1:len-2);
else
    str=str(1:len-1);
    len=len+1;
end

if str(len-4:len-2)=='bar'
    sym=1;
    oddsym=1;
    str=str(2:len-5);
else
    str=str(2:len-2);
end

len=length(str);

str=strcat(str,'/');

slash=findstr('/',str);
strpos=1;
plypos=1;
slashpos=1;
plydir=0;

while strpos<len+1
    if str(strpos:strpos+1)=='+-'
        plydir(plypos)=str2num(str(strpos+2:slash(slashpos)-1));
        plydir(plypos+1)=-str2num(str(strpos+2:slash(slashpos)-1));
        plypos=plypos+2;
        strpos=slash(slashpos)+1;
    elseif str(strpos:strpos+1)=='-+'
        plydir(plypos)=-str2num(str(strpos+2:slash(slashpos)-1));
        plydir(plypos+1)=str2num(str(strpos+2:slash(slashpos)-1));
        plypos=plypos+2;
```

```
        strpos=slash(slashpos)+1;
    elseif str(strpos)=='('
        closepar=findstr(')',str(strpos:len))+strpos-1;
        slash2=findstr('/',str(closepar(1):len+1))+closepar(1)-1;
        digits=slash2(1)-closepar(1)-1;
        [newplydir,slashnum]=parentheses(str(strpos:closepar(1)+1));

        if slashpos==1
            plydir=newplydir;
        else
            plydir=[plydir,newplydir];
        end

        slashpos=slashpos+slashnum;
        strpos=slash(slashpos)+1;
        [y,z]=size(plydir);
        plypos=z+1;
    else
        plydir(plypos)=str2num(str(strpos:slash(slashpos)-1));
        plypos=plypos+1;
        strpos=slash(slashpos)+1;
    end
    slashpos=slashpos+1;
end

if sym==1
    if oddsym==1
        [y,z]=size(plydir);
        plydir=[plydir(1:z-1),fliplr(plydir)];
    else
        plydir=[plydir,fliplr(plydir)];
    end
end
dir=plydir.';
```

Subroutine: parentheses

```
function [plydir,slashnum]=parentheses(str)
% PARENTHESES converts parenthetical shorthand ply angle notation
% [plydir,slashnum]=PARENTHESES(str) outputs the ply direction plydir
%   and the number of slashes slashnum in the string str.
%
% See also DIRECTIONS

len=length(str);
str=strcat(str(1:len-2),'/',str(len-1:len));
mult=str2num(str(len+1));

slash=findstr('/',str);
[z,slashnum]=size(slash);
slashnum=slashnum-1;
strpos=2;
plypos=1;
slashpos=1;

while strpos<len
```

```
    if str(strpos:strpos+1)~='+-' & str(strpos:strpos+1)~='-+'
        plydir(plypos)=str2num(str(strpos:slash(slashpos)-1));
        plypos=plypos+1;
        strpos=slash(slashpos)+1;
    elseif str(strpos:strpos+1)=='+-'
        plydir(plypos)=str2num(str(strpos+2:slash(slashpos)-1));
        plydir(plypos+1)=-str2num(str(strpos+2:slash(slashpos)-1));
        plypos=plypos+2;
        strpos=slash(slashpos)+1;
    else
        plydir(plypos)=-str2num(str(strpos+2:slash(slashpos)-1));
        plydir(plypos+1)=str2num(str(strpos+2:slash(slashpos)-1));
        plypos=plypos+2;
        strpos=slash(slashpos)+1;
    end
    slashpos=slashpos+1;
end

plydir1=plydir;

for a=2:mult
    plydir=[plydir,plydir1];
end
```

Subroutine: ABD

```
function [K,Q,S,Qbar,Sbar,T,z,z0]=ABD(plydir,plythick,E1,E2,G12,nu12)
% ABD calculates the laminate stiffness matrix of the form [A,B;B,D].
% All referenced equations are from Gibson, Principles of Composite
Material Mechanics, 1994
%   [K,Q,S,Qbar,Sbar,T,z,z0]=ABD(plydir,plythick,E1,E2,G12,nu12)
%
%   Inputs:
%   plydir: string of the form '[90/+-45/(-+30)3/90bar]s' or column
matrix of ply directions.  Note
%       that the variables make more sense with the z-axis down;
following this convention, the
%       first ply is the most negative.
%   plythick: column vector of ply thicknesses.  If thick is a scalar,
the thickness is applied to
%       all plys.
%   E1: column vector of Young's modulii in the fiber direction of each
ply.  If E1 is a scalar,
%       the modulus is applied to all plys.
%   E2: same as E1, in transverse directions.
%   G12: same as E1, but shear modulii.
%   nu12: same as E1, but Poisson's ratios.
%
%   Outputs:
%   K: laminate stiffness (ABD) matrix
%   Q: ply stiffness.  3D array with Q(:,:,k) the stiffness matrix for
the kth ply.
%   S: ply compliance.  Also 3D array, same convention.
%   Qbar: transformed ply stiffness.  Also 3D array, same convention.
%   Sbar: transformed ply compliance.  Also 3D array, same convention.
```

```
%   T: transformation matrix.  Also 3D array, same convention.  Q, S,
Qbar, Sbar, and T are
%       throughput for use by other functions.
%   z: column vector of z postions, kth entry is z postion of bottom of
kth ply.
%   z0: z position of top of first ply (most negative).
%
%   See also DIRECTIONS, PLANESTRESS



%---------Housekeeping---------
%Converts shorthand ply orientation to matrix
if ischar(plydir)
    plydir=directions(plydir);
end

%Checks laminate property sizes and orients in column vector form
[m,n]=size(plydir);

[o,p]=size(plythick);
if p ~= 1
    plythick = plythick.';
    o = p;
end

[q,r]=size(E1);
if r ~= 1
    E1 = E1.';
    q = r;
end

[s,t]=size(E2);
if t ~= 1
    E2 = E2.';
    s = t;
end

[u,v]=size(G12);
if v ~= 1
    G12 = G12.';
    u = v;
end

[w,x]=size(nu12);
if x ~= 1
    nu12 = nu12.';
    w = x;
end

%Expands uniform ply properties
if o==1
   plythick=ones(m,1)*plythick;
elseif o~=m
    error('Thickness should be entered either as a scalar or as a
vector of length n, where n is the number of plys in the laminate')
end
```

```
if q==1
   E1=ones(m,1)*E1;
elseif q~=m
    error('E1 should be entered either as a scalar or as a vector of
length n, where n is the number of plys in the laminate')
end

if s==1
   E2=ones(m,1)*E2;
elseif s~=m
    error('E2 should be entered either as a scalar or as a vector of
length n, where n is the number of plys in the laminate')
end

if u==1
   G12=ones(m,1)*G12;
elseif u~=m
    error('G12 should be entered either as a scalar or as a vector of
length n, where n is the number of plys in the laminate')
end

if w==1
   nu12=ones(m,1)*nu12;
elseif w~=m
    error('nu12 should be entered either as a scalar or as a vector of
length n, where n is the number of plys in the laminate')
end


%---------Computation-----------
%Sets z values for bottom of each ply.  z0 is top of 1st ply.
z0=-sum(plythick)/2;
z(1)=z0+plythick(1);
for k=2:m
   z(k)=z(k-1)+plythick(k);
end

%Calcs stiffnesses and compliances.  Each is placed into a 3-D matrix,
where Q(:,:,k) corresponds to the kth ply.
for k=1:m

[Q(:,:,k),S(:,:,k),Qbar(:,:,k),Sbar(:,:,k),T(:,:,k)]=planestress(E1(k),
E2(k),G12(k),nu12(k),plydir(k));
end

%Assembling A, B, and D.  Eqs 7.38, 7.39, 7.40
for i=1:3
   for j=1:3
      A(i,j)=Qbar(i,j,1)*(z(1)-z0);
      B(i,j)=1/2*Qbar(i,j,1)*(z(1)^2-z0^2);
      D(i,j)=1/3*Qbar(i,j,1)*(z(1)^3-z0^3);
      for k=2:m
         A(i,j)=A(i,j)+Qbar(i,j,k)*(z(k)-z(k-1));
         B(i,j)=B(i,j)+1/2*Qbar(i,j,k)*(z(k)^2-z(k-1)^2);
         D(i,j)=D(i,j)+1/3*Qbar(i,j,k)*(z(k)^3-z(k-1)^3);
      end
```

```
   end
end

%Putting it all together.
K=[A,B;B,D];
```

Subroutine: planestress

```
function [Q,S,Qbar,Sbar,T]=planestress(E1,E2,G12,nu12,theta)
% PLANESTRESS calculates the stiffness and compliance matrices of a
lamina
%   All referenced equations are from Gibson, Principles of Composite
Material Mechanics,
%   1994 except as noted.
%
%   Inputs:
%   E1: Young's modulus in the fiber direction.
%   E2: Young's modulus in the transverse direction.
%   G12: Shear modulus.
%   nu12: Poisson's ratio.
%   theta: angle between ply fibers (1-direction) and x-direction, in
degrees.
%
%   Outputs:
%   Q: stiffness matrix in 12 (fiber) coordinates.
%   S: compliance matrix in 12 (fiber) coordinates.
%   Qbar: transformed stiffness matrix in xy (general) coordinates.
%   Sbar: transformed compliance matrix in xy (general) coordinates.
%   T: transformation matrix.


%--------Computation-------
%Change theta to radians.
theta=theta*pi/180;

nu21 = nu12*E2/E1;

%Calculating S and Q.  Eqs 2.24, 2.4, 2.6
S=[1/E1, -nu12/E1, 0; -nu12/E1, 1/E2, 0; 0, 0, 1/G12];
Q=inv(S);
%Q = [E1/(1-nu12*nu21), nu12*E2/(1-nu12*nu21), 0;nu12*E2/(1-nu12*nu21),
E2/(1-nu12*nu21),0;0,0,G12];

%Transformation matrices.  Eq 2.32, Ifju's class notes, 2/7/02
T=[(cos(theta))^2, (sin(theta))^2, 2*cos(theta)*sin(theta);
(sin(theta))^2, (cos(theta))^2, -2*cos(theta)*sin(theta); -
cos(theta)*sin(theta), cos(theta)*sin(theta), (cos(theta))^2-
(sin(theta))^2];
R=[1,0,0;0,1,0;0,0,2];

%Calculating Qbar and Sbar.  Ifju's class notes, 2/7/02
Qbar=inv(T)*Q*R*T*inv(R);
Sbar=R*inv(T)*inv(R)*S*T;
```

Subroutine: hygrothermal

```
function
[Nh,Mh,alpha,beta]=hygrothermal(deltaT,c,alpha12,beta12,Qbar,T,z0,z)
% hygrothermal outputs the thermal and moisture induced forces and
moments
% on a laminate.
% All referenced equations are from Gibson, Principles of Composite
Material Mechanics, 1994
%   Nh: hygrothermal force.
%   Mh: hygrothermal moment.
%   alpha: matrix of coeff thermal expansions in laminate coords.
alpha is 3xn,
%       where n is the number of plies.  The kth column is
[alpha_x;alpha_y;alpha_xy]
%       for the kth ply.
%   beta: same as alpha, but coeff hygroscopic expansions.
%   deltaT: change in temperature from cure temp.
%   c: moisture concentration.
%   alpha12: matrix of coeffs of thermal expansion, in material coords.
alpha12
%       is 2xn or 3xn,  where n is the number of plies.  If alpha12 is
2x1 or
%       3x1, the CTEs are assumed to apply to all plies.  Row 1 is CTE
in the
%       fiber direction, row 2 is CTE in the transverse direction, and
row 3
%       is 0.
%   beta12: matrix of coeffs of hygroscopic expansion.  Same format as
alpha12.
%   Qbar: transformed stiffness matrix.
%   T: transformation matrices, 3x3xn.
%   z0: z position of top of 1st ply.
%   z: column matrix of z positions of bottom of plies.


%--------Housekeeping--------
[m,n]=size(z);
%determining number of plies

[o,p]=size(alpha12);
if o==2
    alpha12(3,:)=0;
end
if p==1
    for k=2:n
        alpha12(:,k)=alpha12(:,1);
    end
end

[o,p]=size(beta12);
if o==2
    beta12(3,:)=0;
end
if p==1
    for k=2:n
```

```
        beta12(:,k)=beta12(:,1);
    end
end
%adding shear component to CTE and CHE matrices for calculations
%   and expanding uniform ply properties

%--------Computation--------
for k=1:n
    alpha(:,k)=inv(T(:,:,k))*alpha12(:,k);
    beta(:,k)=inv(T(:,:,k))*beta12(:,k);
end
alpha(3,:)=alpha(3,:)*2;
beta(3,:)=beta(3,:)*2;
%calculating laminate direction CTEs and CHEs--note that
%   alpha12*inv(T)=[alpha_x;alpha_y;alpha_xy/2], and the third row
%   must be multiplied by 2 to give the shear CTE.  Same for beta.
%   Eq. 5.22

Nt = deltaT*Qbar(:,:,1)*alpha(:,1)*(z(1)-z0);
Nm = c*Qbar(:,:,1)*beta(:,1)*(z(1)-z0);
Mt = deltaT/2*Qbar(:,:,1)*alpha(:,1)*(z(1)^2-z0^2);
Mm = c/2*Qbar(:,:,1)*beta(:,1)*(z(1)^2-z0^2);
%0-index workaround again...see below

for k=2:n
    Nt = Nt + deltaT*Qbar(:,:,k)*alpha(:,k)*(z(k)-z(k-1));
    Nm = Nm + c*Qbar(:,:,k)*beta(:,k)*(z(k)-z(k-1));
    Mt = Mt + deltaT/2*Qbar(:,:,k)*alpha(:,k)*(z(k)^2-z(k-1)^2);
    Mm = Mm + c/2*Qbar(:,:,k)*beta(:,k)*(z(k)^2-z(k-1)^2);
end
% calculating thermal and hygroscopic forces and moments.  Eqs 7.87-
7.91

Nh=Nt+Nm;
Mh=Mt+Mm;
% summing for hygrothermal forces and moments
```

LIST OF REFERENCES

1. Bert, C. W., and Thompson, G. L., "A Method for Measuring Planar Residual Stresses in Rectangularly Orthotropic Materials," *Journal of Composite Materials*, Vol. 2, No. 2, April, pp. 244-253, 1968.

2. Carman, G. P., and Sendechyj, G. P., "Review of the Mechanics of Embedded Optical Sensors," *Journal Composites Technology & Research*, Vol. 17, No. 3, pp. 183-193, 1995.

3. Chapman, T. J., Gillespie, J. W., Pipes, R. B., Manson, J. E., "Prediction of Process-Induced Residual Stresses in Thermoplastic Composites," *Journal Composite Materials,* Vol. 24, pp. 616-643, 1990.

4. Choi, S., Sankar, B.V., *A Micromechanics Method to Predict the Microcracking of the LH_2 Composite Tank at Cryogenic Temperature*, Department of Mechanical and Aerospace Engineering, University of Florida, 2003.

5. Daniel, I. M., and Liber, T., "Effect of Laminate Construction on Residual Stresses in Graphite/Polyimide Composites," *Experimental Mechanics,* Vol. 1, pp. 21-25, 1977.

6. Daniel, I. M., and Liber, T., "Lamination Residual Stresses in Fiber Composites," *IITRI Report D6073-I, for NASA-Lewis Research Center, NASA CR-134826,* 1975.

7. Daniel, I. M., Liber, T., and Chamis, C. C., "Measurement of Residual Strains in Boron/Epoxy and Glass/Epoxy laminates," *Composite Reliability, ASTM STP 580, American Society for Testing and Materials,* pp. 340-351, 1975.

8. Daniel, I. M., Wang, T., "Determination of Chemical Cure Shrinkage in Composite laminates," *Journal of Composites Technology & Research*, Vol. 12, No. 3, pp. 172-176, 1989.

9. Daniel, I. M., Wang, T. –M., Karalekas, D. and Gotro, J. T., "Determination of Chemical Cure Shrinkage in Woven_Glass/Epoxy Laminates," *Annual Technical Conference-Society of Plastics Engineers*, New York, USA, May 1-4, pp. 632-634, 1989.

10. Fakuda, H., Takahashi, K., and Toda, S., "Thermal Deformation of Anti-Symmetric Laminates At Cure," *Proceedings of ICCM-10,* Whistler, B.C., Canada, August, Vol.3, pp. 141-148, 1995.

11. Fenn, R. H., Jones, A. M., and Wells, G. M., "X-Ray Diffraction Investigation of Triaxial Residual Stresses in Composite Materials," *Journal Composite Materials,* Vol. 27, No. 14, pp. 1338-1351, 1993.

12. Final Report of the X-33 Liquid Hydrogen Tank Test Investigation Team, NASA George C Marshall Space Flight Center, Huntsville, AL 35812, May 2000.

13. Gibson, R. F., *Principles of Composite Material Mechanics,* McGraw-Hill, New York, New York, 1994.

14. Griffith, A.A., "The Phenomena of Rupture and Flow in Solids," *Philosophical Transactions of the Royal Society*, Vol. 221A, pp. 163-198, 1920.

15. Groover, M.P., *Fundamentals of Modern Manufacturing*, Prentice Hall, Upper Saddle River, New Jersey, 1996.

16. Hahn, H. T., "Residual Stresses in Polymer Matrix Composite Laminates," *Composite Materials,* Vol. 10, pp. 265-277, 1976.

17. Hyer, M. W., "Calculation of Room-Temperature Shapes of Unsymmetrical Laminates," *Journal Composite materials,* Vol. 15, July, pp. 296-310, 1981.

18. Ifju, P.G., Myers, D., Schulz, W., "Residual Stress and Thermal Expansion of Graphite Epoxy Laminates Subjected to Cryogenic Temperatures," *Proceedings of the American Society for Composites 18th Technical Conference*, October 19-23, 2003.

19. Ifju, P.G., Haftka, R., Myers, D., Schulz, W., Singer, T., "Statistics Properties and Reliability Based Optimiztion of Laminates for Cryogenic Environments," *AIAA-2003-1935, 44th AIAA/ASME/ASCE/AHS Structures, Structural Dynamics, and Materials Conference,* 7-10 April 2003.

20. Ifju, P.G., Niu, X., Kilday, B.C., Liu, S.C., Ettinger, S.M., "Residual Strain Measurement in Composites Using the Cure-referencing Method," *Journal of Experimental Mechanics*, Vol. 40, No. 1, pp. 22-30, 2000.

21. Ifju, P.G., Niu, X., Kilday, B.C., Liu, S.C., "A Novel Means to Determine Residual Stress In Laminated Composites," *Journal of Composite Materials*, Vol. 33, No. 16, 1999.

22. Jain, L. K., and Mai, Y. W., "On Residual Stress Induced Distortions during Fabrication of Composite Shells," *Proceedings of the American Society for Composites-Tenth Technical Conference*, Santa Monica, CA, USA, Oct. 18-20, pp.261-270, 1995.

23. Jeronimidis, G., and Parkyn, A. T., "Residual Stresses in Carbon Fiber-Thermoplastic Matrix Laminates," *Journal Composites Materials,* Vol. 22, pp. 401-415, May 1988.

24. Joh, D., Byun, K. Y., and Ha, J., "Thermal Residual Stresses in Thick Graphite/Epoxy Composite Laminates-Uniaxial Approach," *Experimental Mechanics,* Vol. 33, No., pp. 70-76, 1993.

25. Kam, T. Y., "Nonlinear and First-Ply Failure Analyses of laminated Composite Cross-Ply Plates," *Journal of Composite Materials*, Vol. 29, No.4, pp. 463-482, 1995.

26. Kim, K. S., and Hahn, H.T., "Residual Stress Development during Processing of Graphite/ Epoxy Composite," *Composite Science and Technology*, 36, pp. 121-132, 1989.

27. Kim, R. Y., and Hahn, H. T., "Effect of Curing Stresses on the First Ply-failure in Composite Laminates," *Journal Composite Materials,* Vol. 13, January, pp. 2-16, 1979.

28. Lake, B. R., Appl, F. J., and Bert, C. W., "An Investigation of the Hole-drilling Technique for Measuring Planar Residual Stress in Rectangularly Orthotropic Materials," *Experimental Mechanics,* Vol. 10, June, pp. 233-239, 1970.

29. Lawrence, C., Nelson, D.V., Bennett, T.E., Spingarn, J.R., "Embedded Fiber Optic Sensor Method for Determining Residual Stresses in Fiber-Reinforced Composite Materials," *Journal of Intelligent Material Systems and Structures*, Vol. 9, pp. 788-799, 1999.

30. Lee, J., and Czarnek, R., "Measuring Residual Strains in Composites Laminates Using Moiré Interferometry," *Proceedings of the 1991 SEM Conference on Experimental Mechanics,* Milwaukee, WI, USA, June 1-3, pp. 405-415, 1991.

31. Lee, J., Czarnek, R., and Guo, Y. "Interferometric Study of Residual Strains in Thick Composites," *Proceedings of the 1989 SEM Conference on Experimental Mechanics*, Cambridge, MA, USA, June 7-10, pp. 356-364, 1989.

32. Månson, J. E., and Seferis, J.C. "Process Simulated Laminate (PSL)" A Methodology to Internal Stress Characterization in Advanced Composite Materials," *Journal Composite Materials,* Vol. 26, No. 3, pp. 405-431, 1992.

33. Mathar, J., "Determination of Initial Stress by Measuring the Deformations Around Drilled Holes," *Transaction of ASME*, Vol. 56, p.249, 1934.

34. "Measurement of Thermal Expansion Coefficient," *Tech Note TN-513*, Measurements Group, pp. 1-24.

35. "Measurement of Residual Stresses by the Hole-Drilling Strain-Gage Method," *Tech Note TN-503,* Measurement Group, pp. 1-15, 1988.

36. Nicoletto, G., “Moiré Interferometry Determination of Residual Stresses in the Presence of Gradients,” *Experimental Mechanics,* Vol. 31, No. 3, pp. 252-256, 1991.

37. Niu, X., *Process Induced Residual Stresses and Dimensional Distortions in Advanced Laminated Composites*, University of Florida, 1999.

38. Park, J., Lee, S., Lee, J., “Nondestructive Sensing Evaluation of Single Carbon Fiber/Polymer Composites Using Electro-Micromechanical Technique,” *International SAMPE Symposium and Exhibition (Proceedings)*, Vol. 47, pp190-203, 2002.

39. Post, D., Han, B., and Ifju, P. G., *High Sensitivity Moiré: Experimental Analysis for Mechanics and Materials*, Springer Verlag, New York, 1994.

40. Predecki, P., and Barrett, C. S., “Stress Measurement in Graphite/Epoxy Composites by X-Ray Diffraction from Fillers,” *Journal Composite Materials,* Vol. 13, pp. 61-71, 1979.

41. Qu, X., Venkataraman, S., Haftka, R.T., Johnson, T.F., “Reliability, Weight, and Cost Tradeoffs in the Design of Composite Laminates for Cryogenic Environments,” *AIAA Paper 2001-1327, Proceedings 42nd AIAA/ASME/ASCE/AHS/ASC Structures, Structural Dynamics and Material Conference*, Seattle, WA, April, 2001.

42. Rendler, N. J., and Vigness, I., “Hole-drilling Strain-gage Method of Measuring Residual Stresses,” *Experimental Mechanics*, pp. 577-586, December 1966.

43. Schajer, G. S., and Yang, L., “Residual-stress Measurement in Orthotropic Materials Using the Hole-drilling Method,” *Experimental Mechanics,* Vol. 34, No. 4, pp. 324-333, 1994.

44. “Standard Test Method for Tensile Properties of Polymer Matrix Composite Materials,” *ASTM Standards D3039*, Vol. 15.03, pp 98-108.

45. “Standard Test Method for Shear Properties of Composite Materials by the V-Notched Beam Method,” *ASTM Standards D5379*, Vol. 15.03, pp 226-238.

46. Sunderland, P., Yu, W. J., and Månson, J. E., "A Technique for the Measurement of Process-Induced Internal Stresses in Polymers and Polymer Composites,” *Proceedings of ICCM-10,* Whistler, B. C., Canada, August, Vol. 3, pp. 125-132, 1995.

47. Tanaka, N., Okabe, Y., Takeda, N., “Temperature-Compensated Strain Measurement Using FBG Sensors Embedded in Composite Laminates,” *Proceedings of SPIE-The International Society for Optical Engineering*, Vol. 4694, pp. 304-313, 2002.

48. "Polymer Matrix Composites: Materials, Usage, Design, and Analysis," *The Composite Materials Handbook Mil 17,* Vol. 3, pp. 9.1-9.12, ASTM, West Conshohocken, PA, 2002.

49. Unger, W. J., and Hansen, J. S., "The Effect of Thermal Processing on Residual Strain Development in Unidirectional Graphite Fiber Reinforced PEEK," *Journal Composite Materials,* Vol. 27, No. 1, pp. 59-81, 1993.

50. Wang, S., Chung, D.D.L., "Electrical Behavior of Carbon Fiber Polyer-Matrix Composites in the Through-Thickness Direction," *Journal of Materials Science*, Vol. 35, pp. 91-100, 2000.

51. Wang, T.-M., Daniel, I. M., and Gotro, J. T., "Thermoviscoelastic Analysis of Residual Stresses and Warpage in Composite Laminates," *Journal of Composite Materials*, Vol. 26, No. 6, pp. 883-899, 1992

BIOGRAPHICAL SKETCH

Donald Myers was born on August 26, 1978, in North Miami Beach, Florida. He lived in Miramar, Florida, an area between Miami and Ft. Lauderdale, where he attended Miramar High School and graduated as Valedictorian in the spring of 1996. Later that year he began his undergraduate education at the University of Florida in the Department of Aerospace Engineering, Mechanics, and Engineering Science. He graduated with honors in May 2001 with a Bachelor of Science in Aerospace Engineering. After obtaining the B.S., he continued his education at the University of Florida in August of 2001 pursuing a Master of Science from the Department of Mechanical and Aerospace Engineering. He served as a Graduate Research Assistant under Dr. Bhavani Sankar in the Advanced Center for Composites Laboratory, from August 2001 till May of 2002. In May of 2002 he transitioned to the Experimental Stress Analysis Laboratory where he has been serving as a Graduate Research Assistant under the tutelage of Dr. Peter Ifju. While in the Experimental Stress Analysis Lab he has been conducting research into material characterization of graphite/epoxy composites involved in the storage of cryogenic fuels.